MODEL ORDER REDUCTION AND OPTIMAL CONTROL OF WIND ENERGY CONVERSION SYSTEMS

BY INTESSAR TAEES HWAIDY AL-IEDANI

A dissertation submitted to the

Graduate School—New Brunswick

Rutgers, The State University of New Jersey

in partial fulfillment of the requirements

for the degree of

Doctor of Philosophy

Graduate Program in Electrical and Computer Engineering

Written under the direction of

Professor Zoran Gajic

and approved by

_____

_____

_____

_____

_____

New Brunswick, New Jersey

January, 2021

ABSTRACT OF THE DISSERTATION

MODEL ORDER REDUCTION AND OPTIMAL CONTROL OF WIND ENERGY CONVERSION SYSTEMS

by INTESSAR TAEES HWAIDY AL-IEDANI
Dissertation Director: Professor Zoran Gajic

The increased demand on energy resources worldwide, along with the expectations of future depletion of fossil fuels: coal, oil, and gas, have encouraged considering the renewable energy as an alternative to traditional resources. Renewable resources including wind, solar, hydro, biomass, and geothermal are naturally abundant and can be harnessed to meet the energy demand without exacerbating the environmental contamination.

During the last few decades, wind energy has become one of the fastest growing and most promising renewable energy resources, due to their availability and minimal impact on the environment. As variable-speed wind turbine generators (WTGs) became advent, they gained increasing popularity due to their ability to work efficiently over wide ranges of wind speeds. The double fed induction generators (DFIGs) are widely used in variable-speed wind energy systems, since they consume less reactive power, inflict less mechanical stress on turbines, and allow decoupled control of the active and reactive power. This dissertation focuses on model reduction and optimal control of variable-speed wind turbines with DFIG systems.

To reduce the complexity of the power system model when a large number of WTGs

is integrated to the power grid, and to obtain a simplified model that adequately simulates such systems, the methods of balancing transformation and singular perturbations were utilized to reduce the order of a DFIG-based wind turbine model. We show that the order of the considered wind turbine model can be reduced from eight to six via the balancing transformation. Further reduction via the aforementioned method results in a significant increase in the error bound. In contrast, the method of singular perturbations shows that the order of the model can be further reduced to four, or even to two, and still provide very good approximations to the system model, in terms of its transient step response. Moreover, we show that the reduction in model order achieved via singular perturbations is superior from the optimal performance point of view to that achieved via balancing when the linear-quadratic near-optimal controllers are considered, and when the wind turbulence and a large-signal disturbance are applied to the system.

The state-space model of wind farms of different sizes, under different wind speed conditions, was also studied in this thesis. Model order reduction methods: balanced truncation, balanced residualization, cross Gramians, and singular perturbation were applied to the one-mass model to obtain simplified equivalents to wind farms of different sizes. This helps in reducing the computational complexity when controlling such systems. Examining the controllability and observability of the system, in both the vector and diagonal forms of the input control matrix, showed a considerable loss of controllability and observability in the case of the latter form.

The main obstacles that are associated with wind energy conversion systems are their intermittent behavior and dependence on the geographical location and weather conditions. Such randomness and uncertainty introduce nonlinearities when modeling the system dynamics. Therefore, designing optimal and robust controllers are crucial to deal with all the nonlinearities and uncertainties associated with wind energy systems. Based on time scale decomposition, an optimal controller for a DFIG-based wind turbine was designed by decomposing the algebraic Riccati equation (ARE) of the singularly perturbed wind turbine system into two reduced-order AREs that correspond to the slow and fast time scales. In addition, we derive a mathematical expression to

obtain the optimal regulator gains with respect to the optimal pure-slow and pure-fast, reduced-order Kalman filters and linear quadratic Gaussian (LQG) controllers. Using this method allows the design of the linear controllers for the slow and fast subsystems independently, thus, achieving complete separation and parallelism in the design process. This solves the corresponding numerical ill-conditioning problem, and reduces the complexity that arises when the number of wind turbines integrated to the power system increases. The reduced-order systems were compared to the original full-order system to validate the performance of the proposed method when a wind turbulence and a large-signal disturbance are applied to the system. In addition, we showed that the similarity transformation does not preserve the performance index value in the case of Kalman filter and the corresponding LQG controller.

Studying the wind turbine with DFIG system as a high order singularly perturbed system led to the introduction of a new recursive algorithm for solving the algebraic Sylvester equation that defines the cross Gramian of singularly perturbed linear systems. The cross Gramian matrix provides aggregate information about the controllability and observability of a linear system. The solution was obtained in terms of reduced-order algebraic Sylvester equations that correspond to the slow and fast subsystems of the singularly perturbed system. The rate of convergence of the proposed algorithm is $O(\epsilon)$, where ϵ is a small singular perturbation parameter that indicates the separation of slow and fast state variables. Several real physical system examples were solved to demonstrate the efficiency of the proposed algorithm.

Acknowledgements

As I sit down to write the acknowledgments section of my dissertation, I feel overwhelmed when I remember all the people who were vital in my arriving to this point. Words alone can never truly express my sincere and heartfelt thanks to everyone who has supported me, in some form or another, during this long and arduous journey, full of uncontrollable situations.

First and foremost, I would like to express my sincere appreciation and eternal gratitude for my advisor Professor Zoran Gajic, for his guidance and contribution towards this research throughout my time as a graduate student. His unwavering support and immense knowledge have been a major inspiration for me to carry on and have kept me from giving up during some of the most difficult times in my life. When my PhD program was hindered by illness, he provided his technical and moral support, and never grew frustrated with my slowing progress. I am extremely fortunate to have him as an advisor and owe him all my achievements during my graduate studies. He deserves more gratitude than I can articulate here.

I would also like to extend my thanks and appreciation to my committee members: Professor Hana Godrich, Professor Jinjang Yi, and Professor John McGarvey for making the time and effort to review my dissertation and to provide their valuable suggestions. My special thanks to Dr. Muhidin Lelic for agreeing to be an outside committee member in my defense, and for his thoughtful comments.

I would like to acknowledge the financial support provided by the Higher Committee for Education Development in Iraq (HCED), and the incredible opportunity to pursue my PhD studies in the United States. I am also grateful that I had the privilege to receive a fellowship from the Electrical and Computer Engineering Department (ECE) at Rutgers University, for three consecutive years, which provided me with additional

financial support.

I would like to express my gratitude to my friends, from whom I have gained knowledge and shared useful discussions during the control systems talks, Dr. John McGarvey, Dr. Sumati Sehajpal, Dr. Kliti Kodra, and Miss. Lingyi Xu.

I am immensely grateful to Dr. John McGarvey for his endless support and friendship throughout the years. I appreciate very much all the many wonderful conversations and endless encouragements. Thank you for being a welcoming and genuine friend and thank you for always being willing to listen to me talk about my research and life.

My precious friend Christy, your friendship has been a light in my darkest moments. Thank you for your prayers, your listening ears, your kind thoughts, and your open heart. I will never forget all the support you gave me, the encouraging words, tears, and laughter.

I would like to extend my gratitude to my friends in Iraq and the United States, including Dr. Israa Al-Saadi, Dr. Aseel Mansi, Dr. Ahmed Al-Abdel Abass, and Mrs. Safaa Al-Joorany. Thank you for your help, prayers unwavering encouragement and support.

I would like to express my gratitude to my mother, my sisters, and brothers for their unconditional love, and for providing their support for my current endeavors. I love you all more than words can describe; even though you were thousands of miles away, you were always there for me.

To my sister Nour, thank you for caring about me and my family. I am thankful to you for being incredibly patient, kind, understanding, and encouraging. I appreciate that more than words can say.

My dearest husband Ali:

Thank you for being in my life and for standing by my side through all of this. Thank you for being my research colleague and my best friend, for listening to my complaints and frustrations and loving me throughout my darkest moments. Thank you for proofreading my chapters and correcting my grammar. I could not have completed this work without your love, humor, emotional support, and help, especially during times of illness. I am eternally grateful for your phenomenal patience and understanding.

To my amazing daughter Maryam and my strong boy Wissam, thank you for being in my life, and for enlightening my days. You are the reason that I keep going.

Lastly, I was fortunate to have so many friends and supporters during this journey, whom I would love to acknowledge, but that would take so many more pages. To all of them, none of this would have been possible without any of you; there are not enough words to express how much I truly appreciate all of your love and support. Thank you all!

Dedication

To my family and my advisor, Dr. Zoran Gajic,

your support, understanding, and encouragement have been exceptional.

Table of Contents

List of Tables

List of Figures

Chapter 1

Introduction

Harnessing wind energy, one of the most efficient forms of renewable energy, has exponentially increased in the last few decades. The significant improvement in wind turbine technology, low cost of operation and maintenance in comparison to other forms of renewable energy, and its negligible effect on the environment are the main reasons behind its dramatic growth. According to the annual Wind Technologies Market Report in 2018, the average hub height and the average rotor diameter of the newly installed turbines in the United States has increased by 57% and 141%, respectively since 1998–1999 [1]. Higher towers and larger rotors help maximize the captured energy leading to very efficient power generation. Furthermore, the cost of wind energy has dramatically decreased, making wind energy a true competitor of the lowest-cost sources of electricity nowadays [1, 2].

According to the axis of rotation, industrial wind turbines fall into two main types: vertical-axis wind turbines (VAWTs) and horizontal-axis wind turbines (HAWTs). A VAWT rotates around a vertical axis, its rotation does not depend on the wind direction, and needs only low wind speed to start. Therefore, the main components, such as the gearbox and the generator can be built near to the ground, which facilitates maintenance and service. A HAWT, in comparison, rotates around a horizontal axis and has many blades fixed on the top of a tall tower. Since wind is stronger on higher elevations, the higher the tower, the more the captured energy, resulting in very efficient power generation [3].

Figure 1.1 shows the main components of the HAWT. These are the blades, nacelle (including the other components inside, such as the gearbox, breaker, and generators), and tower. The rotating blades are connected to the shaft of an electric generator
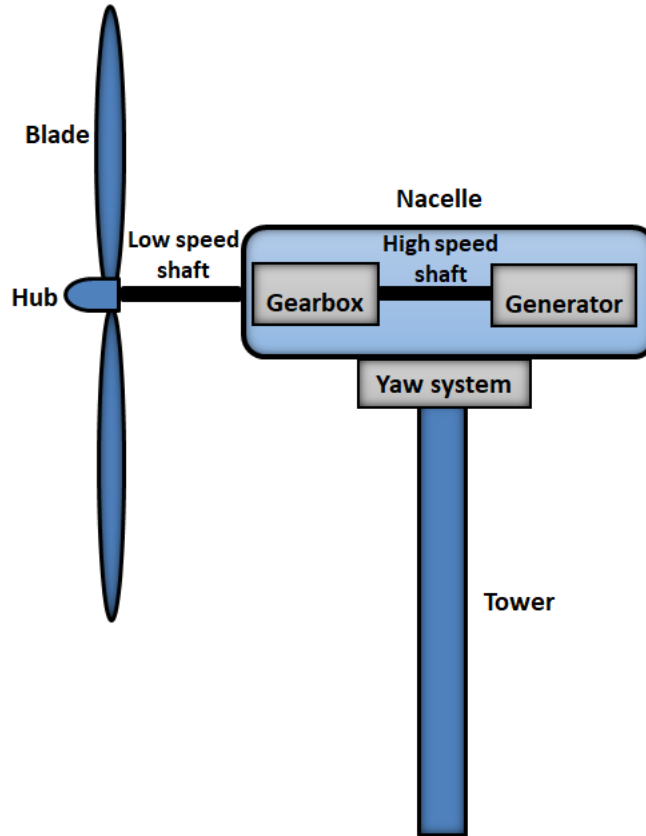
Figure 1.1: Horizontal axis wind turbine components

to produce electricity. The blades are attached firmly to the shaft and shaped like airfoils. The nacelle contains the drive train components: the rotor shaft, gearbox, breaks, and electric generator. The rotor shaft is attached to the blades and rotates at a relatively low speed; therefore the gearbox is used to increase the speed of rotation to the speed required by the generator to generate electricity. A rotation speed of 15 to 20 revolution per minute (rpm) could be increased to between 1800 and 2000 (rpm) by the gearbox. However, the gearbox is one of the most vulnerable parts of the turbine and its breakdown causes a major fault and reduces the reliability of the system. It contributes along with the generator to the most frequent downtime of the wind turbine [1,4]. The gearbox can be eliminated through the use of a direct-drive system which has fewer components and it is more reliable, easily maintained and able to generate power at much lower speeds [4–6].

The early models of wind turbines were all based on fixed-speed wind turbine generators (WTGs), which are connected directly to the utility grid [5–7]. In this type of generators, extracting the maximum energy can only be achieved at a specific speed of rotation that occurs at a certain wind speed. The efficiency of such a generator deteriorates as the wind speed moves further away from that set point. As variable-speed WTGs became advent, they gained increasing popularity due to their ability to work efficiently over wide ranges of wind speeds. Two types of variable-speed electric generators are commonly used nowadays: the double-fed induction generator (DFIG) and permanent-magnet synchronous generator (PMSG). Variable-speed generators are connected to the utility grid through power electronic converters. When the wind speed increases a pitch drive can be used to turn the blades away from the wind direction. Sometimes, when the wind becomes too strong a mechanical break should be used to completely turn off the turbine in order to protect the blades from damage. As the extracted wind energy is highly related to the wind speed, fluctuations of the latter lead to significant power fluctuations. Therefore, when the wind speed is too high, pitch drive control moves the blades to the best angle that reduces power fluctuations and maximizes wind energy capturing. Moreover, the nacelle usually rotates about its vertical axis with an angle called the yaw angle. Yaw control moves the nacelle such that the blades will always face the coming wind.

The tower is a tall structure that carries and supports the turbine components. The size of the tower depends on the size of the turbine. Moreover, the higher the tower, the more wind energy that will be captured by the turbine, since the wind is usually stronger at higher elevations.

Wind energy conversion systems (WECS) exhibit highly nonlinear behavior, as both the generated power and aerodynamic torque are nonlinear functions of the wind speed and rotational speed of the rotor. To control such complicated systems, optimal control theory has been utilized with different objective functions, design constraints, and algorithms. For WECS, the main objective functions aim to maximize energy extraction, minimize the cost of energy and fatigue damage, maintain the stability and robustness of the system, and reject the disturbance. For this purpose, a linearized model of the

WECS is obtained around the optimal operating points, and suitable linear controllers are utilized according to the control objective [8]. One major drawback of linear control methods is that they require prior knowledge of all parameters and measurements of the system, which are sometimes unavailable. Therefore, measurement devices and/or dynamic estimators may be used to estimate these parameters. Furthermore, having mechanical and electrical components, wind turbines are known to operate in at least two time scales: the slow time scale, in which mechanical state variables evolve; and the fast time scale, in which electrical and electronic state variables evolve.

1.1 Wind Turbines Operating Regions

Based on wind speed, variable-speed wind turbines can operate within one of four possible regions, shown in Figure 1.2. In the first region (region I), there is no power generated, since wind speed is too low to turn on the turbine and generate energy. The minimum wind speed required to generate power is called cut-in speed and it is typically above $4\,[\text{m/s}]$. In region II, the generated electrical power increases as the wind speed rises above the cut-in speed until the power reaches its maximum value generated by the wind turbine that is called the rated power. In this region, the control objective is to maximize the extracted power by keeping the pitch angle constant while controlling the generator torque. This can be achieved by the torque–speed lookup table of the generator or the optimal relationship between generator's speed and torque; that is known as maximum power point tracking (MPPT) of the power coefficient function.

The main objectives of the controller design in region III are to regulate the generated power such that it does not exceed the rated output power of the WECS and to reduce fatigue load damages. For this purpose, blade pitch angle control can be used when wind speed goes above the rated speed in order to limit the rotational speed and/or the generated power to their rated values. The generator torque is kept constant in this case. Pitch control can be achieved collectively or individually through adjusting the angles of the blades. In collective pitch control (CPC), the blades are set simultaneously to the same angle, whereas, in the individual pitch control (IPC), the blades are set to different angles.
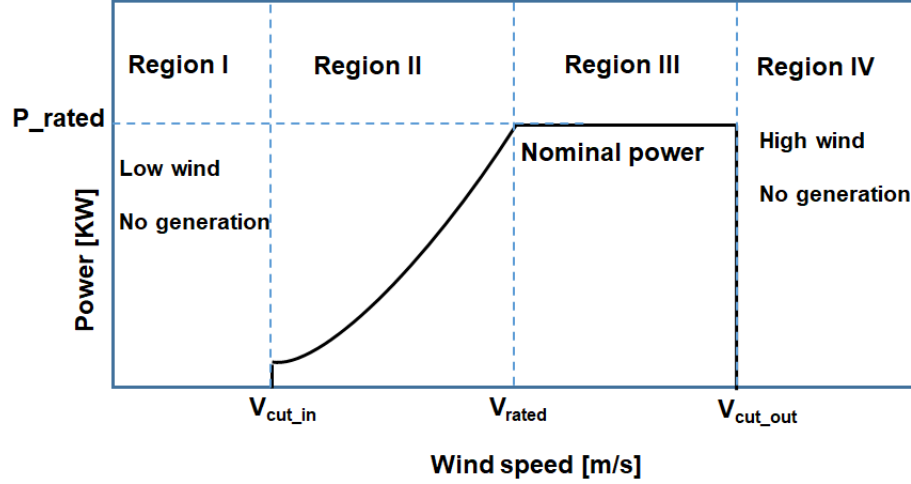
Figure 1.2: Operation regions of wind turbines

At very high wind speed (region IV), turbines are usually shut down at what is called the cut-off wind speed using a breaking system. It is not safe to turn on the wind turbines beyond the cut-off speed, since that might expose their electrical and mechanical parts to sever damages.

1.2 Research Objectives

In this thesis, we address three problems that are related to the control of WECS. First, we consider the problem of reducing the complexity of the power system model when a large number of WTGs is integrated to the power grid, with the objective of obtaining a simplified model that adequately simulates such systems. To address this problem, a small-signal and time-scale analyses-based investigation of the dynamic performance of WECS with DFIG connected to the utility grid was conducted. Furthermore, the order reduction methods that are based on balancing, i.e., balanced truncation and balanced residualization, and singular perturbations theory were compared based on their transient responses and linear-quadratic near-optimal control performance criteria. In order to enhance the modeling and control of wind farms when a large number of WTGs is integrated to the power grid, and to develop the corresponding simplified equivalent models, the controllability and observability of the WECS, over different forms of the input control matrix, are investigated through the application of the aforementioned

order reduction methods.

The second problem we consider here involves the design of an optimal controller for a DFIG-based WECS by decomposing the algebraic Riccati equation (ARE) of the singularly perturbed wind turbine system into two reduced-order AREs corresponding to the slow and fast time scales. This allows the design of independent linear controllers for the slow and fast subsystems, and avoids the corresponding ill-conditioning problem associated with singularly perturbed systems.

Inspired by the use of cross Gramians in reducing the order of wind farms of different sizes and the time-scale analysis of the singularly perturbed WECS system, the third objective constitutes in the development of a new recursive algorithm that solves the algebraic Sylvester equation, which defines the cross Gramian of singularly perturbed linear systems, while avoiding the ill-conditioning problem.

1.3 Thesis Structure and Contributions

This thesis is organized in the following manner.

In **Chapter 1**, a succinct overview of the main parts of the wind turbine and its operating regions were presented. The objectives, structure, and contributions of this thesis are also introduced.

Chapter 2 presents a theoretical background of the dynamics and modeling of the wind turbine and DFIG. The chapter further reviews the model order reduction methods based on balancing (balanced truncation and residualization) and singular perturbation theory. The state-space model of the wind turbine with DFIG connected to the utility grid presented in [9–11] is reduced using the aforementioned methods. The performances of the obtained reduced order systems are compared on the basis of their transient responses and linear-quadratic near-optimal control criteria. Simulation and comparisons were also conducted when wind turbulence and large-signal disturbance are applied to the system.

The main finding of this chapter is the advantage that the singular perturbation method has over the balancing methods, in terms of the accuracy in approximating

the dynamics of the considered system. The order of the considered wind turbine model is reduced from eight to six via the balancing transformation. Further reduction results in a significant jump in the error bound. In contrast, the method of singular perturbation shows that an order reduction to four, or even two, can still provide very good approximation to the system model. These results were published in [12].

In **Chapter 3**, the order reduction methods constituting in the balanced truncation, balanced residualization, and cross Gramian are applied to the state-space representations of wind farms consisting of different numbers of identical and non-identical one-mass wind turbines. The reduced order systems are compared to the original system based on step responses, maximum absolute, and mean errors.

Examining the controllability and observability of the system, in both the vector and diagonal forms of the input control matrix, showed a considerable loss of controllability and observability in the case of the latter form.

Chapter 4 utilizes the method of singular perturbation to design LQR, Kalman filter, and LQG optimal controllers in two independent time scales for a fifth-order single-cage DFIG wind turbine. The algebraic Riccati equation (ARE) of the singularly perturbed wind turbine system is decomposed into two reduced-order AREs, which correspond to the slow and fast time scales. The reduced-order systems are compared to the original full-order system to validate the performance of the proposed method when wind turbulence and large-signal disturbance are applied to the system. Using this method allows designing linear controllers for the slow and fast subsystems independently, thus, achieving complete separation and parallelism in the design process. The advantages of such an approach include the alleviation of stiffness difficulties and reduction of computational complexities and dimensionality burdens resulting from the increased penetration of wind turbines to the power grid.

A mathematical expression is derived to obtain the optimal regulator gains with respect to the optimal pure-slow and pure-fast, reduced-order Kalman filters and linear quadratic Gaussian (LQG) controllers. In addition, we show that the similarity transformation does not preserve the performance index value in the case of Kalman filter and the corresponding LQG controller. The results of this chapter were published

in [13]

In **Chapter 5**, a new recursive algorithm for solving the ill-defined algebraic Sylvester equation that defines the cross Gramian of singularly perturbed linear systems is developed. The solution is obtained in terms of the well-defined reduced-order algebraic Sylvester equations corresponding to the slow and fast subsystems of a singularly perturbed system. Several examples are solved to demonstrate the efficiency of the proposed algorithm. The algorithm was shown to be very accurate with a rate of convergence of $O(\epsilon)$. Furthermore, it can be directly applied to singularly perturbed systems in the explicit standard forms. If the considered system is in the implicit form, a similarity transformation is necessary to convert it into its explicit form before the utilization of the proposed algorithm. The results of this chapter were published in [14].

Chapter 6, summarizes the conclusions of our research and discusses the future work.

Chapter 2

Order Reduction via the Methods of System Balancing and Singular Perturbations

2.1 Introduction

Due to the increasing penetration of wind energy systems to the existing power systems, it has become necessary to reduce the complexity of the power system models, when large numbers of WTGs are integrated to the power grids, towards obtaining simplified models that adequately simulates such integrated systems. The goal of any order reduction method is obtaining a model with a lower order than the original one, while accurately representing the dynamic characteristics of the system. Rather than following a systematic approach for obtaining a low order model, studies have commonly neglected the transient stator dynamics [15]. For example, a DFIG model of a fifth-order was reduced to the third-order [16–18]. A simplified one-mass model was used in [19] with an algorithm that detects the stator voltage sequence components that bring the fault ride-through capability to the wind turbine connected to the grid. Using aggregation methods to reduce the order of wind farms, studies have followed two distinct approaches. The first approach applies to farms with identical WTGs and constitutes an aggregation of all WTGs into a single equivalent machine, with the size and rated and reactive powers re-scaled to incorporate the underlying multiplicity [20, 21]. The second approach aggregates each group of identical WTGs into an individual, re-scaled equivalent machine [22]. On the other hand, methods based on control theory use linearized state-space models for WTGs. To reduce the model order down to the most relevant modes, [23] uses selective modal analysis. Similar reduction was achieved in [24, 25] through the balance truncation (BT) method. Time-scale and singular perturbation analyses were used in [26–28] to reduce the order of the WECS model by

neglecting the fast modes of the system assuming that the fast states are stable and settle to steady-state values. The same techniques were used in [29–31] to reduce the order of the model and break it into slow and fast components, which are then separately controlled. Alternatively, [32] reduced the complexity of the DFIG model by evaluating the effect of the damping torque, contributed by the different dynamic components of DFIG, on the stability margin and the damping performance of the system. A hybrid approach, combining dominant pole-based modal analysis (DPMA) and BT with aggregation methods, was used in [33] to obtain an equivalent wind farm model.

There are few studies that compare different order reduction methods for wind turbine models. In this chapter, the order reduction methods of balanced truncation, balanced residualization, and singular perturbations are applied to a model of a wind turbine with DFIG that is connected to the utility grid. The linearized eighth-order state-space model presented in [9–11] is used here. The performance of the different model order reduction methods are compared on the basis of their transient responses and their linear-quadratic near-optimal control performance criteria.

The rest of the chapter is organized as follows. In Section 2.2, the wind turbine dynamics will be reviewed. Modeling and control of the DFIG is presented in Section 2.3 along with the state-space model of the considered WECS. Section 2.4 provides a theoretical background for the model order reduction using balancing methods: balanced truncation and residualization. In Section 2.5, the model of the wind turbine with DFIG connected to the utility grid is reduced using the aforementioned methods. In Section 2.6, the near-optimal controllers for the balanced truncation and residualization methods are derived and calculated. The singular perturbations method is used to reduce the wind turbine model in Section 2.7. Near-optimal control using lower-order slow subsystems is derived and the corresponding calculations are presented in Section 2.8. The performances of the reduced models of the considered WTG with DFIG are tested for wind turbulence and gust in Section 2.9 and for voltage sag in Section 2.10. The chapter is concluded in Section 2.11.

2.2   Wind Turbine Dynamics

Wind turbines convert the wind kinetic energy into mechanical energy that rotates the turbine blades. The mechanical energy is then converted into electrical energy by an electrical generator. The mechanical output power that is harvested from the wind is proportional to the third power of wind speed and can be expressed as [5]

$$P_m = \frac{1}{2}\rho\pi R^2 v^3 C_p(\lambda, \beta) \tag{2.1}$$

where ρ is the air density in $[Kg/m^3]$, R is the radius of the turbine in $[m]$, v is the wind speed $[m/s]$, $C_p(\lambda, \beta)$ is the power coefficient of the wind turbine that describes the efficiency of power extraction. C_p is a nonlinear function that depends on the blade pitch angle β and the tip speed ratio λ, which is given by

$$\lambda = \frac{R\omega_r}{v} \tag{2.2}$$

where ω_r is the rotor angular velocity. C_p is a measure for power performance of the wind turbine. Using the turbine characteristics, the latter can be approximated as:

$$C_p(\lambda, \beta) = C_1(\frac{C_2}{\lambda_i} - C_3\beta - C_4)e^{\frac{-C_5}{\lambda_i}} + C_6\lambda \tag{2.3}$$

where λ_i can be calculated approximately as follows

$$\frac{1}{\lambda_i} = \frac{1}{\lambda + 0.08\beta} - \frac{0.035}{\beta^3 + 1} \tag{2.4}$$

The coefficients $C_i, i = 1, 2, \ldots, 6$, depend on the turbine design characteristics and are given in Appendix A.1. The maximum mechanical power P_{opt} collected by the wind turbine is

$$P_{opt} = \rho\pi R^5 C_{p-opt}\omega_{opt}^3/2\lambda_{opt} = k_{opt}\omega_{opt}^3 \tag{2.5}$$

which requires maintaining λ at its optimum value λ_{opt} and the pitch angle at $\beta = 0$.

Figure 2.1 shows a typical wind turbine characteristics with the optimal power

extraction P_{opt}. As the wind speed varies, the controller plays the role of ensuring that the wind turbine follows the optimal power curve in Figure 2.1.(a).

In this chapter, the one-mass derive train model is considered since the derive train acts as a single equivalent mass with nearly equal participation of all inertias [15]. The total inertia constant H_t is the sum of the turbine rotor and generator inertia constants. The dynamic equation of this model can be expressed by the following differential equation

$$2H_t \frac{d\omega_r}{dt} = T_m - T_e \qquad (2.6)$$

where T_m is the mechanical torque and T_e is the electromechanical torques. The generator torque-speed characteristic is shown in Figure 2.1(b).
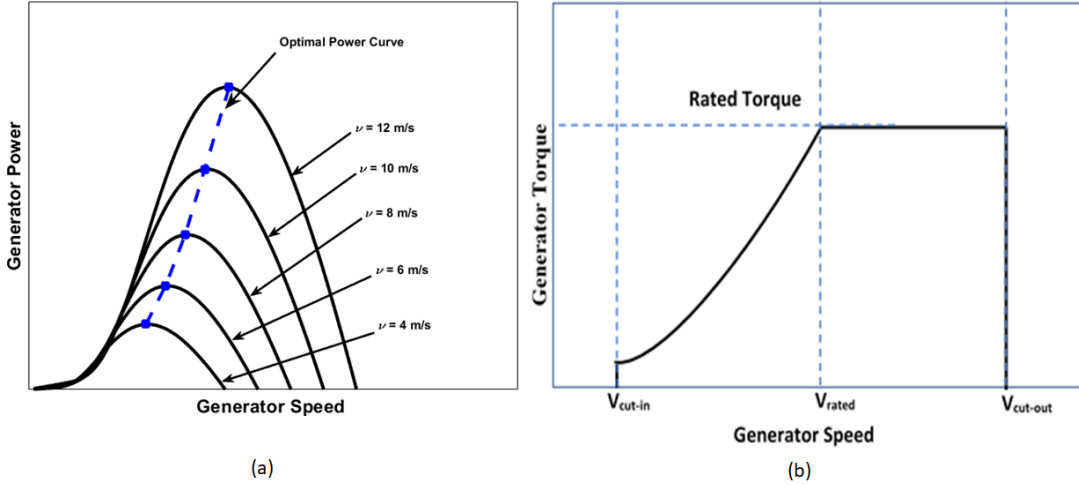
Figure 2.1: Maximum power extraction characteristic for wind turbines. (a) Optimal power-speed characteristics (b) Torque-speed characteristics

2.3 Modeling and Control of DFIG-based Wind Turbine

The variable speed wind turbine with double fed induction generator (DFIG) has gained wide spread attention in the last decade, due to the low cost of installation, ability to control its active and reactive power independently, low consumption of reactive power, and it inflicting less mechanical stress on turbines. The DFIG represents a wound rotor induction generator consisting of three phase rotor and stator windings, which are both connected to the utility grid, hence the term "double fed". It is connected from the

stator side directly to the utility grid, while the rotor side is interfaced to the utility via a back-to-back voltage source converter. The converter consists of grid-side converters (GSCs) and rotor-side converters (RSCs) placed back-to-back with a DC-link capacitor in between. A crowbar circuit is also used to protect the converter and the generator at high voltage situations by limiting the high current in the rotor circuit [34–36]. Figure 2.2 shows a typical configuration of a DFIG used with wind turbine energy systems.
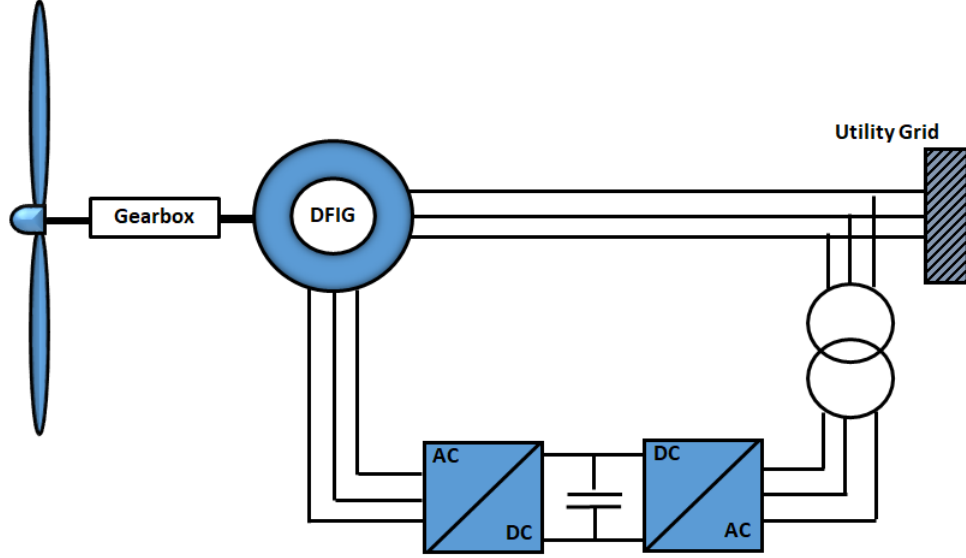
Figure 2.2: A typical configuration for a DFIG-based wind turbine.

In order to simplify the mathematical model analysis of the DFIG, the three-phase stator and rotor quantities (voltages, currents, and flux linkages) are placed in direct (d) and quadrature (q) axes to obtain two-phase dq quantities using the direct-quadrature-zero transformation ($dq0$). More details about the $dq0$ transformation can be found in Appendix B.1 [15].

The dynamic performance and small signal stability analysis of DFIG-based WECS have been investigated by many researchers [11, 35, 37–39]. In this section, we study the linearized state-space model of the DFIG-based WECS presented in [9–11], which was developed by considering the following assumptions:

- All equations of the induction generator are derived in the synchronous reference frame using the direct-quadrature (d-q) transformation.

- The d-axis is assumed to be 90° lagging the q-axis.

- The stator current is assumed to be negative when flowing toward the machine.

The dq synchronous reference frame equations of the stator flux and rotor may be written as [9, 10].

$$
\begin{aligned}
\psi_{ds} &= L_s i_{ds} + L_m i_{dr} \\
\psi_{qs} &= L_s i_{qs} + L_m i_{qr} \\
\psi_{dr} &= L_r i_{dr} + L_m i_{ds} \\
\psi_{qr} &= L_r i_{qr} + L_m i_{qs}
\end{aligned}
\tag{2.7}
$$

where L_s, L_r, and L_m are stator, rotor, and self magnetizing reactances, respectively. L_s and L_r are defined by the following equations

$$
\begin{aligned}
L_s &= L_{ls} + L_m \\
L_r &= L_{lr} + L_m
\end{aligned}
\tag{2.8}
$$

Furthermore, the reactances can be written in terms of inductances as follows [40]

$$
X_{ss} = \omega_s(L_{ls} + \frac{3}{2}L_m) \tag{2.9}
$$

$$
X_{rr} = \omega_r(L_{lr} + \frac{3}{2}L_m) \tag{2.10}
$$

$$
X_m = \frac{3}{2}\omega_s L_m \tag{2.11}
$$

where X_{ss}, X_{rr}, and X_m are stator, rotor, and self magnetizing reactances, respectively. The equivalent circuit for one phase of the DFIG generator can be drawn as in Figure 2.3

The stator and rotor voltage equations in d-q synchronous reference frame are given,
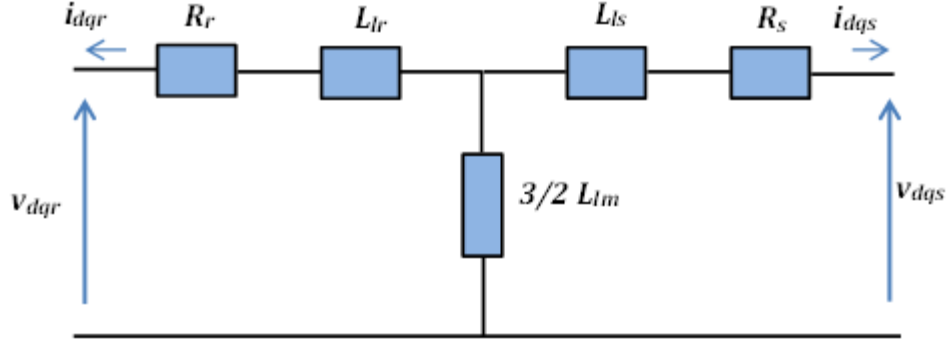
Figure 2.3: DFIG equivalent circuit

respectively by

$$\begin{bmatrix} v_{ds} \\ v_{qs} \end{bmatrix} = -R_s \begin{bmatrix} i_{ds} \\ i_{qs} \end{bmatrix} + \omega_s \begin{bmatrix} -\psi_{qs} \\ \psi_{ds} \end{bmatrix} + \frac{1}{\omega_b} \frac{d}{dt} \begin{bmatrix} \psi_{ds} \\ \psi_{qs} \end{bmatrix} \tag{2.12}$$

$$\begin{bmatrix} v_{dr} \\ v_{qr} \end{bmatrix} = R_r \begin{bmatrix} i_{dr} \\ i_{qr} \end{bmatrix} + s\omega_s \begin{bmatrix} -\psi_{qr} \\ \psi_{dr} \end{bmatrix} + \frac{1}{\omega_b} \frac{d}{dt} \begin{bmatrix} \psi_{dr} \\ \psi_{qr} \end{bmatrix} \tag{2.13}$$

where the subscripts s and r denote the stator and rotor quantities while subscripts q and d denote the components aligned with the q-axis and d-axis reference frames, respectively. In (2.12)-(2.13), R_s and R_r are the stator and rotor resistances, respectively, and ω_s and ω_b are synchronous and base angular frequencies, respectively. s is defined as the slip of the generator and given by $s = (\omega_s - \omega_r)/\omega_s$. The electromechanical torque is given in terms of state variables as follows

$$T_e = L_m(i_{dr}i_{qs} - i_{qr}i_{ds}) \tag{2.14}$$

The electromagnetic torque should be adjusted dynamically to follow wind speed variations and derive the rotor speed of the WTG, so that the system can reach the required operating reference point and extract maximum power from the wind [41]. It is a common practice in stability transient studies of power systems to neglect the stator transients for the fifth-order model of induction generator, as it is much faster

than those of other components [16, 18]. Furthermore, the stator resistance can also be neglected since it is assumed to have a small value ($R_s \approx 0$) [15, 40]. In the q-axis, rotor current $i_{qr,ref}$ is calculated using reference torque values generated by the wind turbine characteristic for maximum power extraction (Figure 2.1(b)) and given by

$$i_{qr,ref} = \frac{\omega_s X_{ss}}{X_m v_{qs}} T_{sp} \tag{2.15}$$

where T_{sp} is the optimal torque set point provided from the torque-speed characteristic for maximum power extraction [10], and $i_{qr,ref}$ is the reference current in the q-axis.

Modeling and control of DFIG-based wind systems are complicated compared to other induction generators. A dominating feature of these systems is having a set of poorly damped eigenvalues with a corresponding natural frequency near the line frequency. Furthermore, the DFIG-based WTG system is sensitive to any grid disturbances, which may lead to system instability at certain operating conditions [39]. The conventional vector control (VC) [42–44] has been widely used in controlling the DFIG-based WECS. Current mode vector control referred to as the $PVdq$ control [5,10,11,44], is adopted in this chapter. This technique enables the independent control of the decoupled active and reactive powers by decomposing the rotor current into two orthogonal components: one, along the d-axis, for regulating the terminal voltage or power factor (PF); whereas the other, along the q-axes, for regulating the torque. For optimal control, proportional and integral (PI) controllers, with parameters accordingly tuned, are commonly used. Such tuning puts these controllers at a disadvantage, though, as it is dependent on the parameters of the system, such as the stator and rotor resistances, inductances, and mutual inductances, in addition to requiring the stability of the system to be sustained even during transient states [45]. Figure 2.4 shows a block diagram of torque control scheme. The complete control scheme was presented in [5, 10, 11].

The error signal produced by the difference in the rotor current i_{qr} from $i_{qr,ref}$ is processed by the PI compensator to produce the rotor voltage v'_{qr}.

$$v'_{qr} = x_1 + K_{p1}(i_{qr,ref} - i_{qr}) \tag{2.16}$$
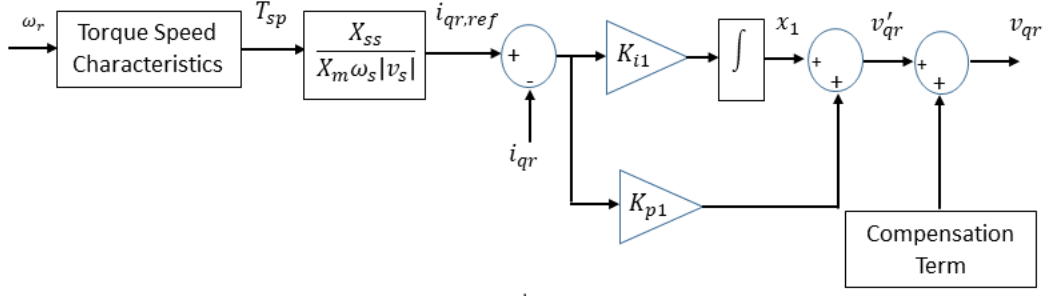
Figure 2.4: PVdq DFIG speed control strategy.

Note that, the compensation term in this control scheme is given by the second and third terms of (2.16). On the other hand, the terminal voltage or power factor control is achieved using the rotor-side converter. The required $d-$axis rotor voltage v_{dr} is obtained through the output of a PI controller and a compensation term which is derived from equation of the rotor voltage in the d-axis. Figure 2.5 shows a block diagram of the terminal voltage control scheme $[5, 10, 11]$
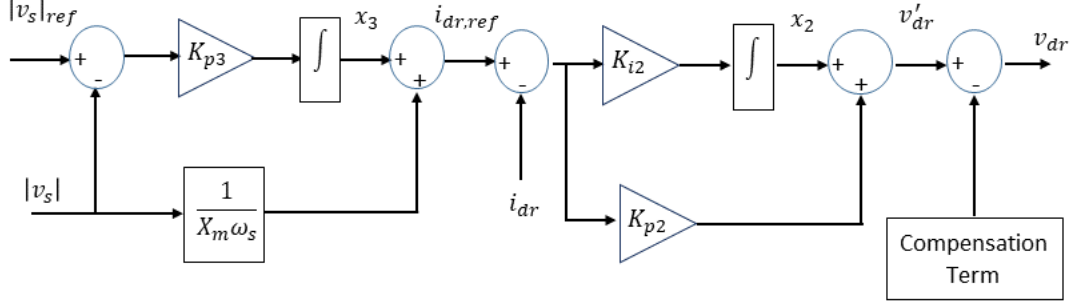
Figure 2.5: PVdq DFIG terminal voltage or power factor control strategy.

In order to simplify the model of the system and to design suitable linear controllers, a linearization process is performed. The behavior of nonlinear system is approximated in the vicinity of its equilibrium points. Small signal analysis can be performed by linearizing the swing mechanical equation (2.6) and the DFIG equations (2.12)-(2.13).

The utility grid is considered, here, an infinite bus, which is represented by a voltage source with constant voltage and frequency. Considering that DFIG is interfaced with the infinite bus through a transmission line, the stator voltage equations can be

rewritten as

$$v_{ds} = v_{q\infty} - X_T i_{qs} + R_T i_{ds} \tag{2.17}$$

$$v_{qs} = v_{d\infty} + X_T i_{ds} + R_T i_{qs} \tag{2.18}$$

where $v_{q\infty}$ and $v_{d\infty}$ are the infinite bus voltages in the q and d reference frames, and $X_T = X_{tr} + X_e$, $R_T = R_e + R_s$

To obtain the complete linearized DFIG model, the state variables and the inputs of the control loops in Figure 2.4 and Figure 2.5 are integrated to the DFIG model and linearized at the operating points. The linearized state space system is given as follows

$$\dot{x}(t) = Ax(t) + Bu(t)$$
$$y(t) = Cx(t) + Du(t) \tag{2.19}$$

The state variables and the control inputs are defined by [11]

$$\dot{x} = \begin{bmatrix} i_{ds} & i_{qs} & i_{dr} & i_{qr} & \omega_r & x_2 & x_1 & x_3 \end{bmatrix}^T \tag{2.20}$$

$$u = \begin{bmatrix} i_{dr} & i_{qr} & v_s & v_{sref} & T_{sp} \end{bmatrix}^T \tag{2.21}$$

The outputs are the rotor currents in the d-axis and q-axis,

$$y = \begin{bmatrix} i_{dr} & i_{qr} \end{bmatrix}^T, \tag{2.22}$$

The system matrices A, B, and C of the wind turbine with DFIG connected to the utility grid are calculated as described in Appendix A.3. All system parameters, DFIG parameters, and operating points used in the linearization procedure can be found in Appendices A.1-A.2. The linearized system and matrices A, B, and C evaluated at the

system's operating points are given by

$$
A = \begin{bmatrix}
-25.17 & 5717 & -89.73 & -5241 & -212.5 & 1617 & 0 & 80.85 \\
-5711 & -27.88 & 5242 & -89.73 & 1646 & 0 & 1617 & 0 \\
-24.38 & 5222.5 & -91.82 & -5050 & -217.4 & 1655 & 0 & 82.74 \\
-5517 & -27.16 & 5050 & -91.82 & 1726 & 0 & 1655 & 0 \\
0.2072 & -0.1225 & -0.1937 & -0.01976 & 0 & 0 & 0 & 0 \\
0.4377 & 0.07021 & -10 & 0 & 0 & 0 & 0 & 10 \\
0.6349 & 0.1018 & 0 & -10 & 9.171 & 0 & 0 & 0 \\
-1.211 & 0.1943 & 0 & 0 & 0 & 0 & 0 & 0
\end{bmatrix}
$$

$$
B = \begin{bmatrix}
-1658 & 0 & 1617 & 0 & 0 \\
0 & -1658 & 0 & 1617 & 0 \\
-1617 & 0 & 1655 & 0 & 0 \\
0 & -1617 & 0 & 1655 & 0 \\
0 & 0 & 0 & 0 & 0.1429 \\
-10 & 0 & -67.47 & 70 & 0 \\
0 & -10 & -8.256 & 0 & 10.24 \\
0 & 0 & -7 & 7 & 0
\end{bmatrix},
$$

$$
C = \begin{bmatrix}
0 & 0 & 1 & 0 & 0 & 0 & 0 & 0 \\
0 & 0 & 0 & 1 & 0 & 0 & 0 & 0
\end{bmatrix}, \quad
D = \begin{bmatrix}
0 & 0 & 0 & 0 & 0 \\
0 & 0 & 0 & 0 & 0
\end{bmatrix}
$$

In the follow-up of this section we will study the DFIG linearized model using the methods of system balancing and singular perturbations.

2.4   Model Order Reduction via System Balancing Methods

Consider the state space realization of an nth-order linear time invariant (LTI) system

$$\dot{x}(t) = Ax(t) + Bu(t)$$
$$y(t) = Cx(t) + Du(t)$$

(2.23)

where $x(t) \in \Re^n$, $u(t) \in \Re^m$, $y(t) \in \Re^p$.

A, B, C and D are constant matrices of appropriate dimensions. The open loop transfer function of the system is given by

$$G(s) = C(sI - A)^{-1}B + D$$

(2.24)

Balancing order reduction is done under the following assumption [46].

Assumption 2.1 *The considered system is controllable, observable, and asymptotically stable.*

The linear time-invariant system is asymptotically stable if all eigenvalues of the system matrix are strictly in the left half of the complex plane, that is, $\Re\{\text{eig}(A)\} < 0$. The controllability and observability Gramians are used to measure the degree of controllability and observability of the system. They are defined respectively as

$$W_C = \int_0^\infty e^{At} BB^T e^{A^T t}\, \mathrm{d}t, \quad W_O = \int_0^\infty e^{A^T t} C^T C e^{At}\, \mathrm{d}t$$

(2.25)

The system is considered to be controllable (observable) if the corresponding Gramian matrix is nonsingular. The integrals (2.25) can be evaluated by solving the corresponding Lyapunov algebraic equations, which are respectively given by

$$AW_C + W_C A^T = -BB^T$$

(2.26)

$$A^T W_O + W_O A = -C^T C$$

(2.27)

Since the system matrix A is Hurwitz (asymptotically stable), the Gramians are positive semidefinite (symmetric) matrices and therefore the eigenvalues of the Gramians matrices are all real and non-negative [47].

It is well known from the Kalman canonical decomposition that state variables that are either uncontrollable or unobservable (their controllability/observability measures are zeros and the corresponding Gramian matrices are singular) can be completely eliminated from the system dynamics since they do not affect the system transfer function, and hence they have no impact on the system input-output behavior. This implies a reduced-order model of a full-order model. The balancing order reduction is an extension of the Kalman canonical decomposition in the case when all system state variables are both controllable and observable, but some of them are weakly controllable and weakly observable corresponding to small eigenvalues of the controllability and observability Gramians. There are several order reduction techniques. The two most popular ones will be reviewed in the rest of this section. Important features of the system balancing order reduction techniques are that the reduced-order models obtained are asymptotically stable, controllable, and observable, and that they can be used for accurate and efficient full-order system controller design techniques [48].

The state space variables $x(t)$ that are associated with small eigenvalues of the Gramians matrices are less controllable and less observable than those associated with larger ones. Therefore, these state variables can be eliminated from the system model without much effect on the system dynamics. This elimination can be achieved using the balanced transformation technique [48]. System balancing is done via the use of a similarity transformation matrix T that transforms the coordinates of the original system into balanced coordinates, such that the controllability and observability Gramians are identical and diagonal, that is, the transformation

$$x_b = T^{-1}x(t), \quad det(T) \neq 0 \tag{2.28}$$

produces a new linear system

$$\dot{x}_b(t) = A_b x_b(t) + B_b u(t), \quad x_b(0) = T^{-1}x(0) = T^{-1}x_0$$
$$y_b(t) = C_b x_b(t) + D_b u(t) \tag{2.29}$$
$$A_b = TAT^{-1}, \quad B_b = TB, \quad C_b = CT^{-1}, \quad D_b = D$$

with

$$W_{C_b} = W_{O_b} = \Sigma = \text{diag}\{\sigma_1, \sigma_2, \ldots, \sigma_n\} \tag{2.30}$$

$$\sigma_1 \geq \sigma_2 \geq, \ldots, \geq \sigma_n$$

where σ_i, $i = 1, 2, \ldots, n$ are known as the Hankel Singular Values (HSVs) of the system, obtained by taking the positive square root of the eigenvalues of the product of the controllability and observability Gramians matrices [48], that is

$$\sigma_i = \sqrt{\lambda_i(W_C W_O)} \tag{2.31}$$

The magnitudes of the HSVs are ordered in descending order with the first Hankel singular value called the "Hankel norm". The Hankel norm of the system represented by $G(s)$ is defined by

$$\|G(s)\|_H = \sigma_1 = \sigma_{max} = \sqrt{\lambda_{max}(W_C W_O)} \tag{2.32}$$

These HSVs can be used to indicate the amount of energy in each state in the original system. The HSVs with larger magnitudes refer to the states that have more energy and are more controllable and observable in the original system. The balanced controllability and observability Gramians are the unique solutions of the following algebraic Lyapunov equations

$$A_b W_{C_b} + W_{C_b} A_b^T + B_b B_b^T = 0,$$
$$A_b^T W_{O_b} + W_{O_b} A_b + C_b^T C_b = 0 \tag{2.33}$$
$$W_{C_b} = W_{O_b} = \Sigma$$

The balanced system can be partitioned as following

$$A_b = \begin{bmatrix} A_1 & A_2 \\ A_3 & A_4 \end{bmatrix}, \quad B_b = \begin{bmatrix} B_1 \\ B_2 \end{bmatrix}, \quad C_b = \begin{bmatrix} C_1 & C_2 \end{bmatrix}, \quad D_b = D$$

$$\Sigma = \begin{bmatrix} \Sigma_1 & 0 \\ 0 & \Sigma_2 \end{bmatrix}$$

$$\Sigma_1 = diag\{\sigma_1, \sigma_2, \ldots, \sigma_r\}, \quad \Sigma_2 = diag\{\sigma_{r+1}, \sigma_{r+2}, \ldots, \sigma_n\}$$

$$(2.34)$$

2.4.1   Model Order Reduction via Balanced Truncation

Based on this partitioning, the reduced-order system obtained via truncation is defined by

$$\dot{x}_1(t) = A_1 x_1(t) + B_1 u(t)$$
$$y(t) = C_1 x_1(t) + D u(t) \tag{2.35}$$

with the corresponding reduced-order transfer function

$$G_r(s) = C_1(sI - A_1)^{-1}B_1 + D \tag{2.36}$$

It has been shown in [49] that

$$\|G(s) - G_r(s)\| \le \sigma_{r+1}^2, \sigma_{r+2}^2, \ldots, \sigma_n^2 \tag{2.37}$$

The reduced-order system can be simply obtained by eliminating the part of the system associated with the small HSVs and retaining the remaining part of the system, which is associated with the larger HSVs.

2.4.2   Model Order Reduction via Balanced Residualization

Reducing the system order using the balanced truncation method gives a very good approximation for the original system at high frequencies. The negligible values of

the impulse response error for the original and approximated system show just that. However, the approximation will be less accurate at low and medium frequencies, due to the DC gain difference between the original system and the reduced order truncated system. Comparing step responses of the original and the reduced-order system, a relatively large error can be observed. In [48], the balanced residualization technique was proposed to overtake this problem. To explain this technique, consider the following balanced linear system

$$
\begin{aligned}
\dot{x}_1(t) &= A_1 x_1(t) + A_2 x_2(t) + B_1 u(t) \\
\dot{x}_2(t) &= A_3 x_1(t) + A_4 x_2(t) + B_2 u(t) \\
y(t) &= C_1 x_1(t) + C_2 x_2(t) + D u(t)
\end{aligned}
\tag{2.38}
$$

where $A_1 \in \Re^{r \times r}$, $A_4 \in \Re^{(n-r) \times (n-r)}$ with the remaining matrices having appropriate dimensions relative to the original system dimensions. It is assumed that the Hankel singular values of this balanced system satisfy $\sigma_r \gg \sigma_{r+1}$. A quasi steady state system can be defined by setting the derivative of $x_2(t)$ state variable to zero as follows

$$
\begin{aligned}
\dot{x}_1(t) &= A_1 x_1(t) + A_2 x_2(t) + B_1 u(t) \\
0 &= A_3 x_1(t) + A_4 x_2(t) + B_2 u(t) \\
y(t) &= C_1 x_1(t) + C_2 x_2(t) + D u(t)
\end{aligned}
\tag{2.39}
$$

Note that, the matrix A_4 is assumed to be invertible [49]. Eliminating $x_2(t)$ from the second equation in (2.39), the residualized, reduced-order system is obtained as [50]

$$
\begin{aligned}
\dot{x}_r(t) &= A_r x_r(t) + B_r u(t) \\
y(t) &= C_r x_r(t) + D_r u(t) \\
A_r &= A_1 - A_2 A_4^{-1} A_3, \quad B_r = B_1 - A_2 A_4^{-1} B_2 \\
C_r &= C_1 - C_2 A_4^{-1} A_3, \quad D_r = D - C_2 A_4^{-1} B_2
\end{aligned}
\tag{2.40}
$$

The residualized reduced-order system preserves the DC gain of the original system.

It also provides a good approximation to the frequency spectrum at low and medium frequencies. However, this method provides less accurate approximation to the frequency spectrum at high frequencies [51], [50]. In contrast to that, the reduced-order system obtained through the balanced truncation method provides a good approximation at high frequencies on the expense of a mismatched DC gain.

2.5   Wind Turbine Model Order Reduction using Balancing Methods

The balanced truncation method requires first to balance the system. The Hankel singular values are then calculated and presented in the following table.

HSVs	20.8363	19.9418	14.3674	12.6774	12.0217	11.3983	0.9975	0.4742

Table 2.1: HSVs for wind turbine with DFIG system

It can be observed that the first six HSVs are much larger than the last two HSVs, hence, the system can be reduced to the sixth-order ($r = 6$) since

$$\| G(s) - G_6(s) \| \leq \sigma_7^2 + \sigma_8^2 = (0.9976)^2 + (0.4742)^2 = 1.220$$

produces a small error. Otherwise, according to the error formula a reduction to order five or less will produce huge errors. For example, for $r = 5$, we have

$$\| G(s) - G_5(s) \| \leq \sigma_6^2 + \sigma_7^2 + \sigma_8^2 = (11.4146)^2 + (0.9976)^2 + (0.4742)^2 = 131.51$$

For $r = 4, 3, 2$, this error becomes considerably bigger.

The step responses of the reduced truncation, residualization, and original systems are shown in Figure 2.6 for the rotor current output in the d-axis i_{dr} only, when $r = 6$. The step response behavior for the rotor current output in the q-axis i_{qr} is similar. It can be observed from Figure 2.6 that reducing the system order using balanced truncation method gives a good approximation for the original system at high frequencies. However, using the balanced residualization method shows better approximation to the original system at low and medium frequencies and preserve the DC gain.

Reducing the system to a second-order, $r = 2$, the step response error increases considerably comparing to the sixth-order system case. The step responses of the original and second-order reduced systems are shown in Figure 2.7.

It can be concluded from this section that the *balancing transformation order reduction method allows the considered system model of order eighth to be reduced only to order six.*
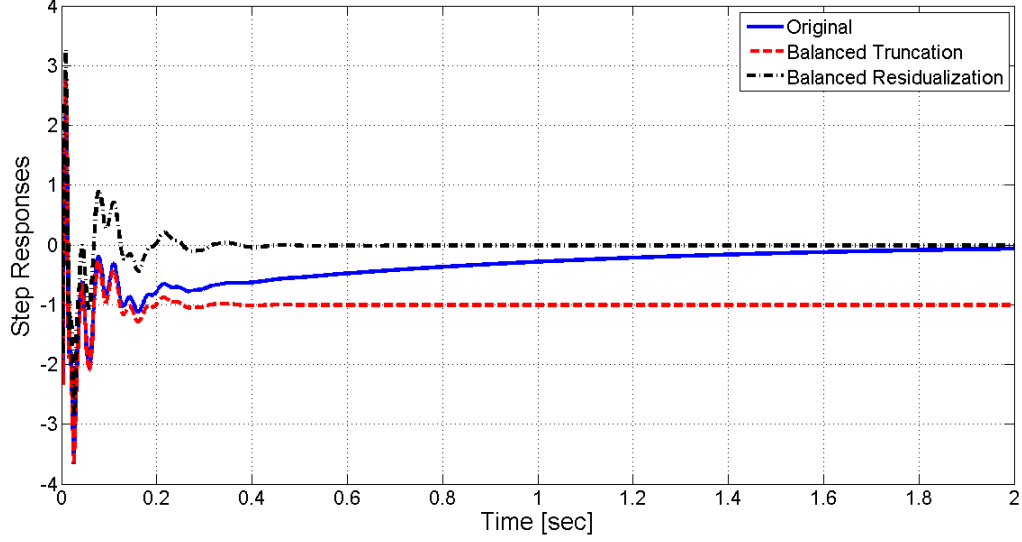
Figure 2.6: Step response of the sixth-order wind turbine with DFIG system
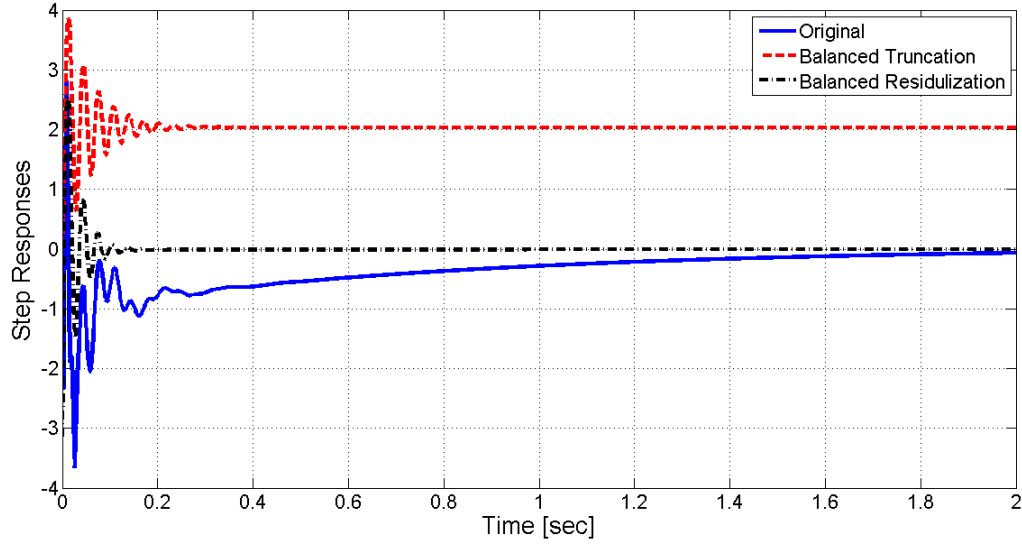
Figure 2.7: Step response of the second-order wind turbine with DFIG system

2.6 Near-optimal Control using the Reduced Order Truncated and Residualized Models

Consider the original system in the balanced coordinates defined by (2.29) and (2.39). The corresponding truncated system is given in (2.35) and the residualized system by (2.40). In the following, we use these reduced-order models to derive the near-optimal controllers for (2.34) obtained by minimizing a quadratic performance criterion defined by

$$
J_b = \frac{1}{2} \int_0^\infty \left[x_b^T(t) C_b^T C_b x_b(t) + u^T(t) R u(t) \right] dt = \frac{1}{2} \int_0^\infty \left\{ \begin{bmatrix} x_1(t) \\ x_2(t) \end{bmatrix}^T \begin{bmatrix} C_1^T C_1 & C_1^T C_2 \\ C_2^T C_1 & C_2^T C_2 \end{bmatrix} \right.
$$
$$
\left. \begin{bmatrix} x_1(t) \\ x_2(t) \end{bmatrix} + u^T(t) R u(t) \right\} dt
$$

(2.41)

where $C_b^T C_b \geq 0$ and $R > 0$ are the penalty matrices. We assume that the matrix D appearing in the system output is zero, that is, $D = 0$, so that in the performance criterion (2.41), we practically optimize the term $y^T(t)y(t)$, in addition to the "square" of the control signal.

2.6.1 Truncated Model Based Near-optimal Control

In this case, since the matrix C_2 is neglected in the truncated model (2.35), the quadratic performance criterion (2.41) changes into

$$
J_{trunc} = \frac{1}{2} \int_0^\infty \left[x_1^T(t) C_1^T C_1 x_1(t) + u^T(t) R u(t) \right] dt \tag{2.42}
$$

Minimizing (2.42) along the trajectories of the truncated system (2.35), that is

$$
\dot{x}_1(t) = A_1 x_1(t) + B_1 u(t)
$$
$$
y(t) = C_1 x_1(t)
$$

(2.43)

leads to the well-known optimal solution for the truncated system given by

$$u_{trunc}^{opt}(t) = -R^{-1}B_1^T P_{trunc}x_1(t) = -F_{trunc}^{opt}x_1(t) \tag{2.44}$$

where P_{trunc} satisfies the algebraic Riccati equation for the truncated system corresponding to the optimization problem defined by (2.42)-(2.43)

$$A_1 P_{trunc} + P_{trunc}A_1^T + C_1^T C_1 - P_{trunc}B_1 R^{-1}B_1^T P_{trunc} = 0 \tag{2.45}$$

Using (2.44), we construct the near-optimal full-state feedback control for the original full-order system (with $D = 0$) in the balanced coordinates

$$\dot{x}_b(t) = A_b x_b(t) + B_b u_b(t) \tag{2.46}$$

as follows

$$u_{trunc}^{subopt}(t) = -F_{trunc}^{opt}x_1(t) = -\begin{bmatrix} F_{trunc}^{opt} & 0 \end{bmatrix}\begin{bmatrix} x_1(t) \\ x_2(t) \end{bmatrix} = -F_{trunc}x_b(t) \tag{2.47}$$

using this near-optimal control (2.44) in (2.46), produces

$$\dot{x}_b(t) = (A - BF_{trunc})x_b(t) \tag{2.48}$$

$$J_b^{trunc} = \frac{1}{2}\int_0^\infty x_b^T(t)(C_b^T C_b + F_{trunc}^T R F_{trunc})x_b(t)dt \tag{2.49}$$

It can be shown that integral (2.49), evaluated along trajectories of (2.48), is given by

$$J_b^{trunc} = \frac{1}{2}x_b^T(0)V_b^{trunc}x_b(0), \quad x_b(0) = T^{-1}x(0) = T^{-1}x_0 \tag{2.50}$$

where V_b satisfies the following algebraic Lyapunov equation

$$(A_b - B_b F_{trunc})V_b^{trunc} + V_b^{trunc}(A_b - B_b F_{trunc})^T + C_b^T C_b - F_{trunc}^T R F_{trunc} = 0 \tag{2.51}$$

2.6.2   Residualized Model Based Near-optimal Control

Eliminating $x_2(t)$ from the quadratic performance criterion (2.41) using the second formula in (2.39), coming from the residualization idea, that is

$$x_2(t) = -A_4^{-1}(A_3 x_1(t) + B_2 u(t)) \tag{2.52}$$

the quadratic performance criterion becomes

$$J_b^{res} = \frac{1}{2} \int_0^\infty [x_r^T(t) C_r^T C_r x_r(t) + 2u^T(t) C_r^T D_r x_r(t) + u^T(t) R_r u(t)] dt \tag{2.53}$$

where $R_r = R + D_r^T D_r$ and with C_r, D_r are defined in (2.40). The residualized system is given as

$$\dot{x}_r(t) = A_r x_r(t) + B_r u(t) \tag{2.54}$$

Minimization of (2.53) subject to (2.54) leads to the following optimal control

$$u_{res}^{opt}(t) = -R_r^{-1}(C_r^T D_r + B_r^T P_{res}) x_r(t) = -F_{res} x_r(t) \tag{2.55}$$

where P_{res} satisfies the following algebraic equation, obtained through the linear-quadratic optimization when the quadratic performance criterion contains a cross-product term [52]

$$(A_r - B_r R_r^{-1} C_r^T D_r) P_{res} + P_{res}(A_r - B_r R_r^{-1} C_r^T D_r)^T + C_r^T(I - D_r R_r^{-1} D_r^T) C_r$$
$$- P_{res} B_r R_r^{-1} B_r^T P_{res} = 0 \tag{2.56}$$

The near-optimal control for obtained via balancing residualization, to be implemented to the original full-order system in the balanced coordinates can be now constructed as

$$u_{res}^{subopt}(t) = -F_{res}^{opt} x_1(t) = - \begin{bmatrix} F_{res}^{opt} & 0 \end{bmatrix} \begin{bmatrix} x_1(t) \\ x_2(t) \end{bmatrix} = -F_{res} x_b(t) \tag{2.57}$$

Using this near-optimal control (2.55) in (2.46), produces

$$\dot{x}_b(t) = (A - BF_{res})x_b(t) \tag{2.58}$$

$$J_b^{res} = \frac{1}{2}\int_0^\infty x_b^T(t)(C_b^T C_b + F_{res}^T R F_{res})x_b(t)dt \tag{2.59}$$

It can be shown that integral (2.59), evaluated along trajectories of (2.58), is given by

$$J_b^{res} = \frac{1}{2}x_b^T(0)V_b^{res}x_b(0) \tag{2.60}$$

where V_b^{res} satisfies the following algebraic Lyapunov equation

$$(A_b - B_bF_{res})^T V_b^{res} + V_b^{res}(A_b - B_bF_{res}) + C_b^T C_b + F_{res}^T R F_{res} = 0 \tag{2.61}$$

Note that the similarity transformation does not change the value of the optimal performance criterion [53], so that its optimal value in the original coordinates is equal to the optimal value in the balance coordinates, that is $J^{opt} = J_b^{opt}$. We compared $J_b^{opt}, J_b^{res}, J_b^{trunc}$. The truncated and residualized systems are of the order six, $r = 6$. The results are presented in Table 2.2.

Performance Criterion	Near-optimal/Optimal Value
J_b^{res}	2.0456
J_b^{trunc}	1.8697
J_b^{opt}	0.7390

Table 2.2: Near-optimal and optimal values of the performance criterion for balancing techniques

It can be seen from Table 2.2, that both the truncation and balancing residualization methods produce large errors ($> 100\%$) when the optimal linear-quadratic controller is considered. Moreover, those errors were obtained when the original system model of order eighth is reduced only to order six. It will be seen in the follow-up of this chapter that the singular perturbation method order reduction produces much better results

than the corresponding balancing order reduction techniques when the system order is reduced to six and even to four.

2.7 Wind Turbine Model Order Reduction using Singular Perturbation Method

Wind turbines with DFIG can be studied as singularly perturbed systems (two-time scale systems), since they contain mechanical and electrical elements that operate in different timescales, with mechanical variables in general being slow and electrical variables in general being fast. This can be observed by finding the eigenvalues of matrix A and checking whether they are located in two or several disjoint groups (clusters) which is caused by the presence of a small singular perturbation parameter denoted by ϵ.

The exact decoupling of the slow and fast subsystems can be obtained by employing the Chang transformation [54]. A standard singularly perturbed linear time invariant system in state-space form is represented by

$$
\begin{aligned}
\dot{x}_1(t) &= A_1 x_1(t) + A_2 x_2(t) + B_1 u(t) \\
\epsilon \dot{x}_2(t) &= A_3 x_1(t) + A_4 x_2(t) + B_2 u(t) \quad \Leftrightarrow \dot{x}_{SP}(t) = A_{SP} x_{SP}(t) + B_{SP} u(t), \quad x(0) = x_0 \\
y(t) &= C_1 x_1(t) + C_2 x_2(t) + D u(t) \quad \Leftrightarrow y(t) = C_{SP} x_{SP}(t) + D_{SP} u(t)
\end{aligned}
\tag{2.62}
$$

where ϵ is a small singular perturbation parameter. Here, $x_1(t)$ and $x_2(t)$ can be considered as the slow and fast state space variables of the system, respectively [48].

The slow and fast subsystems can be approximately decoupled using another method. For sufficiently small ϵ, setting $\epsilon = 0$ in the second equation of (2.62) produces the approximate reduced-order slow subsystem given

$$\dot{x}_{1sappr}(t) = A_0 x_{1sappr}(t) + B_0 u(t)$$

$$y_{appr}(t) = C_0 x_{1sappr}(t) + D_0 u(t)$$

$$A_0 = A_1 - A_2 A_4^{-1} A_3, \qquad B_0 = B_1 - A_2 A_4^{-1} B_2$$

$$C_0 = C_1 - C_2 A_4^{-1} A_3, \qquad D_0 = D - C_2 A_4^{-1} B_2$$

$$(2.63)$$

The following assumption is commonly imposed for singularly perturbed linear systems [55].

Assumption 2.2 *Matrix A_4 is invertible.*

The considered DFIG turbine system is not in the explicit standard singular perturbation form (2.62) in which the derivatives of some of the states are multiplied by a small positive singular perturbation parameter ϵ. The eigenvalues of this system can be calculated as

$$\lambda_i = \begin{bmatrix} -85.3933 \pm 530.1511i \\ -20.4084 \pm 184.6632i \\ -11.8777 \pm 51.0489i \\ -0.1514 \\ -1.1916 \end{bmatrix}, \qquad (2.64)$$

Their locations in the s-plane are shown in Figure 2.8. The three cases are considered here, depending on the dimension of the system order reduction: **Case 1**: when the system is reduced to order two; **Case 2**: when the system is reduced to order four; and **Case 3**: when the system is reduced to order six.

In all these three cases, the rows of matrix A need to be rearranged such that the corresponding sub-matrix A_4 is nonsingular and the system is in the explicit standard singular perturbation form (2.62). As described in [56], such systems can be obtained via the use of the Schur transformation. Algebraically [57], for any given square matrix there exists a unitary similarity transformation known as the Schur's form, , where

$$A_{Schur} = U^T A U, \quad U^T = U^{-1} \qquad (2.65)$$
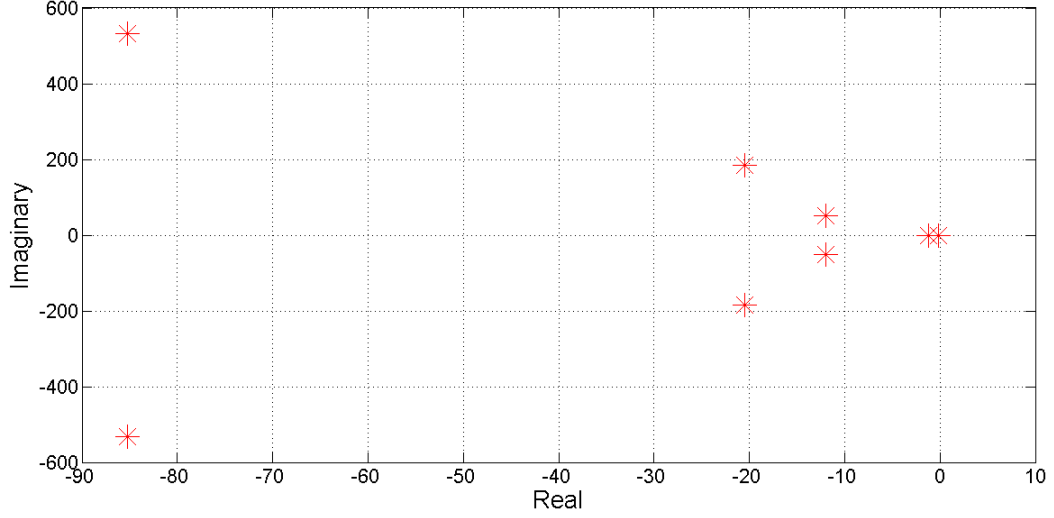
Figure 2.8: Locations of eigenvalues of the wind turbine DFIG system

where the left-hand side constitutes an upper quasi-triangular matrix, such that the real eigenvalues reside on the main diagonal while pairs of complex conjugate eigenvalues constitute 2x2 blocks on the diagonal. MATLAB's implementation of the Schur's form sorts the eigenvalues in a decreasing order, i.e., with the magnitudes of the real parts from the largest to the smallest. When employing U as a similarity transformation for the DFIG system, we also get

$$B_{Schur} = U^T B, \quad C_{Schur} = CU \tag{2.66}$$

To get the singularly perturbed form consistent with (2.62), the order of the eigenvalues needs to be reversed, i.e., the following permutation matrix need to be employed

$$P = \begin{bmatrix} 0 & 0 & 0 & 0 & 0 & 0 & 0 & 1 \\ 0 & 0 & 0 & 0 & 0 & 0 & 1 & 0 \\ 0 & 0 & 0 & 0 & 0 & 1 & 0 & 0 \\ 0 & 0 & 0 & 0 & 1 & 0 & 0 & 0 \\ 0 & 0 & 0 & 1 & 0 & 0 & 0 & 0 \\ 0 & 0 & 1 & 0 & 0 & 0 & 0 & 0 \\ 0 & 1 & 0 & 0 & 0 & 0 & 0 & 0 \\ 1 & 0 & 0 & 0 & 0 & 0 & 0 & 0 \end{bmatrix} \tag{2.67}$$

The singularly perturbed form (2.62) is now achieved by using the following similarity transformation

$$A_{SP} = P^T A P, \quad B_{SP} = P^T B, \quad C_{SP} = C P, \tag{2.68}$$

For the considered DFIG system model, $D_{SP} = D = 0$.

The original system initial conditions, mapped into the new coordinates are given by

$$x_{SP}(0) = P^T U^T x(0) = P^T U^T x_0 \tag{2.69}$$

The singularly perturbed matrices defined in (2.68) and the initial conditions (2.69) are given by

$A_{SP} =$

$$\begin{bmatrix} -0.1514 & 0 & 0 & 0 & 0 & 0 & 0 & 0 \\ 0.2915 & -1.192 & 0 & 0 & 0 & 0 & 0 & 0 \\ 20.439 & 1.612 & -11.878 & -51.168 & 0 & 0 & 0 & 0 \\ -53.174 & 8.308 & 50.93 & -11.878 & 0 & 0 & 0 & 0 \\ -39.962 & -3.679 & -59.826 & -100.76 & -20.408 & -179.13 & 0 & 0 \\ -1.406 & -3.195 & -97.568 & 59.172 & 190.37 & -20.408 & 0 & 0 \\ 1195.5 & 234.29 & -672.89 & -7933.3 & -5499 & -5251.9 & -85.393 & 534.54 \\ -2039 & 2.065 & 7863.1 & -239.84 & -5627.7 & 5258.2 & -525.8 & -85.393 \end{bmatrix}$$

$$B_{SP} = \begin{bmatrix} -0.0311 & 0.0906 & 0.1432 & -0.0251 & -0.00068 \\ 1.213 & 0.1005 & 1.0621 & -1.4192 & 0.2104 \\ 12.356 & 2.3046 & -20.782 & 4.443 & -8.329 \\ -2.003 & 11.927 & -73.393 & 18.304 & -1.4643 \\ 23.757 & -25.504 & 31.864 & -44.994 & -3.177 \\ -27.177 & -24.969 & 8.6312 & -21.95 & 4.8073 \\ 2128.1 & -912.39 & -2126.4 & 911.74 & 0.1259 \\ 912.36 & 2128.1 & -910.69 & -2126.9 & 0.04145 \end{bmatrix}$$

$$C_{SP} = \begin{bmatrix} -0.0004 & 0.0021 & -0.374 & -0.175 & 0.239 & -0.524 & -0.647 & -0.279 \\ -0.0006 & 0.0035 & 0.142 & -0.368 & -0.543 & -0.226 & 0.279 & -0.647 \end{bmatrix}$$

$$x_{SP} = \begin{bmatrix} 0.9813 & 0.8988 & -1.0125 & 0.7402 & -0.7957 & 0.1002 & -0.727 & -1.8667 \end{bmatrix}^T$$

It will be seen that all the three cases considered produce very good results. To the contrary, the balancing method order reduction produced satisfactory results only for the system reduced to order six.

Case 1: Since the absolute real parts of the first two eigenvalues are much smaller than those of the last six, the system exhibits two-time scales and a reasonable approximation is supposed to be obtained if the system is reduced into the second-order slow mode subsystem. The singular perturbation parameter is chosen to be the ratio of the real parts of the fastest slow eigenvalue to the slowest fast one and is equal to $\epsilon_1 = 1.1915/11.8777 = 0.1003$. Then, the approximation method defined in (2.63) is applied to decouple the original system into the slow subsystem with eigenvalues: -0.1514 and -1.1915. The step responses of the original system and the second-order slow mode approximate singularly perturbed subsystems, presented in Figure 2.9, show that the latter provides a very good approximation to the actual response of the original system.
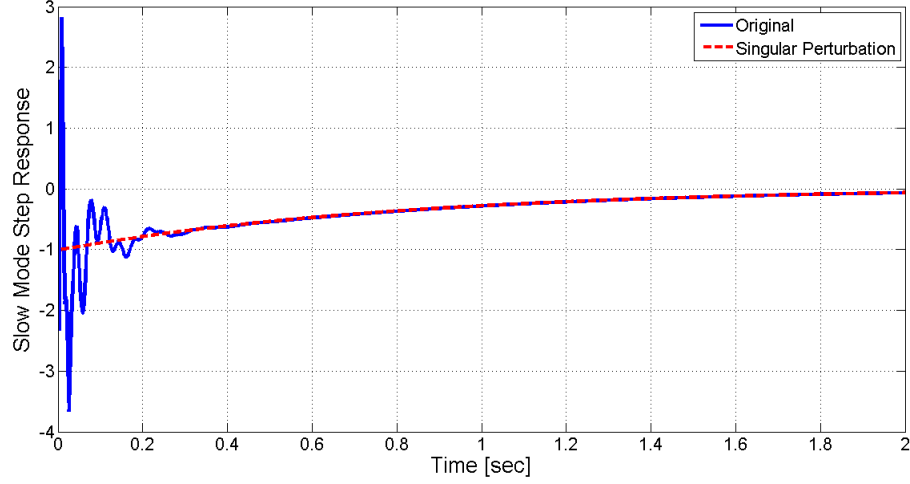
Figure 2.9: Step responses of the original and the second-order approximate slow mode singularly perturbed WT-DFIG system

Case 2: In order to get a better approximation, the original system is decomposed into fourth-order slow and fourth fast subsystems. The small singular perturbation parameter is chosen to be $\epsilon_2 = -11.8777/-20.4804 = 0.5820$. The step responses of the original system and the fourth-order approximate slow mode subsystem are shown in Figure 2.10.
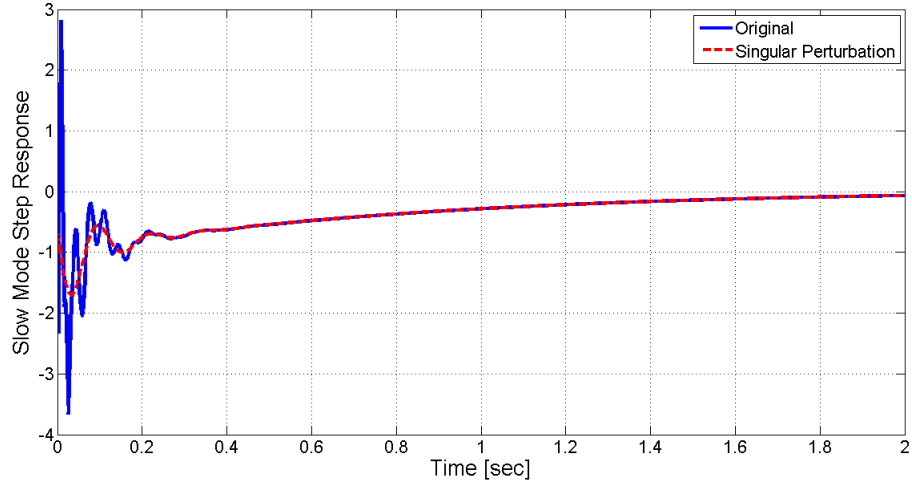
Figure 2.10: Step responses of the original and fourth-order approximate slow mode singularly perturbed WT-DFIG systems

Case 3: The system can also be approximated into a sixth-order slow subsystem, as suggested by the balancing methods. The singular perturbation parameter is chosen

to be the ratio of the fastest slow eigenvalue to the slowest fast one and is equal to $\epsilon_3 = 20.4804/85.3933 = 0.2390$. The step responses of the original system and the sixth-order approximate slow mode singularly perturbed subsystem are shown in Figure 2.11. It shows a better approximation compared to the second and fourth-order slow mode subsystems in Cases 1 and 2.
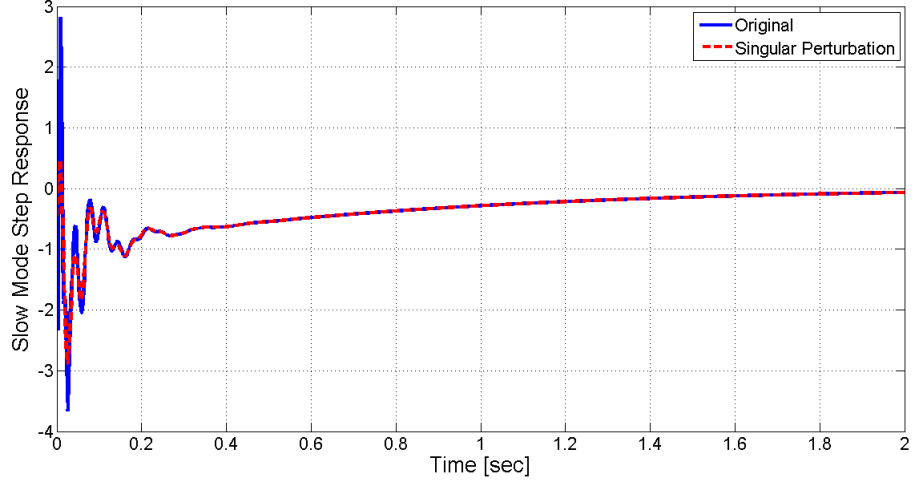
Figure 2.11: Step response of the original and sixth-order approximate slow mode singularly perturbed WT-DFIG systems

It follows from this section that the singular perturbation method allows system model order reduction even to order two, which is a surprising result due to the fact that the balancing order reduction method allows system model order reduction only to order six. In general, these two system model order reduction techniques produce consistent results, but in the case of the considered DFIG system, the singular perturbation method is definitely superior.

2.8 Near-optimal Control using Lower Order Slow Subsystems

In addition to the comparison done with respect to the system responses, in the case of the system order reduction via the method of singular perturbations, these three cases are compared from the optimality point of view for the linear-quadratic optimal controller.

In the case of the approximate slow subsystem (2.63) the derivations are similar to

derivations presented for the residualized model based near-optimal control. Setting $\epsilon = 0$ in the second equation in (2.62), $x_2(t)$ is obtained as

$$x_2(t) = -A_4^{-1}(A_3 x_1(t) + B_2 u(t)) \tag{2.70}$$

Eliminating $x_2(t)$ from the original singularly perturbed system (2.62) and the quadratic performance criterion (2.41) produces

$$J_{SP} = \frac{1}{2} \int_0^\infty \left[x_{1sappr}^T(t) C_0^T C_0 x_{1sappr}(t) + 2 x_{1sappr}^T(t) C_0^T D_0 u(t) + u^T(t) R_0 u(t) \right] dt \tag{2.71}$$

where $R_0 = R + D_0^T D_0$ and with C_0, D_0 defined in (2.63). The approximate slow system is given in (2.72) as

$$\dot{x}_{1appr}(t) = A_0 x_{1appr}(t) + B_0 u(t) \tag{2.72}$$

Minimization of (2.71) subject to (2.72) leads to the following optimal control

$$u_{appr}^{opt}(t) = -R_0^{-1}(C_0^T D_0 + B_0^T P_{appr}) x_{1appr}(t) = -F_{appr} x_{1appr}(t) \tag{2.73}$$

where P_{appr} satisfies the algebraic equation obtained through the linear-quadratic optimization when the quadratic performance criterion contains a cross-product term [52].

$$(A_0 - B_0 R_0^{-1} C_0^T D_0) P_{appr} + P_{appr}(A_0 - B_0 R_0^{-1} C_0^T D_0)^T + C_0^T(I - D_0 R_0^{-1} D_0^T) C_0$$
$$- P_{appr} B_0 R_0^{-1} B_0^T P_{appr} = 0$$

$$\tag{2.74}$$

The near-optimal control to be implemented to the original full-order can be now constructed as

$$u_{appr}^{subopt}(t) = -F_{appr}^{opt} x_1(t) = -\begin{bmatrix} F_{appr}^{opt} & 0 \end{bmatrix} \begin{bmatrix} x_1(t) \\ x_2(t) \end{bmatrix} = -F_{appr} x_{SP}(t) \tag{2.75}$$

Using this near-optimal control in (2.73) and the performance criterion, produces

$$\dot{x}_{SP}(t) = (A_{SP} - B_{SP}F_{appr})x_{SP}(t) \tag{2.76}$$

$$
\begin{aligned}
J_{SP} &= \int_0^\infty \left[x_{SP}^T(t)C^TCx_{SP}(t) + u^T(t)Ru(t) \right] dt \\
&= \frac{1}{2}\int_0^\infty x_{SP}^T(t)\left[C^TC + F_{appr}^T R F_{appr} \right] x_{SP}(t)dt
\end{aligned} \tag{2.77}
$$

It can be shown that integral (2.77), evaluated along trajectories of (2.76), is given by

$$J_{SP}^{appr} = \frac{1}{2}x_{SP}^T(0)V_{SP}^{appr}x_{SP}(0) \tag{2.78}$$

where V_{SP}^{appr} satisfies the following algebraic Lyapunov equation

$$(A_{SP}-B_{SP}F_{appr})V_{SP}^{appr}+V_{SP}^{appr}(A_{SP}-B_{SP}F_{appr})^T+C_{SP}^TC_{SP}+F_{appr}^TRF_{appr} = 0 \tag{2.79}$$

For the considered wind turbine model, the results are presented in Table 2.3 for the cases when the singularly perturbed system is reduced to order two, four, and six.

r	J_r
2	4.3303
4	1.3066
6	0.7493
8	0.7390

Table 2.3: Comparison of the optimal and reduced-order near-optimal performance criteria

It can be seen from this Table 2.3 and system response figures presented in this section, that the system model order reduction to $r = 4$ produces excellent results both from the system response and optimality points of view, which indicates superiority of the singular perturbation approach over the balancing approach for the considered DFIG system.

2.9 Wind Speed Variations

The performances of the reduced models of the considered WTG with DFIG are also tested for wind turbulences and gust. In this chapter, the wind turbulences and gust shown in Figure 2.12 are considered. The total variation in wind speed was modelled after the normal turbulence model (NTM) [58], for an average of $9m/s$, with the addition of a wind gust (modelled as a hamming-shaped dip in wind speed) of width $30s$. We divided the total variance suggested by the NTM into turbulence and gust variations with the proportions of $1/3$ and $2/3$, respectively.
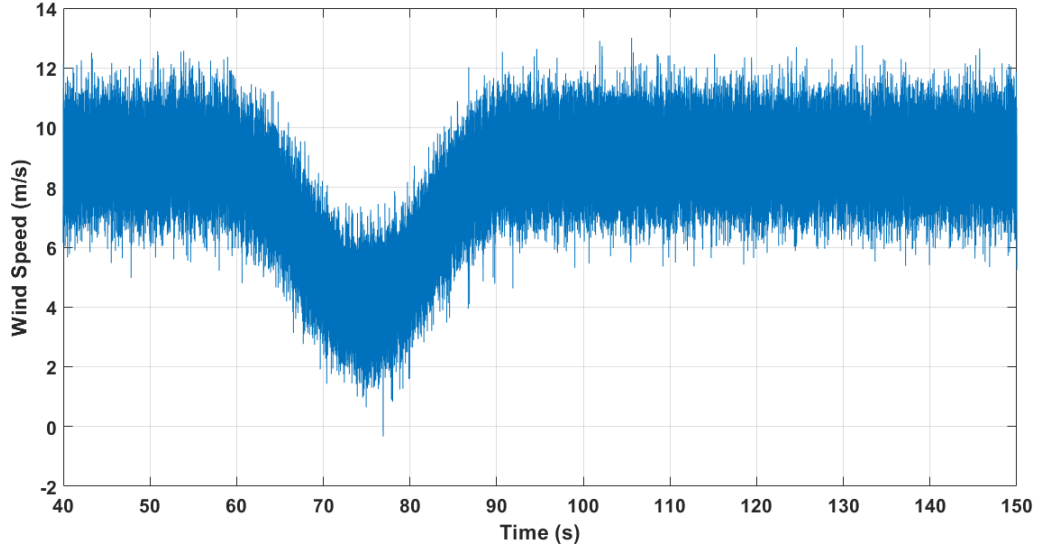
Figure 2.12: Wind turbulences and wind gust

The responses of the reduced balanced truncation and residualization and singular perturbation models to wind turbulences and gust were compared to that of the full-order system in Figures 2.13, 2.14, and 2.15, respectively for the second, fourth, and sixth orders.

The mean and maximum absolute errors, with respect to the full-order system, were also calculated and given in Tables 2.4 and 2.5, respectively, to compare the performances of the reduced models. Both mean and maximum absolute error values show the superiority of the singular perturbation reduced model over the balanced truncation and residualization reduced models. It should be pointed out that by employing

the appropriate filters, the noise appearing in Figures 2.13, 2.14, and 2.15 could be removed.
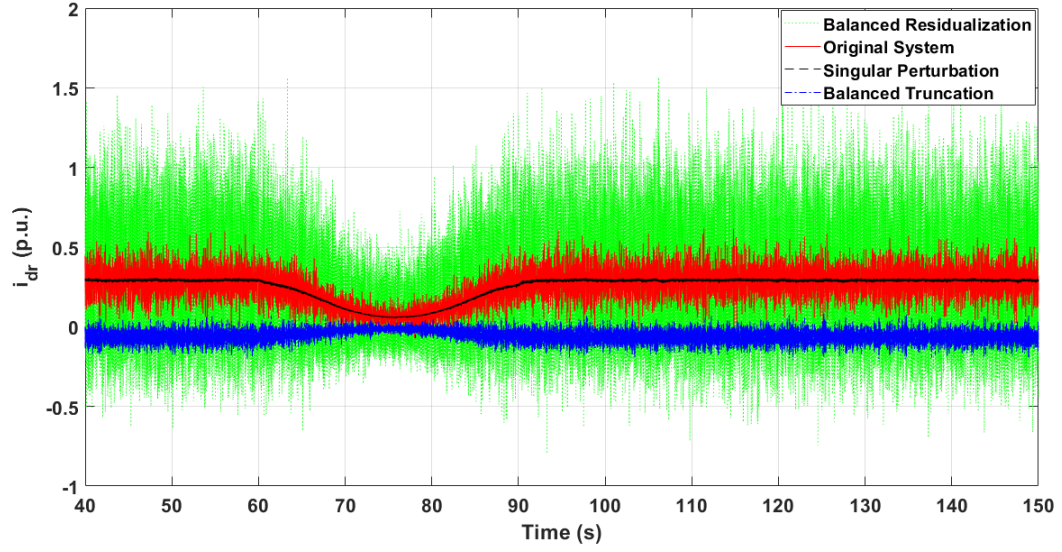
Figure 2.13: Response of the original and second-order reduced models to wind turbulences
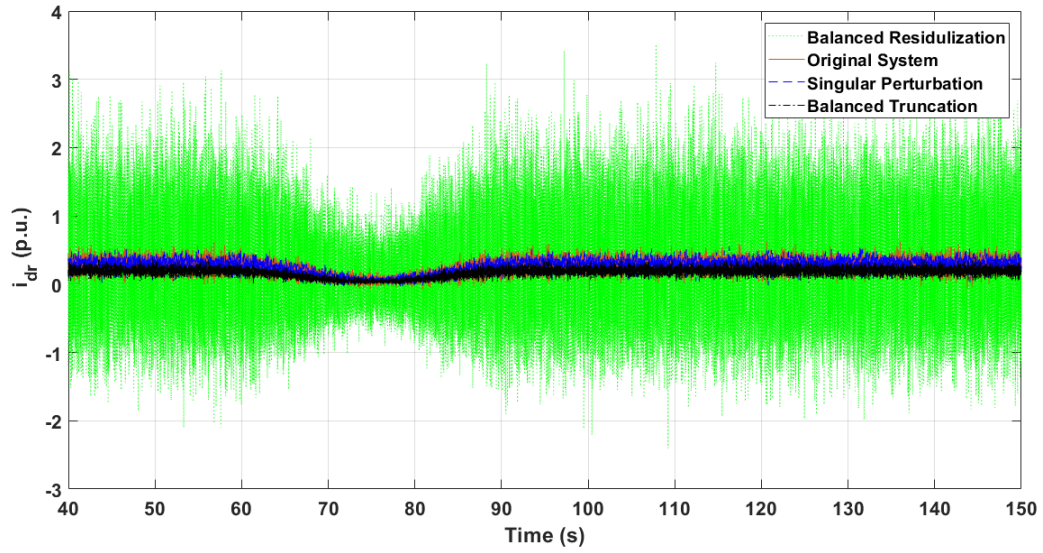
Figure 2.14: Response of the original and fourth-order reduced models to wind turbulences
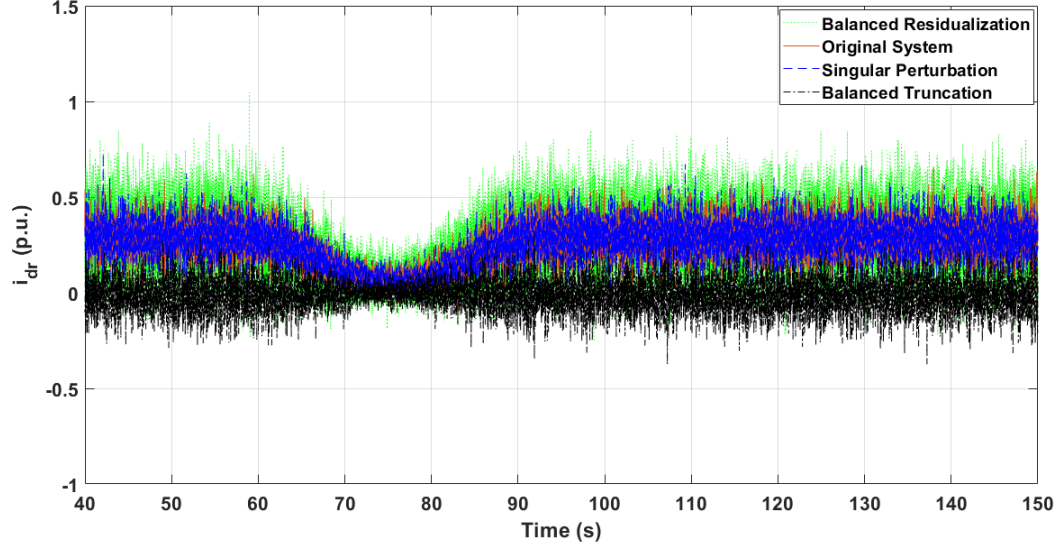
Figure 2.15: Response of the original and sixth-order reduced models to wind turbulences

r	Balanced Truncation	Balanced Residualization	Singular Perturbation
2	-3.2165×10^{-1}	1.4950×10^{-3}	-1.4784×10^{-4}
4	-8.4731×10^{-2}	1.5982×10^{-3}	-2.3263×10^{-5}
6	-2.7915×10^{-1}	1.6708×10^{-3}	4.5829×10^{-5}

Table 2.4: Mean error considering wind turbulences and wind gust

r	Balanced Truncation	Balanced Residualization	Singular Perturbation
2	1.1936	1.629	1.3152
4	0.8489	3.3711	0.45793
6	0.82205	0.83902	0.60111

Table 2.5: Maximum absolute error considering wind turbulences and wind gust

2.10   Voltage Sag

To study the dynamic performance of the different reduced order models, a large-signal disturbance voltage sag is also considered in this chapter. A voltage drop of 50% is applied to the original and reduce models for 1 sec. The responses of the reduced balanced truncation and residualization and singular perturbation models to voltage sag were compared to that of the full-order system in Figure 2.16, Figure 2.17, and Figure 2.18 , respectively for the second, fourth, and sixth orders.

The mean and maximum absolute errors, with respect to the full-order system, were also calculated and given in Tables 2.6 and 2.7, respectively, to compare the performances of the reduced models. Again, the mean and maximum absolute error values show the advantage the singular perturbation reduced model has over the balanced truncation and residualization reduced models.
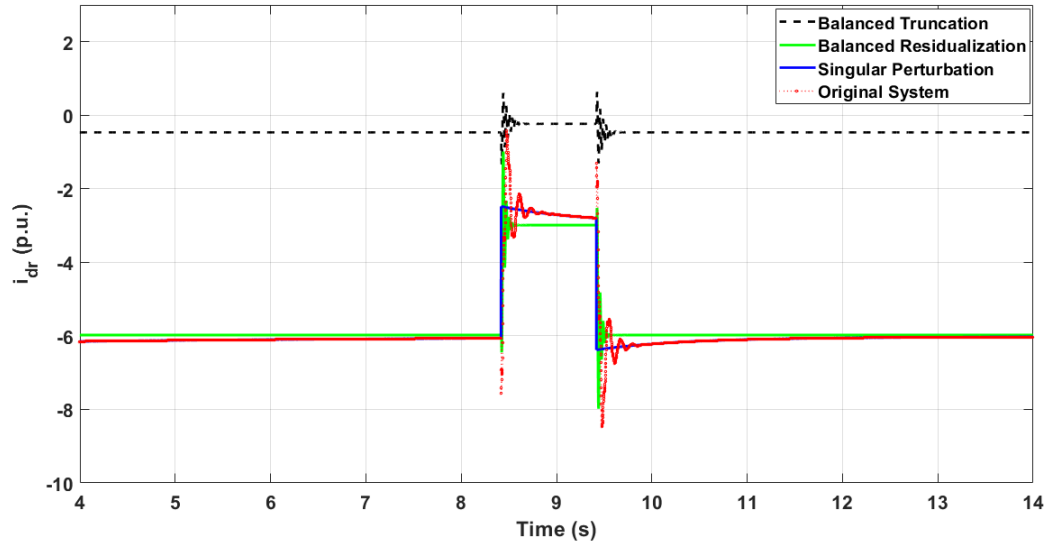
Figure 2.16: Response of the original and second-order reduced models to voltage sag
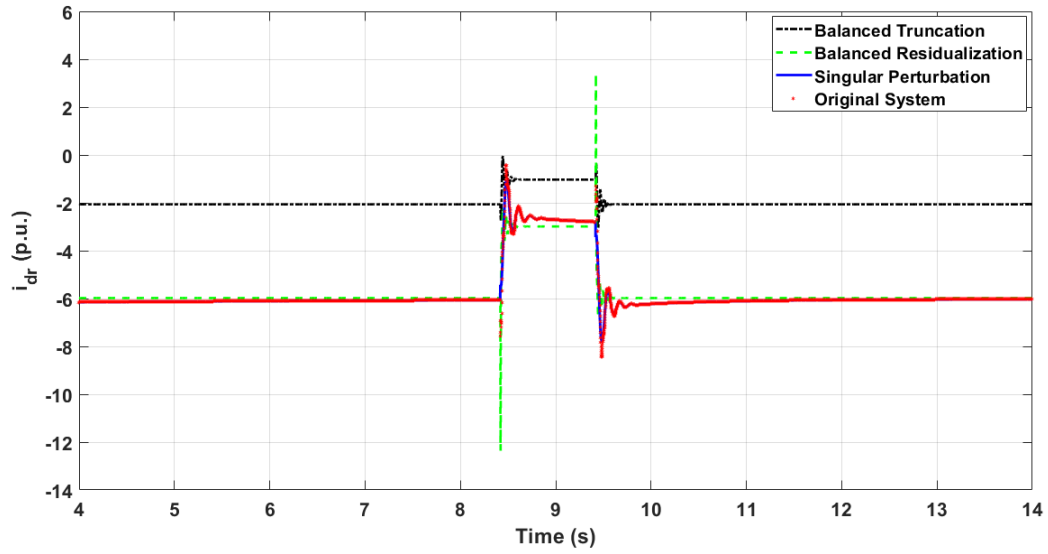
Figure 2.17: Response of the original and fourth-order reduced models to voltage sag
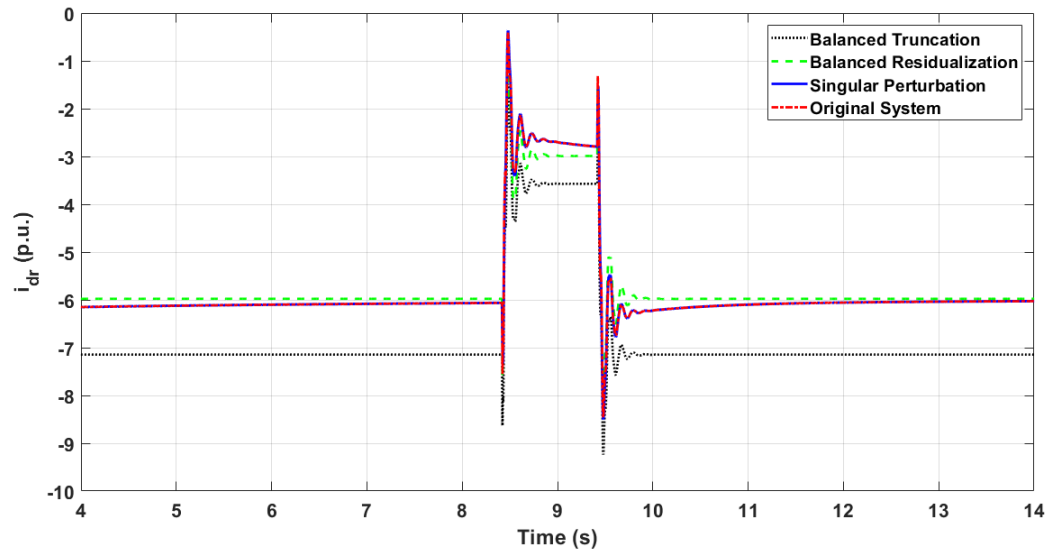
Figure 2.18: Response of the original and sixth-order reduced models to voltage sag

r	Balanced Truncation	Balanced Residualization	Singular Perturbation
2	5.4951	1.3952×10^{-1}	-6.4284×10^{-3}
4	3.945	1.4344×10^{-1}	-1.9616×10^{-3}
6	-9.8912×10^{-1}	1.4246×10^{-1}	-1.2117×10^{-4}

Table 2.6: Mean error considering voltage sag

r	Balanced Truncation	Balanced Residualization	Singular Perturbation
2	11.092	7.0802	10.14
4	9.2731	10.04	4.0685
6	1.1399	1.694	1.1448

Table 2.7: Maximum absolute error considering voltage sag

2.11 Conclusion

In this chapter, an eighth-order wind turbine system with the DFIG connected to the utility grid is investigated. Two methods were used to obtain the reduced-order model of the wind turbine system and to design the corresponding linear-quadratic near-optimal controllers: the methods of system balancing (including balanced truncation and balanced residualization) and singular perturbations. The original and reduced systems were compared through their step responses as well as from the optimality point of view. Simulation and comparisons were also performed when wind turbulence and a large-signal disturbance are applied to the system. The results presented clearly indicate that the method of singular perturbations is superior to that of system balancing for this particular DFIG system.

Chapter 3

Wind Farm Order Reduction via Balancing and Cross Gramians Methods

3.1 Introduction

The power generated by a wind turbine depends, in general, on the wind speed and the size of the turbine itself. It ranges, in a modern wind turbine, from hundreds of watts to several megawatts. Therefore, a large number of identical or different wind turbine generators (WTGs) are usually placed in one location to generate a large amount of electrical power. Such a setting is called a wind farm. Wind turbines are usually distributed uniformly in rows more than three times the lengths of their blades apart from each other and with more than five times the lengths of the blades between the rows. This is usually done for an aesthetic purpose and to increase visual perspicacity especially if the wind farm is built in birds' migration paths. There are many common trends available in modeling wind farms, such as the detailed modeling method and the equivalent modeling method. In the detailed method [59, 60], each wind turbine in the farm is represented with its complete dynamic equations. As the number of wind turbines increases, the order of the farm's mathematical model increases too, leading to more complexity and longer simulation times. Assuming that equating the wind speed experienced by identical wind turbines has low impact on accuracy, several studies [21, 61–63] showed that a wind farm with a large number of identical wind turbines can be approximated by an equivalent model containing only a single turbine. The size, rated, and reactive powers of the equivalent model are equal to the sum of sizes, total rated, and total reactive powers of these wind turbines, respectively.

Alternatively, reduction methods based on control theory can be utilized to obtain reduced order models of wind farms. In balanced truncation [24], the controllability

and observability Gramians are obtained by solving the algebraic Lyapunov equations. The balanced realization of the original system is truncated after that to obtain the reduced-order system. For further reduction in complexity and simulation time, the cross Gramian method can also be used for wind farm order reduction [64, 65]. In this method only one Sylvester equation needs to be solved to obtain the cross Gramian which carries information about the controllability and observability. Truncation is applied after that to obtain the reduced-order system without the need for balancing.

For WECS, studying controllability and observability has a major impact on the efficiency of the control system since it provides important information about the dynamic behavior of the WECS and the relation between the states, control inputs, and outputs. Controllability refers to the ability to control and move the system from any initial state to any desired final state using the appropriate input within finite time. Observability on the other hand, is the ability to estimate the complete dynamic behavior of the states of the system using only the output information [66]. In control theory, the full rank test for the controllability and observability matrices gives a precise answer to whether or not a given system is controllable and/or observable, respectively. Rather than giving a binary answer to the question about controllability and observability of the system, measuring the degree of controllability (DOC) and the degree of observability (DOO) provides further quantitative information about "how controllable/observable" the system is [67]. The relationship between DOC and MPPT efficiency of the wind turbine is studied in [68] for the one-mass and two-mass models. It is observed that the variation of DOC versus the structural parameters of the wind turbine is in accordance with that of MPPT efficiency, therefore higher MPPT efficiency can be achieved with the increase of DOC. Furthermore, reducing rotor inertia and optimum tip-speed ratio increase the DOC measure of the WECS [68, 69]. The influence of model parameters on the controllability of DFIG-based WECS is further investigated in [70], where it is shown that a high ratio of DFIG leakage reactance to its resistance results in uncontrollable slow resonant modes.

In this chapter, the Hankel singular values are adopted as measures of the controllability and observability of the wind farm system. The value of each HSV has a physical

meaning related to the energy content in the corresponding state of the system. The higher the values of the HSV the larger the DOC and the DOO.

The rest of this chapter is organized as follows. Section 3.2 presents the state-space representation of a linearized wind farm model. In Section 3.3, the balanced truncation and balanced residualization methods are used to reduce the order of wind farm models of different sizes, and the DOC and DOO of the reduced systems are calculated. Section 3.4 provides a theoretical background about the cross Gramian and its application to the order reduction of the wind farm model. Section 3.5 concludes the chapter.

3.2 State-space Representation of a Wind Farm

Wind turbines are nonlinear systems, for the power generated by a wind turbine is proportional to the third power of wind speed. In order to simplify the model of the system and to design suitable linear controllers, a linearization process is usually performed. The behavior of a nonlinear system is approximated in the vicinity of its equilibrium points. Therefore, this approximation may not be valid for large deviations from these nominal points. In this section, the linearization process for the farm of one-mass wind turbines with DFIG presented in [24] is considered. Assuming that the wind turbine is operating under the maximum power point tracking conditions, the mechanical power collected from the wind is given by [5]:

$$P_m = \frac{1}{2}\rho\pi R^2 v^3 C_p(\lambda, \beta) \tag{3.1}$$

the mechanical and electromechanical torques, per unit, can be expressed as follows [24]

$$T_m = \frac{K_p v^3}{\omega_r} \tag{3.2}$$

$$T_e = K_p \omega_r^2 \tag{3.3}$$

where v is the wind speed per unit and ω_r is the angular speed of the rotor per unit. The scaling factor k_p depends on the turbine characteristics and indicates the maximum

output power of the turbine at the base wind speed. It is given by

$$k_p = \frac{\rho \pi R^2 v^3 C_p(\lambda_{opt}, \beta_{opt}) v^3}{2 P_{base}} \qquad (3.4)$$

Recalling the nonlinear swing equation (2.6), in which the turbine rotor and generator are considered as one-mass, the linearization process can be performed for small deviations in the wind and rotor speeds, v_Δ and $\omega_{r\Delta}$, respectively, from the initial values, i.e. $v = v_0 + v_\Delta$, $\omega = \omega_0 + \omega_\Delta$. By substituting (3.2) and (3.3) in (2.6), we get [24]

$$2H_t \frac{d\omega_\Delta}{dt} = \frac{3K_p v_0^2}{\omega_0} v_\Delta - (\frac{-K_p v_0^3}{\omega_0^2} + 2K_p \omega_0)\omega_\Delta \qquad (3.5)$$

Equation (3.5) can be rewritten to describe the state space representation of the wind turbine as follows [24]

$$\frac{d\omega_\Delta}{dt} = \frac{3K_p v_0^2}{2H_t \omega_0} v_\Delta - \frac{1}{2H_t}(\frac{-K_p v_0^3}{\omega_0^2} + 2K_p \omega_0)\omega_\Delta \qquad (3.6)$$

$$P_\Delta = 3K_p \omega_0^2 \omega_\Delta \qquad (3.7)$$

where the input is the wind speed deviation while the output is the electrical power deviation. The general linearized state-space model is given by

$$\dot{x}(t) = Ax(t) + Bu(t)$$
$$y(t) = Cx(t) + Du(t) \qquad (3.8)$$

where $A, B, C,$ and D represent the system state, input, output, and feed forward matrices, respectively. The state-space equations for a wind farm containing N wind turbine generators are

$$[\dot{\boldsymbol{\omega}}_\Delta]_{(n \times 1)} = [\boldsymbol{A}]_{n \times n} \cdot [\boldsymbol{\omega_\Delta}]_{n \times 1} + [\boldsymbol{B}]_{n \times n} \cdot [\boldsymbol{V}_\Delta]_{n \times 1} \qquad (3.9)$$

$$\boldsymbol{P}_{F\Delta} = [\boldsymbol{C}]_{1 \times n} \cdot [\boldsymbol{\omega_\Delta}]_{n \times 1} \qquad (3.10)$$

where $\mathbf{P}_{F\Delta}$ is the output power of the wind farm and $\mathbf{v}_\Delta$ is the wind velocities vector.

Elements in matrices $\mathbf{A}$, $\mathbf{B}$ and $\mathbf{C}$ are calculated as follows [24]

$$a_{i,i} = -\frac{1}{2H_{t_i}}\left(\frac{-K_{pi}v_{0i}^3}{w_{0i}^2} + 2K_{pi}w_{0i}\right), \ a_{i,j} = 0$$

$$b_{i,i} = \left(\frac{K_{pi}v_{0i}^3}{2H_{t_i}w_{0i}^2}\right), \ b_{i,j} = 0 \tag{3.11}$$

$$c_{1,i} = 3K_{pj}w_{0j}^2$$

where $i, j = 1, 2, ...n$ and $i \neq j$. For linearization and simulation purposes, we assume wind turbines to be working at a base wind speed equal to $12[m/s]$, and producing an output power of 0.73 per unit (pu). Furthermore, we assume that $v_0 = 1$ pu, $\omega_0 = 1$ pu and $K_p = 0.73$.

3.3 Wind Farm Model Reduction via Balanced Truncation and Balanced Residualization Methods

It can be observed from (3.11) that when the inertia H has identical elements then $A \in \Re^{n \times n}$ and $B \in \Re^{n \times n}$ reduce into diagonal matrices with identical elements on their diagonal, whereas $C \in \Re^{1 \times n}$ assumes the shape of a row vector with identical values. In this study, the matrix B will be represented in two different forms. In the first form, $B \in \Re^{n \times n}$ is a diagonal matrix calculated using (3.11). In the second form, B will be a column vector with elements equal to those of the diagonal of the corresponding $B \in \Re^{n \times n}$ matrix. Using these two forms allows us to compare the degree of controllability and observability for each system form. Using the second form of B the system matrices are given by

$$A = \begin{bmatrix} a & 0 & \cdots & 0 \\ 0 & a & \cdots & 0 \\ \vdots & \vdots & \ddots & \vdots \\ 0 & \cdots & \cdots & a \end{bmatrix}, \ B = \begin{bmatrix} b \\ b \\ \vdots \\ b \end{bmatrix}, \ C = \begin{bmatrix} c & c & \cdots & c \end{bmatrix} \tag{3.12}$$

Using equation (2.24), the transfer function in this case is given by

$$G(s) = \begin{bmatrix} c & c & \cdots & c \end{bmatrix} \begin{bmatrix} s-a & 0 & \cdots & 0 \\ 0 & s-a & \cdots & 0 \\ \vdots & \vdots & \ddots & \vdots \\ 0 & \cdots & \cdots & s-a \end{bmatrix}^{-1} \begin{bmatrix} b \\ b \\ \vdots \\ b \end{bmatrix} \qquad (3.13)$$

$$G(s) = \begin{bmatrix} \frac{c}{s-a} & \frac{c}{s-a} & \cdots & \frac{c}{s-a} \end{bmatrix} \begin{bmatrix} b \\ b \\ \vdots \\ b \end{bmatrix} \qquad (3.14)$$

$$G(s) = \frac{c}{s-a} + \frac{c}{s-a} + \cdots + \frac{c}{s-a} \qquad (3.15)$$

For n terms (n wind turbines), the system transfer function is

$$G(s) = n \cdot \frac{cb}{s-a} \qquad (3.16)$$

To compare this result with that of the balanced truncation method, the algebraic Lyapunov equations (2.26) and (2.27) are used to calculate the controllability and observability Gramian matrices, respectively

$$W_C = \begin{bmatrix} \frac{-b^2}{2a} & \frac{-b^2}{2a} & \cdots & \frac{-b^2}{2a} \\ \frac{-b^2}{2a} & \frac{-b^2}{2a} & \cdots & \frac{-b^2}{2a} \\ \vdots & \vdots & \ddots & \vdots \\ \frac{-b^2}{2a} & \cdots & \cdots & \frac{-b^2}{2a} \end{bmatrix}, \; W_O = \begin{bmatrix} \frac{-c^2}{2a} & \frac{-c^2}{2a} & \cdots & \frac{-c^2}{2a} \\ \frac{-c^2}{2a} & \frac{-c^2}{2a} & \cdots & \frac{-c^2}{2a} \\ \vdots & \vdots & \ddots & \vdots \\ \frac{-c^2}{2a} & \cdots & \cdots & \frac{-c^2}{2a} \end{bmatrix} \qquad (3.17)$$

The product of the Gramian matrices for this case is

$$W_C W_O = \begin{bmatrix} \frac{b^2 c^2}{2a^2} & \frac{b^2 c^2}{2a^2} & \cdots & \frac{b^2 c^2}{2a^2} \\ \frac{b^2 c^2}{2a^2} & \frac{b^2 c^2}{2a^2} & \cdots & \frac{b^2 c^2}{2a^2} \\ \vdots & \vdots & \ddots & \vdots \\ \frac{b^2 c^2}{2a^2} & \cdots & \cdots & \frac{b^2 c^2}{2a^2} \end{bmatrix} \qquad (3.18)$$

It is easy to see that $W_C W_O$ has rank one, with a single non-zero eigenvalue, leading to the one dominant Hankel Singular value, that is

$$\sigma_1 = \frac{bc}{a}, \; \sigma_2 = \cdots = \sigma_n = 0 \tag{3.19}$$

This means that the system can be reduced to a first-order system.

In this chapter, MATLAB simulation was performed on wind farms containing different numbers of identical wind turbines. Wind farms containing 50, 100, 200, and 300 turbines are considered in this study. Using the balancing method, regardless of the number of turbines in the farm, all the HSVs, other than the first one, were found to be zero. Table 3.1 shows the first five HSVs over different wind farm sizes. These results prove that any wind farm with identical wind turbines can be reduced to a first-order system when the wind speed is assumed equal for all the turbines in that farm.

HSVs	Number of Turbines in the Farm			
	50	100	200	300
1	54.7500	109.5000	219.0000	328.5000
2	5.4706×10^{-15}	1.0941×10^{-14}	2.1882×10^{-14}	3.2823×10^{-14}
3	5.4706×10^{-15}	1.0941×10^{-14}	2.1882×10^{-14}	3.2823×10^{-14}
4	5.4706×10^{-15}	1.0941×10^{-14}	2.1882×10^{-14}	3.2823×10^{-14}
5	5.4706×10^{-15}	1.0941×10^{-14}	2.1882×10^{-14}	3.2823×10^{-14}

Table 3.1: First five HSVs for wind farms with different numbers of identical SISO wind turbines

In general, wind speed is not the same for all wind turbines in a farm, especially for the turbines placed in different rows within the same farm, or those placed long distances apart from each other. The system matrices are calculated in the same manner using (3.11). In this case, the matrix B is a column vector with different elements, and the system transfer function is calculated as

$$G(s) = \begin{bmatrix} \frac{c}{s-a} & \frac{c}{s-a} & \cdots & \frac{c}{s-a} \end{bmatrix} \begin{bmatrix} b_1 \\ b_2 \\ \vdots \\ b_n \end{bmatrix} \tag{3.20}$$

$$G(s) = \frac{c}{s-a}[b_1 + b_2 + \cdots + b_n] \tag{3.21}$$

This system is still a first-order system.

Another way to represent matrix B is by putting it in a diagonal form, with non-identical elements.

$$A = \begin{bmatrix} a & 0 & \cdots & 0 \\ 0 & a & \cdots & 0 \\ \vdots & \vdots & \ddots & \vdots \\ 0 & \cdots & \cdots & a \end{bmatrix}, \ B = \begin{bmatrix} b_1 & 0 & \cdots & 0 \\ 0 & b_2 & \cdots & 0 \\ \vdots & \vdots & \ddots & \vdots \\ 0 & \cdots & \cdots & b_n \end{bmatrix}, \ C = \begin{bmatrix} c & c & \cdots & c \end{bmatrix} \tag{3.22}$$

The simulation results were similar to the previous case in that only the first HSV in each wind farm is non-zero. Table 3.2 shows the first five HSVs over different wind farms consisting of 50, 100, 200, and 300 identical wind turbines. Matrix $B \in \Re^{n \times n}$ has the corresponding appropriate size in each case. Comparing the HSVs in Table 3.1 with the corresponding HSVs in Table 3.2, it can be seen that the system is still very well approximated by a first-order system, but it is significantly less controllable and observable when the input matrix B is in the diagonal form. The controllability and observability, in terms of the first HSV, were approximately down by 85% (form 54.75 to 7.7428) for $N = 50$, and 94% (from 328.5 to 18.9659) for $N = 300$.

HSVs	Number of Turbines in the Farm			
	50	100	200	300
1	7.7428	10.9500	15.4856	18.9659
2	7.6588×10^{-16}	1.0886×10^{-15}	1.5434×10^{-15}	1.8919×10^{-15}
3	7.6588×10^{-16}	1.0886×10^{-15}	1.5434×10^{-15}	1.8919×10^{-15}
4	7.6588×10^{-16}	1.0886×10^{-15}	1.5434×10^{-15}	1.8919×10^{-15}
5	7.6588×10^{-16}	1.0886×10^{-15}	1.5434×10^{-15}	1.8919×10^{-15}

Table 3.2: First five HSVs for wind farms with different numbers of identical MIMO wind turbines

The accuracy of the reduced-order system can be measured by comparing its step response to that of the original system. The maximum absolute and mean errors in the

step response are calculated for both the balanced truncation and balanced residual-
ization methods. Note that the mean error ($\bar{e}$) is given by

$$\bar{e} = \frac{\sum_{i=1}^{n} e_i}{n} \tag{3.23}$$

where e_i is the error at instant t_i. The maximum absolute and mean errors were zero
regardless of the size of the wind farm, which consolidates our conclusion that any wind
farm with identical wind turbines can be reduced to a first-order system when the wind
speed is assumed equal over all the turbines in that farm.

Choosing different values for the inertia in (3.11) means that the wind farm may
contain different turbines. The corresponding system would have the following matrices
if the matrix B is put in the vector form

$$A = \begin{bmatrix} a_1 & 0 & \cdots & 0 \\ 0 & a_2 & \cdots & 0 \\ \vdots & \vdots & \ddots & \vdots \\ 0 & \cdots & \cdots & a_n \end{bmatrix}, \ B = \begin{bmatrix} b_1 \\ b_2 \\ \vdots \\ b_n \end{bmatrix}, \ C = \begin{bmatrix} c & c & \cdots & c \end{bmatrix} \tag{3.24}$$

A MATLAB simulation was performed on wind farms containing 50, 100, 200, and
300 different wind turbines, with inertias distributed uniformly between $3[s]$ and $5[s]$
[24]. Using the balancing method, the first five HSVs are shown in Table 3.3. The first
two HSVs of each wind farm are the most dominant. Hence, the system can be reduced
to a second-order system.

| HSVs | Number of Turbines in the Farm | | | |
	50	100	200	300
1	54.4651	108.8727	217.9701	326.8562
2	0.2835	0.6246	1.0252	1.6360
3	0.0012	0.0026	0.0045	0.0076
4	5.998×10^{-6}	1.0588×10^{-5}	1.8815×10^{-5}	3.0016×10^{-5}
5	2.071×10^{-8}	4.2423×10^{-8}	6.6234×10^{-8}	1.2725×10^{-7}

Table 3.3: First five HSVs for wind farms with different numbers of non-identical,
uniformly distributed SISO wind turbines

Table 3.4 lists the HSVs when putting the matrix B into the diagonal form. For

each wind farm, the system can still be reduced to a second-order system, since the first two HSVs are the most dominated. Again, comparing the HSVs in Table 3.3 to the corresponding HSVs in Table 3.4, we can deduce that the system is less controllable and less observable when the matrix B is in the diagonal form. Furthermore, the approximation by the first-order system is not as accurate as in the previous case, since the second and third HSVs now have increased to 0.5572 and 0.0371, respectively.

HSVs	Number of Turbines in the Farm			
	50	100	200	300
1	7.7226	10.9185	15.4491	18.9184
2	0.5572	0.8270	1.0595	1.338
3	0.0371	0.0534	0.0709	0.0914
4	0.0025	0.0034	0.0045	0.0057
5	0.0001	0.0002	0.0002	0.0003

Table 3.4: First five HSVs for wind farms with different numbers of non-identical, uniformly distributed MIMO wind turbines

In the third simulation scenario, the inertia values are generated randomly such that they are clustered around $3[s]$, $5[s]$, and $7[s]$. Matrices A, B, and C, are then calculated using (3.11). Wind farms consisting of 60, 120, 240, and 300 turbines are considered, first when matrix B is in the column vector form, and second when matrix B is in the diagonal form.

For the matrix B in the column vector form, the simulation results are shown in Table 3.5. The first three HSVs were more significant than the remaining HSVs. Therefore, the system can be reduced to a third-order system. When the matrix B is put in the diagonal form, the simulation results for the first five HSVs are as shown in Table 3.6. The first three HSVs were also the most significant HSVs, therefore, the system was also reduced to the third-order. However, comparing these results with the corresponding HSVs in Table 3.6, it can be concluded that the system is still far less controllable and observable when matrix B is in the diagonal form.

HSVs	Number of Turbines in the Farm			
	60	**120**	**240**	**300**
1	63.8425	127.7102	255.1476	318.7120
2	1.8305	3.6360	7.5357	9.6359
3	0.0266	0.0531	0.1155	0.1506
4	0.0002	0.0004	0.0009	0.0013
5	3.645×10^{-6}	9.028×10^{-6}	1.572×10^{-5}	2.792×10^{-5}

Table 3.5: First five HSVs for wind farms with different numbers of non-identical, normally distributed SISO wind turbines

HSVs	Number of Turbines in the Farm			
	60	**120**	**240**	**300**
1	8.3610	11.8255	16.7148	18.6812
2	1.4157	1.9953	2.8725	3.2482
3	0.1707	0.2413	0.3557	0.4061
4	0.0173	0.0232	0.0329	0.0382
5	0.0019	0.0031	0.0041	0.0055

Table 3.6: First five HSVs for wind farms with different numbers of non-identical, normally distributed MIMO wind turbines

3.4 Model Order Reduction via Cross Gramian

In general, model order reduction via balancing methods (truncation and residualization) is relatively expensive computationally. Calculating the controllability and observability Gramians using Lyapunov equations (2.26) and (2.27), followed by balancing and HSV calculation requires computational cost and storage of $O(n^3)$ and $O(n^2)$, respectively. An alternative approach that requires calculation of only one single matrix called the cross Gramian matrix, is proposed in [71]. In this section, model order reduction is achieved using what is called the cross Gramian matrix, which contains information about both controllability and observability and corresponds to a solution of the Sylvester equation.

Cross Gramian was first defined in 1981 by Fernando [71] for single input single output (SISO) linear dynamic systems given by

$$\frac{dx(t)}{dt} = Ax(t) + Bu(t)$$
$$y(t) = Cx(t)$$

(3.25)

where $x(t) \in \Re^n$, are state variables, $u(t) \in \Re^m$ are control inputs, and $y(t) \in \Re^p$ are measured outputs. Assuming that the system in (3.25) is asymptotically stable, controllable observable, and square, i.e., *the number of inputs equals the number of outputs* $m = p$, the cross Gramian matrix is defined by

$$W_X = \int_0^\infty e^{At} BC e^{At} \, dt \tag{3.26}$$

and represented by the solution to the algebraic Sylvester equation

$$AW_X + W_X A = BC \tag{3.27}$$

In this context, the Sylvester algebraic equation (3.27) has a unique solution if and only if A and $-A$ have distinct eigenvalues [72]. The definition in (3.26) was extended in [73], [74] and [75] to include Multi-Input Multi-Output (MIMO) systems. Furthermore, for MIMO symmetric systems, the relation between controllability and observability, on one hand, and the cross Gramian on the other hand, is given by [76]

$$W_X^2 = W_C W_O \tag{3.28}$$

from which the Hankel singular values of system (3.25) are given by the magnitude of the eigenvalues of the cross Gramian

$$\sigma_i = |\lambda(W_X)| = \sqrt{\lambda(W_C W_O)} \tag{3.29}$$

For model order reduction, the cross Gramian matrix obtained as a solution for Sylvester equation (3.27) is decomposed using the singular value decomposition (SVD) and then partitioned without any need for balancing as follows

$$W_X = U \Sigma V^T = \begin{bmatrix} U_1 & U_2 \end{bmatrix} \begin{bmatrix} \Sigma_1 & 0 \\ 0 & \Sigma_2 \end{bmatrix} \begin{bmatrix} V_1^T \\ V_2^T \end{bmatrix} \tag{3.30}$$

where $U, V \in \Re^{n \times n}$, $\quad \Sigma_1 = diag\{\sigma_1, \sigma_2, \ldots, \sigma_r\}$, $\quad \Sigma_2 = diag\{\sigma_{r+1}, \sigma_2, \ldots, \sigma_n\}$. Here,

the order of the reduced model r can be chosen based on the following threshold criteria

$$\sum_{k=r+1}^{n} \sigma_k \leq \epsilon \tag{3.31}$$

By taking the projection in the U_1 subspace direction [77], the reduced order system can be defined as

$$\dot{x}_c(t) = A_c x_c(t) + B_c u(t)$$
$$y_c(t) = C_c x_c(t) \tag{3.32}$$

where $A_c = U_1^T A U_1, \quad B_c = U_1^T B, \quad C_c = C U_1, \quad x_{c0} = U_1^T x_{c0}$

3.4.1 Wind Farm Model Reduction via the Cross Grammian

In this section, the cross Gramian is used to investigate model order reduction for the system (3.11). A MATLAB simulation for wind farms containing different numbers of identical wind turbines was performed. Wind farms containing 50, 100, 200, and 300 turbines are considered again in this section. Using the cross Gramian truncation method, with a threshold value of 0.01 (see equation (3.31)), we got first-order reduced system models for the wind farms of different sizes. These results agree with those we got using the balanced truncation and residualization methods, showing that any wind farm with identical wind turbines can be reduced to a first-order system when the wind speed is assumed to be equal over all the turbines in that farm.

To compare the accuracy of the reduced-order system to that of the original full-order system, the maximum absolute and mean errors in the step responses of the systems reduced using balanced truncation, balanced residualization, and cross Gramian methods are calculated. The results are shown in Tables 3.7 and 3.8, respectively.

The maximum absolute and mean error values show that a first-order approximation to the original system is accurate. Comparing these results to those of the balanced truncation and balanced residualization methods, where the maximum absolute and mean errors were zero for all wind farm sizes, we conclude that the balancing method is slightly more accurate when reducing wind farms that comprise identical turbines

Reduction Method	Number of Turbines in the Farm			
	50	100	200	300
Balanced Truncation	0	0	0	0
Residulization	6.31×10^{-30}	4.74×10^{-29}	1.81×10^{-27}	1.12×10^{-27}
Cross Gramian	2.56×10^{-13}	1.023×10^{-12}	2.44×10^{-12}	2.96×10^{-12}

Table 3.7: Maximum absolute errors in the step responses of the order-reduced wind farms comprising different numbers of identical SISO WTs

Reduction Method	Number of Turbines in the Farm			
	50	100	200	300
Balanced Truncation	0	0	0	0
Residulization	3.22×10^{-32}	2.42×10^{-31}	9.23×10^{-30}	5.69×10^{-30}
Cross Gramian	-6.17×10^{-14}	3.10×10^{-13}	1.08×10^{-13}	8.89×10^{-13}

Table 3.8: Mean errors in the step responses of the order-reduced wind farms comprising different numbers of identical SISO WTs

into first-order systems. Choosing a different threshold value would reduce the system into an order higher than one, with smaller maximum absolute and mean errors. The step responses of the original and reduced-order systems for each of the aforementioned reduction methods are shown in Figure 3.1.
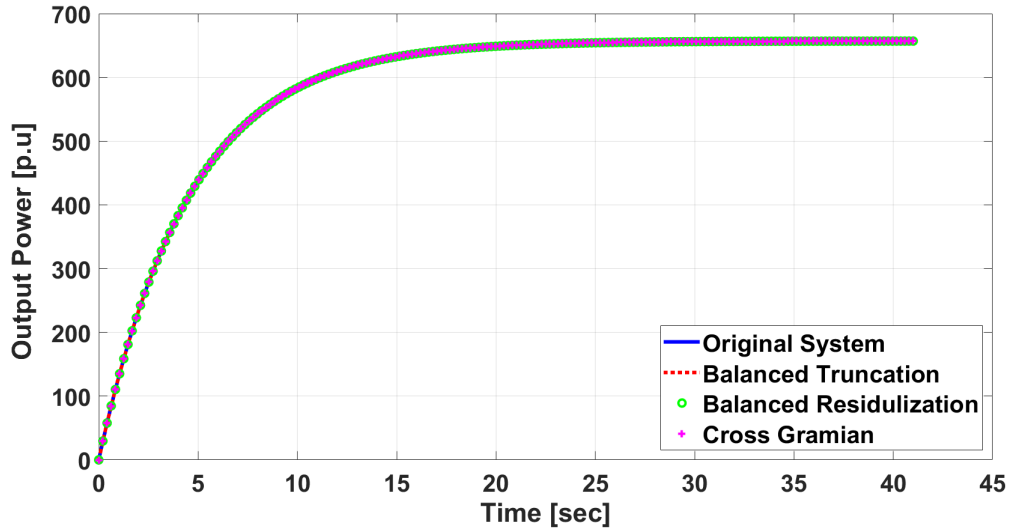
Figure 3.1: Step responses of the reduced order system models of a wind farm comprising 300 identical WTs

Wind farms containing wind turbines with different inertia are also studied using the cross Gramian method. Wind farms containing 50, 100, 200, and 300 different

wind turbines are considered here. The inertia values of these turbines were uniformly distributed between $3[s]$ and $5[s]$. Using MATLAB simulation, the system is successfully reduced to a second-order system for a threshold value of 0.01 (see equation (3.31)). To compare the accuracy of the reduced-order system to the original full-order system, the maximum absolute and mean errors in the step responses, for each of the aforementioned methods, are calculated. The results are shown in Tables 3.9–3.10. It can be observed that the maximum absolute and mean error values are relatively small. However, error values increase as the wind farm size increases, since the precision of reducing the farm size to second-order decreases.

Reduction Method	Number of Turbines in the Farm			
	50	100	200	300
Balanced Truncation	5.307×10^{-4}	0.00121	0.0023	0.0035
Residulization	0.002	0.0047	0.0091	0.0138
Cross Gramian	0.00502	0.011	0.0218	2.003×10^{-5}

Table 3.9: Maximum absolute errors in the step responses of reduced wind farms comprising different numbers of non-identical uniformly distributed SISO WTs

Reduction Method	Number of Turbines in the Farm			
	50	100	200	300
Balanced Truncation	1.27×10^{-4}	2.9×10^{-4}	5.6×10^{-4}	8.54×10^{-4}
Residulization	-9.17×10^{-6}	-4.1×10^{-5}	-4.7×10^{-5}	-7.62×10^{-5}
Cross Gramian	0.0007	0.0015	0.0032	-6.36×10^{-6}

Table 3.10: Mean errors in the step responses of reduced wind farms comprising different numbers of non-identical uniformly distributed SISO WTs

Furthermore, the step responses of the original and reduced-order systems for each of the aforementioned reduction methods are shown in Figure 3.2.

Wind turbines with inertias distributed normally around $3[s]$, $5[s]$ and $7[s]$ are also investigated here, using the cross Gramian method. Wind farms containing 60, 120, 240, and 300 different wind turbines are considered. MATLAB simulation shows that these systems can be reduced into the third-order using a threshold equal to 0.01 (see equation (3.31)). The maximum absolute and mean errors of the step responses are calculated to test the accuracy of this reduction, as shown in Tables 3.11–3.12. Despite the increase in error values with the increase in the size of the wind farm, the low values

of the maximum absolute and mean errors show that a third-order model provides a reasonable approximation to the original system. The step responses of the original and reduced-order systems for each of the aforementioned reduction methods are plotted in Figure 3.3.
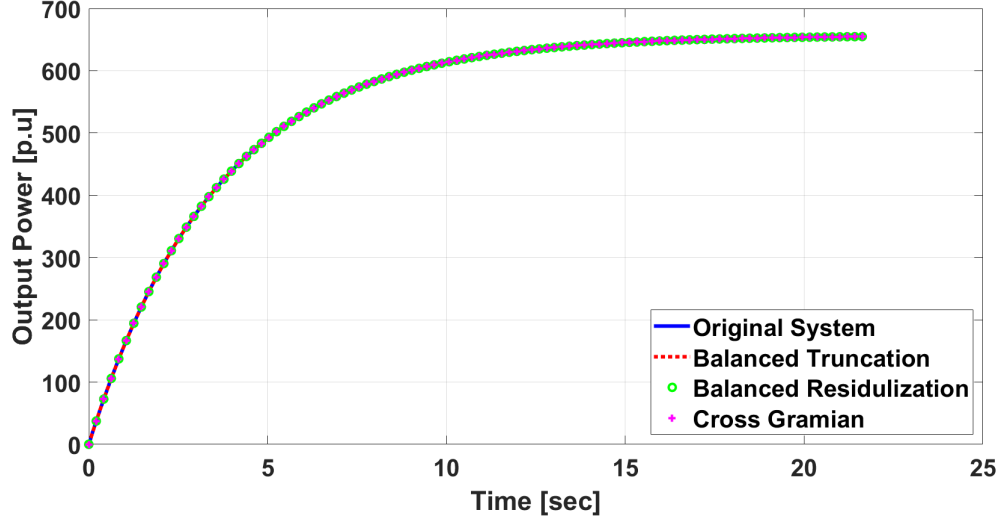
Figure 3.2: Step responses of reduced-order system models for a wind farm comprising 300 non-identical uniformly distributed WTs

Reduction Method	Number of Turbines in the Farm			
	60	120	240	300
Balanced Truncation	2.166×10^{-4}	1.871×10^{-4}	6.581×10^{-4}	0.0012
Residulization	7.193×10^{-4}	6.297×10^{-4}	0.0022	0.0024
Cross Gramian	4.543×10^{-3}	0.0028	0.0113	0.0180

Table 3.11: Maximum absolute errors in the step responses of reduced wind farms comprising different numbers of non-identical normally distributed WTs

Reduction Method	Number of Turbines in the Farm			
	60	120	240	300
Balanced Truncation	2.62×10^{-5}	3.31×10^{-5}	1.23×10^{-4}	-4.43×10^{-6}
Residulization	1.42×10^{-5}	-7.22×10^{-6}	-6.34×10^{-6}	7.56×10^{-5}
Cross Gramian	9.91×10^{-4}	3.73×10^{-4}	0.0018	0.0047

Table 3.12: Mean errors in the step responses of reduced wind farms comprising different numbers of non-identical normally distributed WTs
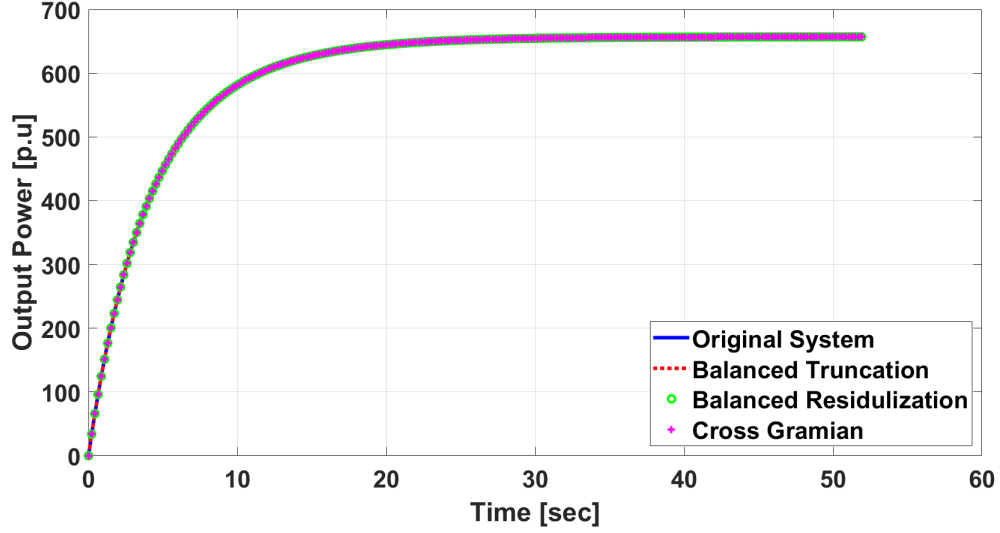
Figure 3.3: Step responses of reduced-order system models for a wind farm comprising 300 non-identical normally distributed WTs

3.5   Conclusions

In this chapter, we discussed the reduced models of wind farms of different sizes using the balancing techniques and the cross Gramian method. The cross Gramian truncation method behaves in a similar manner to the balanced truncation method, i.e., the error has relatively higher values at the low and mid frequencies and relatively low values at high frequencies. The order of the reduced system depends, significantly, on the selected threshold value. However, the system produced by the cross Gramian truncation method seems to be less accurate than the corresponding reduced system obtained using the balancing techniques. Nevertheless, the cross Gramian method reduces the computational complexity by calculating only one Gramian without the need for balancing. Furthermore, examining the degree of controllability and observability of the system, in both the vector and diagonal forms of the control input matrix, showed a considerable loss of controllability and observability in the case of the latter form.

Chapter 4

Optimal Control of Wind Turbine Systems via Time-Scale Decomposition

4.1   Introduction

Wind turbines, having mechanical and electrical components, are known to operate in at least two time-scales: the slow time scale, in which mechanical state variables evolve, and the fast time scale, in which electrical and electronic state variables evolve. The result is the "stiff" numerical problem that occurs naturally in power systems due to the presence of "parasitic" parameters, such as small time constants, masses, resistances, inductances, capacitances, moments of inertia, etc. Singular perturbation methods eliminate the stiffness problem and decouple the mathematical model of the original system into slow and fast reduced-order subsystems. A reduced-order system can be obtained by ignoring the fast subsystem and compensating for its effect by introducing a "boundary layer" correction to the slow subsystem towards a better approximation of the original system. Various methods have been proposed [54,78] to obtain the exact slow and fast subsystems. The Chang transformation [79] has been widely used to get the exact pure-slow and pure-fast subsystems, even when the perturbation parameter ϵ is not very small. Moreover, a number of recursive algorithms [14,80,81] have been developed to avoid the problems involving ill-conditioned systems and to obtain an approximate solution to the ARE, which can be decomposed after that into slow and fast parts.

The main obstacles associated with the renewable resources are their intermittent behavior and their dependence on the geographical location and weather conditions. Such randomness and uncertainty introduce nonlinearities when modeling the system dynamics. Therefore, designing optimal and robust controllers is crucial to dealing

with all the nonlinearities and uncertainties associated with energy systems. Different control strategies that have been applied to WECS are reviewed in [82–84].

The most vital steps in optimal control problems are defining the objective function, which specifies a relationship between the state and control variables, and finding a control law that optimizes this function subject to the given constraints. Multi-objective optimization problems deal with more than one objective function simultaneously. Maximizing the extracted energy while minimizing the cost of production and fatigue damage is the most common setup in the literature involving multi-objective optimization problems of energy systems.

Optimal control of the WECS, based on time scale analysis, has been studied by many researchers [29–31, 85–87]. LQR and LQG controllers were designed in [85, 87] for deterministic and stochastic wind energy systems with permanent magnet synchronous generators using time-scale analysis. Independent linear optimal controllers were designed for the slow and fast subsystems of a DFIG-based wind turbine in [13, 31] by decomposing the algebraic Riccati equation of the singularly perturbed wind turbine system into two reduced-order AREs, corresponding to the slow and fast time scales. In [86], a WECS with Gaussian noise is decoupled into lower-order slow and fast subsystems. Then, slow and fast Kalman filters are designed separately to estimate the states along with their corresponding slow and fast model predictive controllers.

In this chapter, the method of singular perturbation will be used to design LQR, Kalman filter, and LQG optimal controllers in two independent time scales for a fifth-order, single-cage DFIG wind turbine. Here, the ARE of the singularly perturbed wind turbine system is decomposed into two reduced-order AREs that correspond to the slow and fast time scales. Using this method allows designing linear controllers for the slow and fast subsystems independently, thus, achieving complete separation and parallelism in the design process. The advantages of such an approach are alleviating the stiffness difficulties and reducing the computational complexities and dimensionality burdens resulting from the increased penetration of wind turbines to the power grid.

The rest of this chapter is organized as follows. The next section reviews the exact decomposition method of the ARE of the singularly perturbed system. The optimal

performance-invariance of the LQR under the similarity transformation is considered in Section 4.2.1. In Section 4.2.2, the slow and fast decomposition of the optimal performance criteria is provided. The Kalman filtering time scale analysis is reviewed in Section 4.3. The effect of the similarity transformation on the optimal performance of Kalman filter is derived in Section 4.3.1. In Section 4.4, optimal LQG control is discussed. The performance index of the LQG under the similarity transformation and LQG slow and fast optimal performance criteria are derived in Section 4.4.1 and 4.4.2, respectively. The state-space model of the fifth-order, single-cage DFIG wind turbine and the corresponding simulation results are presented in Section 4.5. The chapter is concluded in Section 4.6.

4.2 Exact Decomposition of the Algebraic Riccati Equation

Consider the linear singularly perturbed control system

$$\dot{x}_1(t) = A_1 x_1(t) + A_2 x_2(t) + B_1 u(t),$$
$$\epsilon \dot{x}_2(t) = A_3 x_1(t) + A_4 x_2(t) + B_2 u(t),$$

(4.1)

where $x_i(t) \in \Re^n$, $i = 1, 2$, $u(t) \in \Re^m$ are the state variables and control variables, respectively. ϵ is a small positive singular perturbation parameter that indicates system separation into slow and fast time scales. We assume that the singularly perturbed system (4.1) has the standard singular perturbation form [54]. Hence, the fast subsystem matrix A_4 is nonsingular, which is a standard assumption in the singular perturbation theory [54]. The corresponding linear-quadratic optimal control problem of (4.1) is defined by

$$\dot{x}_1(t) = A_1 x_1(t) + A_2 x_2(t) + B_1 u(t), \quad x_1(0) = x_{10}$$
$$\epsilon \dot{x}_2(t) = A_3 x_1(t) + A_4 x_2(t) + B_2 u(t), \quad x_2(0) = x_{20}$$

(4.2)

where the control vector $u \in \Re^m$, has to be chosen such that the following performance criterion, J, is minimized

$$\min_u J = \min_u \frac{1}{2} \int_0^\infty \left\{ \begin{bmatrix} x_1(t) \\ x_2(t) \end{bmatrix}^T Q \begin{bmatrix} x_1(t) \\ x_2(t) \end{bmatrix} + u^T(t) R u(t) \right\} dt \qquad (4.3)$$

where $R > 0$ and $Q \geq 0$ are the weighting matrices. The optimizing performance criterion (4.3) of the closed-loop optimal control problem, subject to the singularly perturbed system differential equation (4.2), has the solution

$$u(t) = -R^{-1} B^T P_r x(t) = -F_1 x_1 - F_2 x_2 \qquad (4.4)$$

where P_r is the positive semidefinite solution of the regulator algebraic Riccati equation given by [88]

$$0 = P_r A + A^T P_r + Q - P_r Z P_r, \qquad (4.5)$$

with

$$A = \begin{bmatrix} A_1 & A_2 \\ \frac{1}{\epsilon} A_3 & \frac{1}{\epsilon} A_4 \end{bmatrix}, \quad Q = \begin{bmatrix} Q_1 & Q_2 \\ Q_2^T & Q_3 \end{bmatrix} \qquad (4.6)$$

$$B = \begin{bmatrix} B_1 \\ \frac{1}{\epsilon} B_2 \end{bmatrix}, \quad P_r = \begin{bmatrix} P_{1r} & \epsilon P_{2r} \\ \epsilon P_{2r}^T & \epsilon P_{3r} \end{bmatrix}, \quad Z = B_1 R^{-1} B_2^T,$$

The optimal regulator gains F_1 and F_2 are given by

$$F_1 = R^{-1}(B_1^T P_{1r} + B_2^T P_{2r}^T),$$
$$F_2 = R^{-1}(\epsilon B_1^T P_{2r} + B_2^T P_{3r}). \qquad (4.7)$$

The solution of the algebraic Riccati equation (4.5) will be found in term of solutions of the reduced-order, pure slow and pure fast algebraic Riccati equation. For this purpose, a nonsingualr transformation $\boldsymbol{T}$ [55, 89] is applied for the state-costate equations such that they become completely decoupled as independent slow and fast

subsystems in the form

$$\dot{\zeta}_s(t) = (a_1 + a_2 P_{rs})\zeta_s(t)$$

$$\epsilon\dot{\zeta}_f(t) = (b_1 + b_2 P_{rf})\zeta_f(t)$$

(4.8)

where P_{rs} and P_{rf} are the unique solutions of the exact pure-slow and exact pure-fast completely decoupled algebraic regulator Riccati equations

$$0 = P_{rs}a_1 - a_4 P_{rs} - a_3 + P_{rs}a_2 P_{rs}$$

$$0 = P_{rf}b_1 - b_4 P_{rf} - b_3 + P_{rf}b_2 P_{rf}$$

(4.9)

Matrices $a_i, b_i, i = 1, 2, 3, 4$, can be found in [55, 89]. The nonsingular transformation $\boldsymbol{T}$ is given by

$$\boldsymbol{T} = (\Pi_1 + \Pi_2 P_r)$$

(4.10)

The slow and fast subsystems in the new coordinate are related by

$$\begin{bmatrix} \zeta_s(t) \\ \zeta_f(t) \end{bmatrix} = \boldsymbol{T} \begin{bmatrix} x_1(t) \\ x_2(t) \end{bmatrix}$$

(4.11)

Even more, the global solution P_r can be obtained from the reduced-order exact pure-slow and pure-fast algebraic Riccati equations, that is

$$P_{rsf} = \left(\Omega_3 + \Omega_4 \begin{bmatrix} P_{rs} & 0 \\ 0 & P_{rf} \end{bmatrix} \right) \left(\Omega_1 + \Omega_2 \begin{bmatrix} P_{rs} & 0 \\ 0 & P_{rf} \end{bmatrix} \right)^{-1}$$

(4.12)

Known matrices Ω_i, $i = 1, 2, 3, 4$, and Π_1, Π_2 are given in terms of solutions of the Chang decoupling equations [55, 89].

4.2.1 Optimal Performance Invariance to Similarity Transformation

It has been shown in [53] that similarity transformation preserves the optimal performance criteria for the linear quadratic regulator LQR, such that its optimal values in the two coordinate systems are equivalent. This results can be derived briefly as follows

The similarity transformation for the linear quadratic optimal control problem can be derived as fellows

$$
\left.\begin{aligned}
\dot{x} &= Ax + Bu,, \\
x(0) &= x_0, \\
J &= \tfrac{1}{2}\int_0^\infty \left(x^T Q x + u^T R u\right) dt \\
J_{opt} &= \tfrac{1}{2}x_0 P x_0 \\
A^T P + PA + Q - PBR^{-1}B^T P &= 0
\end{aligned}\right\}
\xrightarrow{\ \bar{x} = Tx\ }
\left\{\begin{aligned}
\dot{\bar{x}} &= \bar{A}\bar{x} + \bar{B}u, \\
\bar{x}_0 &= Tx_0, \\
\bar{J} &= \tfrac{1}{2}\int_0^\infty \left(\bar{x}^T \bar{Q}\bar{x} + u^T R u\right) dt \\
\bar{J}_{opt} &= \tfrac{1}{2}\bar{x}_0 \bar{P}\bar{x}_0 \\
\bar{A}\bar{P} + \bar{P}\bar{A} + \bar{Q} - \bar{P}\bar{B}R^{-1}\bar{B}^T \bar{P} &= 0
\end{aligned}\right.
$$

Derivations:

$$
\dot{\bar{x}} = T\dot{x} = TAx + TBu = TAT^{-1}\bar{x} + TBu, \tag{4.13}
$$

$$
\bar{A} = TAT^{-1}, \quad \bar{B} = TB, \quad \bar{Q} = T^{-T}QT, \tag{4.14}
$$

$$
\bar{A}\bar{P} + \bar{P}\bar{A} + \bar{Q} - \bar{P}\bar{B}R^{-1}\bar{B}^T\bar{P} = 0 \tag{4.15}
$$

$$
T^{-T}A^T T^T \bar{P} + \bar{P}TAT^{-1} + \bar{Q} - \bar{P}TBR^{-1}B^T T^T \bar{P} = 0 \tag{4.16}
$$

Multiplying by T^T from the left and by T from the right we get

$$
A^T T^T \bar{P}T + T^T \bar{P}TA + T^T \bar{Q}T - T^T \bar{P}TBR^{-1}B^T T^T \bar{P}P = 0 \tag{4.17}
$$

define $P = T^T \bar{P}T, \quad \bar{P} = T^{-T}PT^{-1}$, then

$$
A^T P + PA + Q - PBR^{-1}B^T P = 0 \tag{4.18}
$$

$$
\bar{J}_{opt} = \frac{1}{2}\bar{x}_0 \bar{P}\bar{x}_0 = \frac{1}{2}x_0^T T^T T^{-T}PT^{-1}Tx_0 = \frac{1}{2}x_0^T P x_0 \tag{4.19}
$$

$$
\bar{J}_{opt} = J_{opt} \tag{4.20}
$$

4.2.2 Slow and Fast Decomposition of the Optimal Performance Criteria

In this section, we calculate the minimized optimal performance J_{opt} for the slow and fast subsystems of the LQR problem. As stated in the previous section, using the nonsingular transformation defined in (4.10) does not change the value of the optimal performance. Therefore, by adding the slow and fast performance indices, we get the total optimal performance J_{opt} obtained in the original coordinates. The quadratic performance criterion to be minimized, calculated in the new coordinates, is given by

$$J = \frac{1}{2} \int_0^\infty \left\{ x^T Q x + u^T R u \right\} dt = \frac{1}{2} \int_0^\infty \left\{ x^T(t)(Q + PSP)x(t) \right\} dt \tag{4.21}$$

$$x(t) = (\Pi_1 + \Pi_2 P)^{-1} \begin{bmatrix} \eta_1(t) \\ \zeta_1(t) \end{bmatrix} = \boldsymbol{T}^{-1} \begin{bmatrix} \eta_1(t) \\ \zeta_1(t) \end{bmatrix} \tag{4.22}$$

$$\begin{aligned} J &= \frac{1}{2} \int_0^\infty \begin{bmatrix} \eta_1(t) \\ \zeta_1(t) \end{bmatrix} T^{-1}(Q + PSP)T \begin{bmatrix} \eta_1(t) \\ \zeta_1(t) \end{bmatrix} dt \\ &= \frac{1}{2} \int_0^\infty \begin{bmatrix} \eta_1(t) \\ \zeta_1(t) \end{bmatrix} \begin{bmatrix} Q_1 & Q_2 \\ Q_2^T & Q_3 \end{bmatrix} \begin{bmatrix} \eta_1(t) \\ \zeta_1(t) \end{bmatrix} dt \end{aligned} \tag{4.23}$$

$$\begin{aligned} \dot{\zeta}_1(t) &= (a_1 + a_2 P_s)\zeta_1(t) \\ \epsilon\dot{\zeta}_2(t) &= (b_1 + b_2 P_f)\zeta_2(t) \end{aligned} \tag{4.24}$$

$$J = \frac{1}{2} \begin{bmatrix} \eta_1(0) \\ \zeta_1(0) \end{bmatrix}^T V \begin{bmatrix} \eta_1(0) \\ \zeta_1(0) \end{bmatrix}, \quad A^T V + V A + \theta = 0 \tag{4.25}$$

$$J = \frac{1}{2} \begin{bmatrix} \eta_1^T(0) & \zeta_1^T(0) \end{bmatrix} \begin{bmatrix} v_1 & \epsilon v_2 \\ \epsilon v_2^T & \epsilon v_3 \end{bmatrix} \begin{bmatrix} \eta_1(0) \\ \zeta_1(0) \end{bmatrix} \tag{4.26}$$

$$J = \frac{1}{2}[\eta_1^T(0)v_1 + \epsilon\zeta_1^T(0)v_2^T \;\; \vdots \;\; \epsilon\eta_1^T(0)v_2 + \epsilon\zeta_1^T(0)v_3] \begin{bmatrix} \eta_1(0) \\ \zeta_1(0) \end{bmatrix} \tag{4.27}$$

$$J = \frac{1}{2}\eta_1^T(0)v_1\eta_1(0) + \frac{1}{2}\epsilon\zeta_1^T(0)v_2^T\eta_1(0) + \frac{1}{2}\epsilon\eta_1^T(0)v_2\zeta_1(0) + \frac{1}{2}\epsilon\zeta_1^T(0)v_3\zeta_1(0) \tag{4.28}$$

$$J = \underbrace{\frac{1}{2}\eta_1^T(0)v_1\eta_1(0)}_{J_{s-opt}} + \underbrace{\epsilon\eta_1^T(0)v_2\zeta_1(0)}_{J_{sf-opt}} + \underbrace{\frac{1}{2}\epsilon\zeta_1^T(0)v_3\zeta_1(0)}_{J_{f-opt}} \tag{4.29}$$

$$J_{opt} = J_{s-opt} + J_{sf-opt} + J_{f-opt} \tag{4.30}$$

$$J_{s-opt} = \frac{1}{2}\eta_1^T(0)v_1\eta_1(0) = \frac{1}{2}\text{tr}\{v_1\eta_1(0)\eta_1^T(0)\} \tag{4.31}$$

$$J_{f-opt} = \frac{\epsilon}{2}\zeta_1^T(0)v_3\zeta_1(0) = \frac{\epsilon}{2}\text{tr}\{v_3\zeta_1(0)\zeta_1^T(0)\} \tag{4.32}$$

$$J_{sf-opt} = \epsilon\eta_1^T(0)v_2\zeta_1(0) = \epsilon\text{tr}\{v_2\zeta_1(0)\eta_1^T(0)\} \tag{4.33}$$

Formula (4.29) constitutes an exact decomposition for the optimal performance criterion into slow and fast components. It can be concluded from (4.29) that the contribution the slow subsystem makes to the performance criterion is $O(1)$, whereas that the fast subsystem makes is only $O(\epsilon)$. Note also that J_{sf-opt} can be negative since v_2 is generally not a square matrix, and in the case it is, it would still be indefinite.

4.3   Kalman Filtering Time Scale Analysis

In this section, an optimal Kalman filter is designed towards estimating the state variables of the wind energy systems with DFIG. Using the duality property between the optimal filter and regulator, the same decomposition method presented in previous section can be applied here so that the optimal Kalman filter is completely decoupled into the pure-slow and pure-fast local filters both driven by the system measurements [88]. Consider the linear continuous-time invariant singularly perturbed stochastic system

$$\dot{x}_1(t) = A_1x_1(t) + A_2x_2(t) + B_1u(t) + G_1w_1(t), \quad E\{x_1(0)\} = x_{10}$$
$$\epsilon\dot{x}_2(t) = A_3x_1(t) + A_4x_2(t) + B_2u(t) + G_2w_1(t), \quad E\{x_2(0)\} = x_{20} \tag{4.34}$$
$$y(t) = C_1x_1(t) + C_2x_2(t) + w_2(t)$$

with the performance criterion

$$J = \lim_{t_f \to \infty} \frac{1}{t_f} \left\{ \int_0^t \left[z^T(t)z(t) + u^T(t)Ru(t) \right] dt \right\}, \quad R > 0 \qquad (4.35)$$

where $x_1(t) \in \Re_1^n$, and $x_2(t) \in \Re_2^n$, are slow and fast state variables, respectively. $u(t) \in \Re^m$ is the control input, $y(t) \in \Re^p$ are system measurements. $w_1(t) \in \Re^r$ and $w_2(t) \in \Re^p$ are zero-mean stationary, white Gaussian noise stochastic process with intensities $W_1 > 0$ and $W_2 > 0$, respectively. $z(t) \in \Re^s$, is the controlled system output given by

$$z(t) = D_1 x_1(t) + D_2 x_2(t) \qquad (4.36)$$

All matrices are of appropriate dimensions and assumed to be constant. The optimal control law for (4.34) with the performance criterion (4.35) is given by

$$u_{opt}(t) = -F_1 \hat{x}_1(t) - F_2 \hat{x}_2(t) \qquad (4.37)$$

where $\hat{x}_1(t)$ and $\hat{x}_2(t)$ are the optimal estimates of the state vectors $x_1(t)$ and $x_1(t)$ obtained from the Kalman filter

$$\dot{\hat{x}}_1(t) = A_1 \hat{x}_1(t) + A_2 \hat{x}_2(t) + B_1 u(t) + K_1 v(t)$$
$$\epsilon \dot{\hat{x}}_2(t) = A_3 \hat{x}_1(t) + A_4 \hat{x}_2(t) + B_2 u(t) + K_2 v(t) \qquad (4.38)$$
$$v(t) = y(t) - C_1 \hat{x}_1(t) - C_2 \hat{x}_2(t)$$

The optimal global Kalman filter (4.38) can be put in the form in which the filter is driven by the system measurements and optimal control inputs, that is

$$\dot{\hat{x}}_1(t) = (A_1 - K_1 C_1)\hat{x}_1(t) + (A_2 - K_1 C_2)\hat{x}_2(t) + B_1 u(t) + K_1 y(t)$$
$$\epsilon \dot{\hat{x}}_2(t) = (A_3 - K_2 C_1)\hat{x}_1(t) + (A_4 - K_2 C_2)\hat{x}_2(t) + B_2 u(t) + K_2 y(t) \qquad (4.39)$$

where the optimal filter gains K_1 and K_2 are obtained from

$$K_1 = (P_{1F}C_1^T + P_{2F}C_2^T)W_2^{-1}$$
$$K_2 = (\epsilon P_{2F}^T C_1^T + P_{3F}C_2^T)W_2^{-1}$$

(4.40)

matrices P_{1F}, P_{2F} and P_{3F} define the positive semidefinite stabilizing solution of the filter algebraic Riccati equation

$$AP_F + P_F A^T - P_F S P_F + G W_1 G^T = 0$$

(4.41)

where

$$A = \begin{bmatrix} A_1 & A_2 \\ \frac{1}{\epsilon}A_3 & \frac{1}{\epsilon}A_3 \end{bmatrix}, \quad G = \begin{bmatrix} G_1 \\ \frac{1}{\epsilon}G_2 \end{bmatrix}, \quad S = C^T W_2^{-1} C, \quad P_F = \begin{bmatrix} P_{1F} & P_{2F} \\ P_{2F}^T & \frac{1}{\epsilon}P_{3F} \end{bmatrix}$$

(4.42)

Using duality, the following matrices have to be formed (see [55, 89])

$$T_{1F} = \begin{bmatrix} A_1^T & -C_1^T W_2^{-1} C_1 \\ -G_1 W_1 G_1^T & -A_1 \end{bmatrix}, \quad T_{2F} = \begin{bmatrix} A_3^T & -C_1^T W_2^{-1} C_2 \\ -G_1 W_1 G_2^T & -A_2 \end{bmatrix},$$

$$T_{3F} = \begin{bmatrix} A_2^T & -C_2^T W_2^{-1} C_1 \\ -G_2 W_1 G_1^T & -A_3 \end{bmatrix}, \quad T_{4F} = \begin{bmatrix} A_4^T & -C_2^T W_2^{-1} C_2 \\ -G_2 W_1 G_2^T & -A_4 \end{bmatrix},$$

(4.43)

The partitions and scaling have to be used here, $x^T(t) = [x_1^T(t) \quad \epsilon x_2^T(t)]$ and $p^T(t) = [p_1^T(t) \quad p_2^T(t)]$. Since matrices T_{1F}, T_{2F}, T_{3F}, and T_{4F} correspond to the system matrices of a singularly perturbed linear system, the slow-fast decomposition is achieved by using the Chang decoupling equations

$$T_{4F}M - T_{3F} - \epsilon M(T_{1F} - T_{2F}M) = 0$$
$$-N(T_{4F} + \epsilon M T_{2F}) + T_{2F} + \epsilon(T_{1F} - T_{2F}M)N = 0$$

(4.44)

Using the following permutation matrices,

$$
E_{1F} = \begin{bmatrix} I_{n_1} & 0 & 0 & 0 \\ 0 & 0 & I_{n_1} & 0 \\ 0 & \frac{1}{\epsilon}I_{n_2} & 0 & 0 \\ 0 & 0 & 0 & I_{n_2} \end{bmatrix}, \quad E_{2F} = \begin{bmatrix} I_{n_1} & 0 & 0 & 0 \\ 0 & 0 & I_{n_1} & 0 \\ 0 & I_{n_2} & 0 & 0 \\ 0 & 0 & 0 & I_{n_2} \end{bmatrix} \tag{4.45}
$$

we can define

$$
\Pi_F = \begin{bmatrix} \Pi_{1F} & \Pi_{2F} \\ \Pi_{3F} & \Pi_{4F} \end{bmatrix} = E_{2F}^T \begin{bmatrix} I_{2n_1} - \epsilon NM & -\epsilon N \\ M & I_{2n_2} \end{bmatrix} E_{1F} \tag{4.46}
$$

Then, the desired transformation is given by

$$
\boldsymbol{T_2} = (\Pi_{1F} + \Pi_{2F}P_F) \tag{4.47}
$$

where P_F is the solution of the ARE (4.41). M and N are the solution of the Chang decoupling algebraic equations (4.44). The transformation $\boldsymbol{T_2}$ is applied to the filter variables as

$$
\begin{bmatrix} \hat{\eta}_s(t) \\ \hat{\eta}_f(t) \end{bmatrix} = \boldsymbol{T_2}^{-T} \begin{bmatrix} \hat{x}_1(t) \\ \hat{x}_2(t) \end{bmatrix} \tag{4.48}
$$

4.3.1 Kalman Filter Under Similarity Transformation

To determine the gain of Kalman filter in the new coordinates under a similarity transformation, the same strategy used in Section 4.2.1 is applied here

$$
\begin{aligned}
\dot{x}(t) &= Ax(t) + Gw_1(t), \quad x(0) = x_0 \\
y(t) &= Cx(t) + w_2(t)
\end{aligned} \tag{4.49}
$$

$$
\dot{\hat{x}} = (A - KC)\hat{x} + Ky, \quad K = P_F C^T W_2, \quad E\{\hat{x}(0)\} = x_0 \tag{4.50}
$$

$$
AP_F + P_F A^T + GW_1 G^T - P_F C W_2^{-1} C^T P_F = 0 \tag{4.51}
$$

$$\dot{\bar{x}}(t) = \bar{A}\bar{x}(t) + \bar{G}w_1(t), \quad x(0) = x_0$$

$$y(t) = \bar{C}\bar{x}(t) + w_2(t), \tag{4.52}$$

$\bar{G} = TG, \quad \bar{C} = CT^{-1}$, in the new coordinates $\bar{K} = \bar{P}_F \bar{C}^T W_2$ and

$$\bar{A}\bar{P}_F + \bar{P}_F \bar{A}^T + \bar{G}W_1 \bar{G}^T - \bar{P}_F \bar{C}^T W_2^{-1} \bar{C}\bar{P}_F = 0 \tag{4.53}$$

$$TAT^{-1}\bar{P}_F + \bar{P}_F T^{-T} A^T T^T + TGW_1 G^T T^T - \bar{P}_F T^{-T} C^T W_2^{-1} CT^{-1}\bar{P}_F = 0 \tag{4.54}$$

Multiplying by T^{-1} from the left and by T^{-T} from the right we get

$$AT^{-1}\bar{P}_F T^{-T} + T^{-1}\bar{P}_F T^{-T} A^T + GW_1 G^T - T^{-1}\bar{P}_F T^{-T} C^T W_2^{-1} CT^{-1}\bar{P}_F T^{-T} = 0 \tag{4.55}$$

$$\bar{K} = TP_F T^T T^{-T} C^T W_2 = TP_F C^T W_2 = TK \tag{4.56}$$

where $P_F = T^{-1}\bar{P}_F T^{-T}, \quad \bar{P} = TP_F T^T$

4.4 Optimal Linear-Quadratic Gaussian Control

In order to obtain the solution of the linear-quadratic Gaussian LQG control problem of a singularly perturbed DFIG wind turbine system, it is necessary to obtain gain matrices of the the optimal LQR and Kalman filters. In this section, the results of Sections 4.2 and 4.3 are utilized by solving the pure-slow and pure-fast, reduced-order AREs and by implementing the pure-slow and pure-fast, reduced-order Kalman filters. Using the separation principle for linear stochastic control, an optimal LQG controller can be designed for slow and fast subsystems independently, thus, achieving complete separation and parallelism in the design process. The structure of a LQG controller with a decoupled slow and fast subsystems of the LQR and Kalman filter is shown in Figure 4.1. The decoupled pure-slow and pure-fast local Kalman filters driven by

system measurements and system control inputs are given by

$$\dot{\hat{\eta}}_s(t) = (a_{1F} + a_{2F}P_{sF})^T \hat{\eta}_s(t) + B_s u(t) + K_s y(t)$$

$$\epsilon \dot{\hat{\eta}}_f(t) = (b_{1F} + b_{2F}P_{fF})^T \hat{\eta}_f(t) + B_f u(t) + K_f y(t)$$

(4.57)

where P_{sF} and P_{fF} are the solutions of the following AREs

$$0 = P_{sF}a_{1F} - a_{4F}P_{sF} - a_{3F} + P_{sF}a_{2F}P_{sF}$$

$$0 = P_{fF}b_{1F} - b_{4F}P_{fF} - b_{3F} + P_{fF}b_{2F}P_{fF}$$

(4.58)

The pure-slow and pure-fast filter gains, K_s, K_f are defined by

$$\begin{bmatrix} K_s \\ \frac{1}{\epsilon}K_f \end{bmatrix} = \boldsymbol{T_2^{-T}} \begin{bmatrix} K_1 \\ \frac{1}{\epsilon}K_2 \end{bmatrix}$$

(4.59)

and the remaining matrices are given by

$$\begin{bmatrix} a_{1F} & a_{2F} \\ a_{3F} & a_{4F} \end{bmatrix} = (T_{1F} - T_{2F}M), \quad \begin{bmatrix} b_{1F} & b_{2F} \\ b_{3F} & b_{4F} \end{bmatrix} = (T_{4F} + \epsilon M T_{2F})$$

(4.60)

In addition, the pure-slow and pure-fast system input matrices are

$$\begin{bmatrix} B_s \\ \frac{1}{\epsilon}B_f \end{bmatrix} = \boldsymbol{T_2^{-T}} \begin{bmatrix} B_1 \\ \frac{1}{\epsilon}B_2 \end{bmatrix}$$

(4.61)

The feedback control in the new coordinates is given

$$u_{opt}(t) = -F\hat{x}(t) = -F\boldsymbol{T_2^{-T}} \begin{bmatrix} \hat{\eta}_s(t) \\ \hat{\eta}_f(t) \end{bmatrix} = - \begin{bmatrix} F_s & F_f \end{bmatrix} \begin{bmatrix} \hat{\eta}_s(t) \\ \hat{\eta}_f(t) \end{bmatrix}$$

(4.62)

where F_s and F_f are obtained from

$$\begin{bmatrix} F_s & F_f \end{bmatrix} = F\boldsymbol{T_2}^T = R^{-1}B^T P(\Pi_{1F} + \Pi_{2F}P_F)^T$$

(4.63)
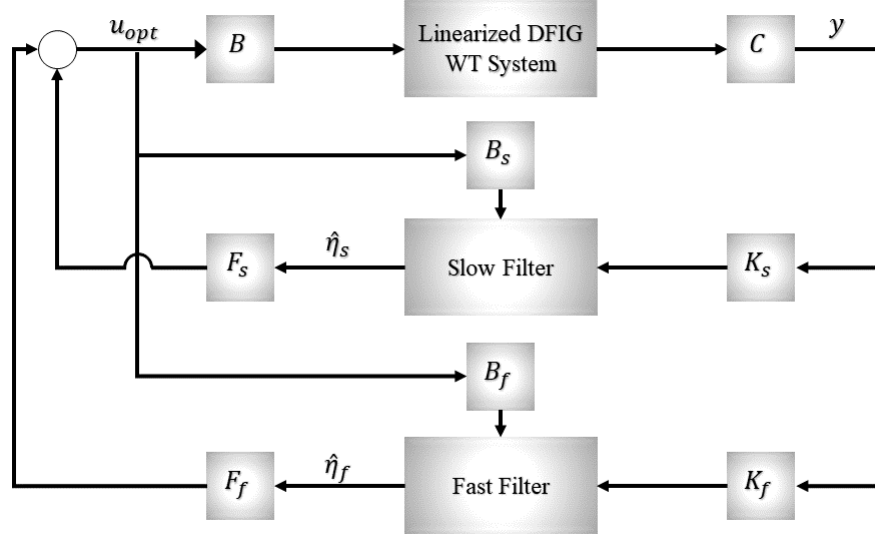
Figure 4.1: Slow-fast LQG controller structure for DFIG wind turbine system.

4.4.1 LQG under Similarity Transformation

The optimal performance index J_{opt} of the LQG follows from the known formula

$$
\begin{aligned}
J_{opt} &= \text{tr}\Big\{ PKW_2K^T + P_FD^TD \Big\} \\
&= \text{tr}\Big\{ PGW_1G^T + P_FF^TRF \Big\}
\end{aligned}
\tag{4.64}
$$

Under the similarity transformation, the performance criteria can be derived as follows. Starting with the second line of (4.64)

$$
\bar{J}_{opt} = \text{tr}\Big\{ \bar{P}\bar{G}W_1\bar{G}^T + \bar{P}_F\bar{F}^TR\bar{F} \Big\}
\tag{4.65}
$$

$$
\bar{J}_{opt} = \text{tr}\Big\{ T^{-T}PT^{-1}TGW_1G^TT^T + TP_FT^TT^{-T}F^TRFT^{-1} \Big\}
\tag{4.66}
$$

where $P_F = T^{-1}\bar{P}_FT^{-T}, \quad \bar{P} = TP_FT^T, F = \bar{F}T$

$$
\bar{J}_{opt} = \text{tr}\Big\{ T^{-T}(PGW_1G^T)T^T + T(P_FF^TRF)T^{-1} \Big\} \neq J_{opt}
\tag{4.67}
$$

Similarly, for the first line in (4.64), we have

$$J_{opt} = \text{tr}\left\{PKW_2K^T + P_F D^T D\right\} \tag{4.68}$$

where $D^T D = Q, \quad \bar{K} = TK$

$$\bar{J}_{opt} = \text{tr}\left\{\bar{P}\bar{K}W_2\bar{K}^T + \bar{P}_F\bar{Q}\right\} \tag{4.69}$$

$$\bar{J}_{opt} = \text{tr}\left\{T^{-T}PT^{-1}TKW_2K^TT^T + TP_FT^TT^{-T}QT^{-1}\right\} \tag{4.70}$$

$$\bar{J}_{opt} = \text{tr}\left\{T^{-T}(PKW_2K^T)T^T + T(P_FQ)T^{-1}\right\} \neq J_{opt} \tag{4.71}$$

Hence, the similarity transformation does not preserve the optimal performance LQG criteria value.

4.4.2   LQG Slow Fast Optimal Performance Criteria

Based on the method proposed in [55], the optimal performance index for the slow and fast subsystems of the LQG controller can be obtained separately as follows

$$J_{opt} = \text{tr}\left\{PKW_2K^T + P_F D^T D\right\} \tag{4.72}$$

where $D^T D = Q; \quad Q = \begin{bmatrix} Q_1 & Q_2 \\ Q_2^T & Q_3 \end{bmatrix}$

$$P = \begin{bmatrix} P_1 & \epsilon P_2 \\ \epsilon P_2^T & \epsilon P_3 \end{bmatrix}, \quad K = \begin{bmatrix} K_1 \\ \frac{1}{\epsilon}K_2 \end{bmatrix}, \quad P_F = \begin{bmatrix} P_{1F} & P_{2F} \\ P_{2F}^T & \frac{1}{\epsilon}P_{3F} \end{bmatrix} \tag{4.73}$$

$$J_{opt} = \text{tr}\left\{\begin{bmatrix} P_1 & \epsilon P_2 \\ \epsilon P_2^T & \epsilon P_3 \end{bmatrix}\begin{bmatrix} K_1 \\ \frac{1}{\epsilon}K_2 \end{bmatrix}W_2\begin{bmatrix} K_1^T & \frac{1}{\epsilon}K_2^T \end{bmatrix} + \begin{bmatrix} P_{1F} & P_{2F} \\ P_{2F}^T & \frac{1}{\epsilon}P_{3F} \end{bmatrix}\begin{bmatrix} Q_1 & Q_2 \\ Q_2^T & Q_3 \end{bmatrix}\right\} \tag{4.74}$$

$$
=\text{tr}\left\{ \begin{bmatrix} P_1 & \epsilon P_2 \\ \epsilon P_2^T & \epsilon P_3 \end{bmatrix} \begin{bmatrix} K_1 w_2 K_1^T & \frac{1}{\epsilon} K_1 w_2 K_2^T \\ \frac{1}{\epsilon} K_2 w_2 K_1^T & \frac{1}{\epsilon^2} K_2 w_2 K_2^T \end{bmatrix} + \right.
$$
$$
\left. \begin{bmatrix} P_{1F} Q_1 + \epsilon P_{2F} Q_2^T & \epsilon P_{1F} Q_2 + \epsilon P_{2F} Q_3 \\ P_{2F}^T Q_1 + P_{3F} Q_2^T & P_{2F}^T Q_2 + P_{3F} Q_3 \end{bmatrix} \right. \tag{4.75}
$$

$$
=\text{tr}\left\{ \begin{bmatrix} P_1 K_1 W_2 K_1^T + P_2 K_2 W_2 K_1^T & \frac{1}{\epsilon} P_1 K_1 W_2 K_2^T + \frac{1}{\epsilon} P_2 K_2 W_2 K_2^T \\ \epsilon P_2^T K_1 W_2 K_1^T + P_3 K_2 W_2 K_1^T & P_2^T K_1 W_2 K_2^T + \frac{1}{\epsilon} P_3 K_2 W_2 K_2^T \end{bmatrix} + \right.
$$
$$
\left. \begin{bmatrix} P_{1F} Q_1 + \epsilon P_{2F} Q_2^T & \epsilon P_{1F} Q_2 + \epsilon P_{2F} Q_3 \\ P_{2F}^T Q_1 + P_{3F} Q_2^T & P_{2F}^T Q_2 + P_{3F} Q_3 \end{bmatrix} \right\} \tag{4.76}
$$

$$
=\text{tr}\left\{ P_1 K_1 W_2 K_1^T + P_2 K_2 W_2 K_1^T + P_{1F} Q_1 + \epsilon P_{2F} Q_2^T \right\} +
$$
$$
\text{tr}\left\{ P_2^T K_1 W_2 K_2^T + \frac{1}{\epsilon} P_3 K_2 W_2 K_2^T + \epsilon P_{2F}^T Q_2 + P_{3F} Q_3 \right\} \tag{4.77}
$$

$$
= \text{tr}\left\{ P_1 K_1 W_2 K_1^T + 2 P_2 K_2 W_2 K_1^T + P_{1F} Q_1 + 2\epsilon P_{2F} Q_2^T + +\epsilon P_{3F} Q_3 + \frac{1}{\epsilon} P_3 K_2 W_2 K_2^T \right\} \tag{4.78}
$$

$$
J_{opt} = \underbrace{\text{tr}\left\{ P_1 K_1 W_2 K_1^T + P_{1F} Q_1 \right\}}_{J_{s-opt}} + \underbrace{2\text{tr}\left\{ P_2 K_2 W_2 K_1^T + \epsilon P_{2F} Q_2^T \right\}}_{J_{sf-opt}}
$$
$$
+ \underbrace{\frac{1}{\epsilon}\text{tr}\left\{ P_3 K_2 W_2 K_2^T + \epsilon P_{3F} Q_3 \right\}}_{J_{f-opt}} \tag{4.79}
$$

$$
J_{s-opt} = \text{tr}\left\{ P_1 K_1 W_2 K_1^T + P_{1F} Q_1 \right\} \tag{4.80}
$$

$$
J_{f-opt} = \frac{1}{\epsilon}\text{tr}\left\{ P_3 K_2 W_2 K_2^T + \epsilon P_{3F} Q_3 \right\} \tag{4.81}
$$

$$
J_{sf-opt} = 2\text{tr}\left\{ P_2 K_2 W_2 K_1^T + \epsilon P_{2F} Q_2^T \right\} \tag{4.82}
$$

The formula for the optimal performance criterion (4.79) exactly decomposes the optimal performance criteria of the LQG controller into slow and fast components and *it shows that in the optimal LQG, the performance criteria is dominated by the fast subsystem.*

4.5   Simulation Results

In this chapter, the current model of a single-cage DFIG wind turbine reported in [9,10] is considered. Recall the swing equation (2.6) for the one-mass derive train model explained in Chapter 2. For a simplified mathematical model, all equations of the induction generator are derived using the direct-quadrature (d-q) transformation. The stator and rotor voltage equations in d-q synchronous reference frame are given in (2.12) and (2.13), respectively. The following assumptions were imposed:

- The stator current is assumed to be negative when flowing toward the machine.

- The q-axis is 90° ahead of the d-axis with respect to the direction of rotation.

The general linearized state-space current model is given by

$$\dot{x}(t) = Ax(t) + Bu(t)$$
$$y(t) = Cx(t) + Du(t)$$

(4.83)

where A, B, C, and D represent the system state, input, output, and feed forward matrices, respectively. The state-space variables, inputs and outputs of the fifth-order single cage DFIG wind turbine can be described by the following vectors

$$\dot{x} = \begin{bmatrix} i_{ds} & i_{qs} & i_{dr} & i_{qr} \end{bmatrix}^T$$
$$u = \begin{bmatrix} v_{ds} & v_{qs} & v_{dr} & v_{qr} \end{bmatrix}, \quad y = \begin{bmatrix} i_{dr} & i_{qr} \end{bmatrix},$$

(4.84)

where the state variables x are the rotor and stator currents, the control signals u are the input voltages and the outputs of the system y are the rotor currents in the d-axis and q-axis, respectively. In terms of state variables, the electromechanical torque can

be formulated as

$$T_e = L_m(i_{dr}i_{qs} - i_{qr}i_{ds}) \tag{4.85}$$

using (2.6) and (4.85) we get

$$\dot{\omega}_m = \frac{T_m}{2H_t} + \frac{L_m}{2H_t}(i_{qr}i_{ds} - i_{dr}i_{qs}) \tag{4.86}$$

The state-space model of the fifth-order single cage DFIG wind turbine is obtained by integrating equations (4.84)-(4.86). The new state variables, control signal and outputs are given as follows

$$\dot{x} = \begin{bmatrix} i_{ds} & i_{qs} & i_{dr} & i_{qr} & \omega_m \end{bmatrix}^T$$
$$u = \begin{bmatrix} v_{ds} & v_{qs} & v_{dr} & v_{qr} & T_m \end{bmatrix}, \quad y = \begin{bmatrix} i_{dr} & i_{qr} \end{bmatrix}, \tag{4.87}$$

The linearized system, control and output matrices A, B, and C, evaluated at the system's operating points, are characterized by [9, 10, 90]

$$A = K_G \cdot \begin{bmatrix} -R_s L_r & \alpha_1 \omega_s & -R_r L_m & -\beta_r \omega_s & a_{15} \\ -\alpha_1 \omega_s & -R_s L_r & -\beta_r \omega_s & -R_r L_m & a_{25} \\ -R_s L_m & \beta_s \omega_s & -R_r L_s & -\alpha_2 \omega_s & a_{35} \\ -\beta_s \omega_s & -R_s L_m & \alpha_2 \omega_s & -R_r L_s & a_{45} \\ K_w i_{qr} & -K_w i_{dr} & -K_w i_{qs} & K_w i_{ds} & 0 \end{bmatrix},$$

$$B = K_G \cdot \begin{bmatrix} -L_r & 0 & L_m & 0 & 0 \\ 0 & -L_r & 0 & L_m & 0 \\ -L_m & 0 & L_s & 0 & 0 \\ 0 & -L_m & 0 & L_s & 0 \\ 0 & 0 & 0 & 0 & \frac{1}{2H_t} \end{bmatrix}, \tag{4.88}$$

$$C = \begin{bmatrix} 0 & 0 & 1 & 0 & 0 \\ 0 & 0 & 0 & 1 & 0 \end{bmatrix}, \quad D = \begin{bmatrix} 0 & 0 & 0 & 0 & 0 \\ 0 & 0 & 0 & 0 & 0 \end{bmatrix}$$

where $\alpha_1 = L_s L_r - s L_m^2$, $\alpha_2 = L_m^2 - s L_s L_r$, $\beta_s = L_m L_s(1-s)$, $\beta_r = L_m L_r(1-s)$, $\sigma = 1 - L_m^2/L_r L_s$, $K_G = \omega_b(L_s L_r \sigma)^{-1}$, $K_w = L_m(2H_t K_G)^{-1}$, $a_{15} = L_m(L_m i_{qs} - L_r i_{qr})$,

$a_{25} = L_m(-L_m i_{ds} + L_r i_{dr}),\ \ a_{35} = L_s(L_m i_{qs} - L_r i_{qr}),\ \ a_{45} = L_s(-L_m i_{ds} + L_r i_{dr}).$

Appendices A.1-A.2 lists the parameters of the system and the DFIG, in addition to the operating points employed in the linearization procedure.

4.5.1 Slow-Fast Decomposition of the WT with DFIG System

Using the wind turbine state-space matrices defined in (4.88), the linearized system, control, and output matrices A, B, and C of the considered fifth-order WT-DFIG, evaluated at the system's operating points (see Appendices A.2- A.1 for the corresponding values), are given as

$$
A = \begin{bmatrix}
0.0260 & -17.4194 & 0.0285 & 16.824 & 0.538 \\
17.419 & 0.026 & -16.824 & 0.028 & -5.308 \\
0.0253 & -16.794 & 0.029 & 16.2094 & 0.551 \\
16.795 & 0.0253 & -16.209 & 0.029 & -5.432 \\
0.207 & -0.129 & -0.197 & -0.014 & 0
\end{bmatrix},
$$

$$
B = \begin{bmatrix}
5.320 & 0 & -5.189 & 0 & 0 \\
0 & 5.320 & 0 & -5.189 & 0 \\
5.189 & 0 & -5.311 & 0 & 0 \\
0 & 5.189 & 0 & -5.311 & 0 \\
0 & 0 & 0 & 0 & -0.187
\end{bmatrix},
$$

$$
C = \begin{bmatrix}
0 & 0 & 1 & 0 & 0 \\
0 & 0 & 0 & 1 & 0
\end{bmatrix}, \quad
D = \begin{bmatrix}
0 & 0 & 0 & 0 & 0 \\
0 & 0 & 0 & 0 & 0
\end{bmatrix}
$$

This DFIG system model is not expressed in the explicit standard singular perturbation form given in (4.1), where it can be noticed that ϵ, a small positive singular perturbation parameter, multiplies the derivatives of some states. Therefore, rearrangement for the rows of matrix A is necessary to ensure the nonsingularity of sub-matrix A_4 and that the system conforms to the explicit standard singular perturbation form (4.1). As described in Section 2.7, such can be established through the use of the Schur transformation. Furthermore, for the singularly perturbed form to conform to (4.1),

the order of the eigenvalues needs to be reversed, i.e., the following permutation matrix need to be employed

$$
P = \begin{bmatrix} 0 & 0 & 0 & 0 & 1 \\ 0 & 0 & 0 & 1 & 0 \\ 0 & 0 & 1 & 0 & 0 \\ 0 & 1 & 0 & 0 & 0 \\ 1 & 0 & 0 & 0 & 0 \end{bmatrix} \tag{4.89}
$$

The singularly perturbed form (4.1) can be established through the relations in (2.68), and using the wind turbine state space matrices defined in (4.88), the system matrices A, B, and C are given by

$$
A_{SP} = \begin{bmatrix} 0.860 & 0 & 0 & 0 & 0 \\ 0.252 & 0.050 & 0 & 0 & 0 \\ -1.390 & -1.007 & -0.839 & 0 & 0 \\ 14.552 & -30.084 & -8.485 & 0.019 & -0.606 \\ -29.236 & -10.565 & -12.575 & 1.674 & 0.019 \end{bmatrix},
$$

$$
B_{SP} = \begin{bmatrix} -0.144 & -0.143 & 0.064 & 0.290 & -0.063 \\ -0.093 & -0.044 & 0.253 & 0.117 & -0.032 \\ 0.433 & -0.021 & -0.432 & 0.089 & 0.173 \\ 0.778 & -7.39 & -0.777 & 7.378 & -0.0003 \\ 7.377 & 0.777 & -7.368 & -0.776 & -0.0118 \end{bmatrix},
$$

$$
C_{SP} = \begin{bmatrix} 0.305 & -0.649 & 0.039 & 0.071 & 0.691 \\ -0.607 & -0.299 & -0.273 & -0.680 & 0.072 \end{bmatrix}
$$

Furthermore, using the relation in (2.69), the initial conditions of the original system, mapped into the new coordinates, are calculated as

$$
x_{sp}(0) = \begin{bmatrix} 27.8963 & 12.4845 & -84.7021 & -120.1073 & 165.7279 \end{bmatrix}^T \tag{4.90}
$$

The closed-loop eigenvalues of the original system are shown in Table 4.1. Since

all eigenvalues are in the left half plane, this indicates that the system is asymptotically stable. Furthermore, the system has two time-scales (three slow and two fast eigenvalues).

Original System Eigenvalues
-7.4441 + 0.5867i
-7.4441 - 0.5867i
-0.3806 + 0.6293i
-0.3806 - 0.6293i
-0.2411

Table 4.1: Eigenvalues of the considered WT with DFIG system

The singular perturbation parameter can be calculated as the ratio between the real part of the fastest slow eigenvalue and the real part of the slowest fast eigenvalue. Here, this ratio is equal to ($\epsilon = 0.05$). The slow and fast subsystems can be obtained using the criteria explained in Section 4.2. Using wind turbine system matrices (4.88), the controllability of the original system has been tested using MATLAB. A full rank controllability matrix was obtained (rank= 5), which guarantees the controllability of the original system. The partitioned matrices $A_1 - A_4$, $B_1 - B_2$, Z, and P_r were obtained as in (4.6), where A_4 is nonsingular. Matrices $(a_i, b_i, i = 1, 2, 3, 4)$, Π_1 and Π_2 were calculated as in [55, 89]. The nonsingular transformation $\boldsymbol{T}$ is then formulated using (4.10). Additionally, the Newton recursive algorithm was used to obtain the solutions P_s and P_f of the AREs (4.9)). The solution P_{rsf} of the ARE was reconstructed again using the obtained slow and fast solutions, P_s and P_f, respectively, as in (4.12). The obtained P_{rsf} is found to be identical to P_r, with the accuracy of $E_{Pr} = 7.4247 * 10^{-13}$, where E_{Pr} is the norm of the absolute maximum error between P_r and P_{rsf}. Finally, the slow and fast subsystems were obtained as in (4.8). The corresponding eigenvalues of the slow and fast subsystems are shown in Table 4.2. Notice that, the eigenvalues in Table 4.2 are equal to those in Table 4.1, which indicates that the method proposed in Section 4.2 successfully decomposed the original system into pure-slow and pure-fast

subsystems.

Slow Subsystem	Fast Subsystem
-0.3806 + 0.6293i	-7.4441 + 0.5867i
-0.3806 - 0.6293i	-7.4441 - 0.5867i
-0.2411	

Table 4.2: Eigenvalues of the slow and fast decomposed subsystems.

4.5.2   Optimal LQR Design for the WT with DFIG System

In order to obtain the optimal gain that minimizes the performance criteria in (4.3), equation (4.5) should be solved. The weighting matrices R and Q of appropriate dimensions are chosen as follows:

$$R = I_5, \quad Q = C_{SP}^T C_{SP} \tag{4.91}$$

The solution of the ARE (4.5) gives the matrix P_r, from which the optimal LQR controller gain K_r for the full-order original system can be obtained as

$$K_r = R^{-1}B^T P_r = \begin{bmatrix} -2.5026 & 0.7102 & -0.7276 & 0.1007 & 0.5132 \\ 0.0660 & 2.2973 & 1.1863 & -0.5426 & 0.0176 \\ 0.4879 & 3.2873 & 0.7781 & -0.1288 & -0.4588 \\ 3.6358 & -0.4617 & 0.0295 & 0.4194 & -0.0303 \\ -0.6583 & -0.2721 & 0.5250 & -0.0094 & -0.0456 \end{bmatrix} \tag{4.92}$$

with the optimal control input u_{opt} given by (4.4). The optimal performance index J_{opt} for the full-order WT with DFIG system is calculated as

$$J_{opt} = \frac{1}{2}x_{sp}^T(0)P_r x_{sp}(0) = 1.9799 \tag{4.93}$$

where $x_{sp}(0)$ is the initial condition of the full-order WT with DFIG system given by (2.69) and calculated as

$$x_{sp}(0) = \begin{bmatrix} 27.8963 & 12.4845 & -84.7021 & -120.1073 & 165.7279 \end{bmatrix}^T \qquad (4.94)$$

In this section, an optimal LQR is designed for the slow and for the fast subsystems, independently. Having obtained the slow and fast solutions P_s and P_f, respectively, from their corresponding AREs (4.12), the optimal LQR controller gain for the slow subsystem can be obtained, as follows

$$K_{sr} = R_s^{-1} B_s^T P_s = \begin{bmatrix} -1.5209 & -4.3229 & 2.6228 \\ -8.6553 & -2.7713 & -2.5414 \\ -0.4911 & 8.3930 & -2.5882 \\ 12.5216 & 4.7245 & 3.7339 \\ -0.6138 & -0.2921 & 0.5316 \end{bmatrix} \qquad (4.95)$$

where R_s is the weighting positive definite matrix for the slow subsystem, chosen as an identity matrix, i.e., $R_s = I_5$. The optimal performance index for the slow subsystem J_{s-opt} can be calculated using (4.31), derived in Section 4.2.2

$$J_{s-opt} = 1.9122 \qquad (4.96)$$

Similarly, the optimal LQR controller gain for the fast subsystem can be obtained as follows

$$K_{fr} = R_f^{-1} B_f^T P_f = \begin{bmatrix} 0.1453 & -0.4403 & -0.1477 & 0.4209 & 0.0096 \\ 0.4693 & 0.0565 & -0.4558 & -0.0606 & -0.0029 \end{bmatrix}^T \qquad (4.97)$$

where R_f is the weighting positive definite matrix for the fast subsystem, chosen as an identity matrix, i.e., $R_f = I_5$. The optimal performance index for the fast subsystem

J_{f-opt} can be calculated using (4.32), derived in Section 4.2.2

$$J_{f-opt} = 0.0785 \tag{4.98}$$

Moreover, the slow-fast term of the optimal performance index is calculated using (4.33), and is equal to $J_{sf-opt} = -0.0108$. Adding up all three values of J_{s-opt}, J_{f-opt}, and J_{sf-opt}, we get

$$J_{total} = J_{s-opt} + J_{sf-opt} + J_{f-opt} = 1.9799 \tag{4.99}$$

which is equal to the exact value of the optimal performance index J_{opt} of the full-order WT with DFIG system obtained in (4.93).

4.5.3 Optimal Kalman Filter Design for the WT with DFIG System

Based on the duality property exhibited by the linear-quadratic optimal filters, on one hand, and the regulators, on the other, the exact decomposition of the singularly perturbed ARE, presented in Section 4.2, is applied here to design an optimal Kalman filter to estimate the state variables of the slow and fast subsystems of the WT with DFIG. The design takes into account that the slow and fast filters are completely decoupled and that both of them are driven by the system measurements, as demonstrated in Section 4.3. After calculating the matrices in (4.43)-(4.46), the similarity transformation $\boldsymbol{T_2}$ can be obtained using (4.47). Using the wind turbine system matrices (4.88), with the weighting matrices chosen as $R = I_5$, $\quad Q = C_{SP}^T C_{SP}$, and the white noise intensity (spectral density) matrices chosen as $W_1 = I_5$, $\quad W_2 = I_2$, the completely decoupled Kalman filters are obtained with pure-slow and pure-fast optimal filter gains K_s and K_f given by

$$K_s \begin{bmatrix} 0.0292 & -0.0395 \\ 0.0165 & -0.0344 \\ -0.0285 & 0.1238 \end{bmatrix}, \quad K_f \begin{bmatrix} 0.0067 & -0.0255 \\ 0.0262 & 0.0028 \end{bmatrix} \tag{4.100}$$

4.5.4 Optimal Linear-Quadratic Gaussian Design for the WT with DFIG System

In this section, a reduced-order optimal LQG controller is applied to the DFIG wind turbine, by combining the closed-loop regulator with the Kalman filter. The inputs to the closed-loop system are the noise of the WT system $w_1(t)$ and the measurements noise $w_2(t)$. All the controllers were implemented using MATLAB/Simulink. Figure 4.2 shows the original and estimated slow and fast states of the considered system, and the performance of the Kalman filter.

In Section 4.4.1 we showed that the similarity transformation does not preserve the value of the optimal performance criteria for the LQG controller. Therefore, the values of the optimal performance indices for the decomposed slow and fast subsystems do not add up to the same exact value of the optimal performance index before decomposition. The optimal performance index for the full-order LQG controller can be calculated using (4.64) as follows

$$J_{opt} = 37.3785 \tag{4.101}$$

Using the derivation in Section 4.4.2, the optimal performance index for the slow subsystem J_{s-opt} can be calculated using (4.80) as

$$J_{s-opt} = 10.0060 \tag{4.102}$$

whereas, the optimal performance index for the fast subsystem J_{f-opt} can be calculated using (4.81)

$$J_{f-opt} = 22.3614 \tag{4.103}$$

(a) First slow state

(b) Second slow state

(c) Third slow state

(d) First fast state

(e) Second fast state
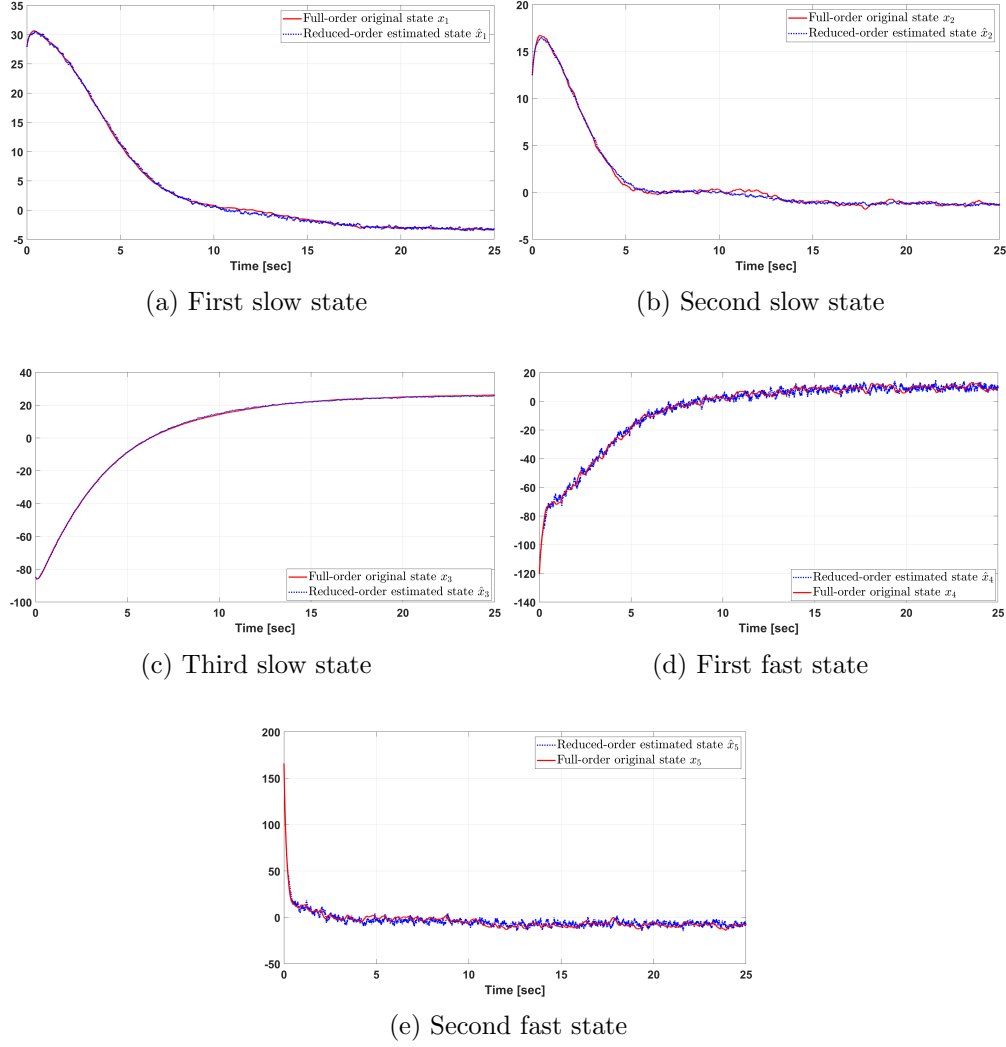
Figure 4.2: The original and reduced-order estimated states of the WT-DFIG

Moreover, the slow-fast term of the optimal performance index is calculated using (4.82), and is equal to $J_{sf-opt} = -10.0845$. Adding up all three values of J_{s-opt}, J_{f-opt}, and J_{sf-opt}, we get

$$J_{total} = J_{s-opt} + J_{sf-opt} + J_{f-opt} = 22.2829 \qquad (4.104)$$

Since, in the case of the LQG problem, the optimal performance at steady state is averaged over an infinite length of time, the initial conditions do not affect the optimal performance value. The original system output, i.e., before filtering, and the

estimated output of the LQG controller of the DFIG WT system after filtering are shown in Figures 4.3 and 4.4 for the rotor current output in the d-axis i_{dr} and q-axis i_{qr}, respectively. It can be observed from Figures 4.3 and 4.4 that the effect of the input white Gaussian noise is reduced successfully by the LQG regulator and its Kalman filter implementation.

| (a) Before filtering. | (b) After filtering. |
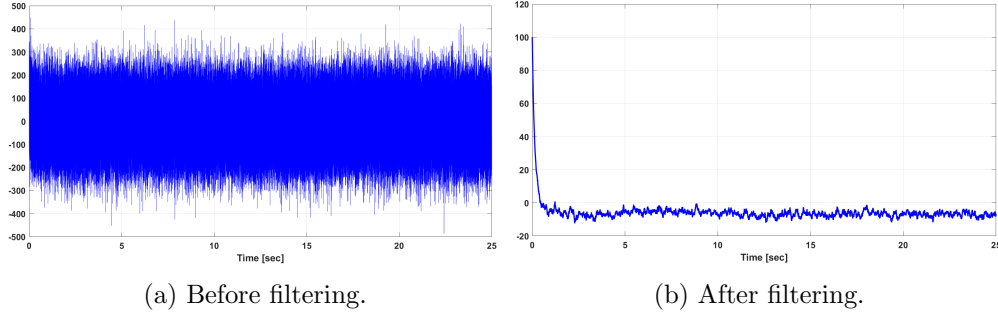
Figure 4.3: Original and reduced-order rotor current output i_{dr} of the LQG-controlled DFIG WT system

| (a) Before filtering. | (b) After filtering. |
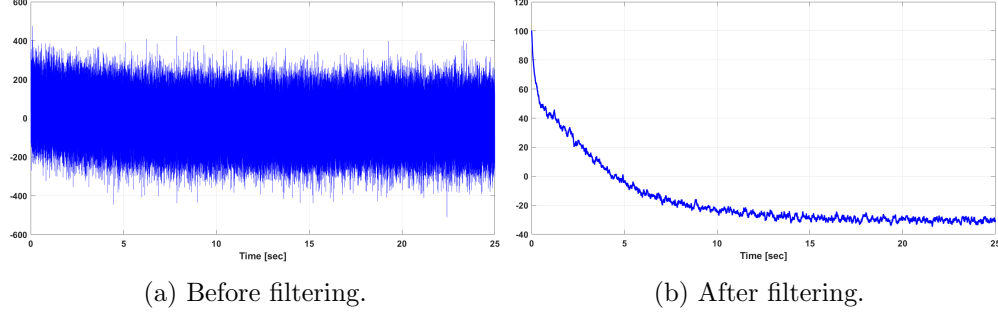
Figure 4.4: Original and reduced-order rotor current output i_{qr} of the LQG-controlled DFIG WT system

4.5.5 Wind Speed Variations

Here, we test the performances of the slow and fast subsystems of the reduced-order DFIG WT under the effects of wind turbulences and gust. The considered wind turbulence and gust are shown in Figure 4.5. In order to model the total variation in wind speed, the normal turbulence model (NTM) [23] was evaluated at an average of 9 m/s.

A wind gust, shaped as a hamming dip, of width 30 s was added. The total variance, as suggested by the aforementioned NTM, was broken between the turbulence and gust with the ratios of 1/3 and 2/3, respectively. The output responses of the rotor current in d-axis i_{dr} and q-axis i_{qr} of the original and reduced-order of the considered DFIG WT system to wind turbulence and gust are shown in Figures 4.6, and 4.7. These figures show the robustness of the designed LQG controller to wind speed variations.
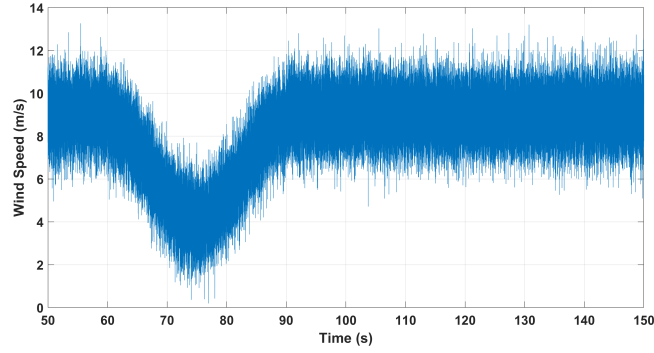
Figure 4.5: Wind turbulence and wind gust.

(a) Before filtering.

(b) After filtering.
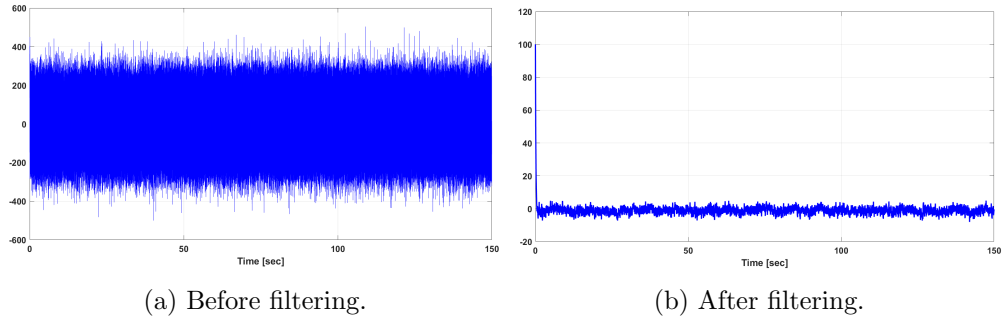
Figure 4.6: Output responses of the rotor current i_{dr} of the original and reduced-order system for wind turbulence and gust

(a) Before filtering.   (b) After filtering.
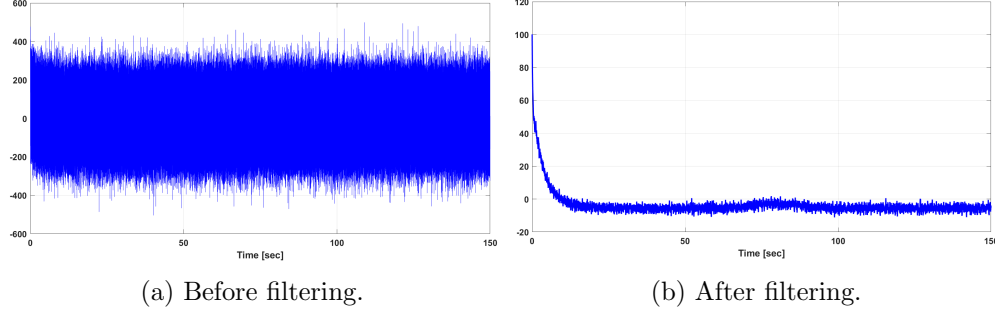
Figure 4.7: Output responses of the rotor current i_{qr} of the full- and reduced-order system for wind turbulence and gust.

4.5.6   Voltage Sag

For the evaluation of the dynamic performance of the models reduced into different orders, we study the effect of a large-signal disturbance voltage sag as well. We apply a voltage drop of 50% lasting for 1 sec to both the full- and reduced-order models. The output responses of the rotor current in d-axis, i_{dr}, and q-axis, i_{qr}, of the original and reduced-order DFIG WT system are shown in Figures 4.8 and 4.9, respectively, which show the robustness of the designed LQG controller.

(a) Before filtering.   (b) After filtering.
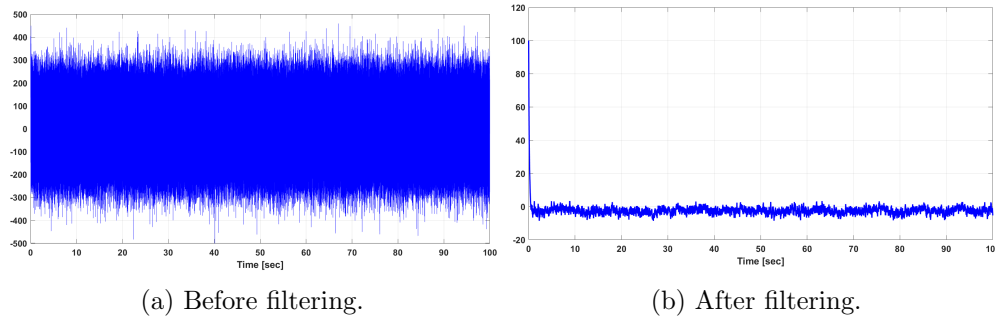
Figure 4.8: Output responses of the rotor current i_{dr} of the original and reduced-order system for voltage sag

(a) Before filtering.

(b) After filtering.
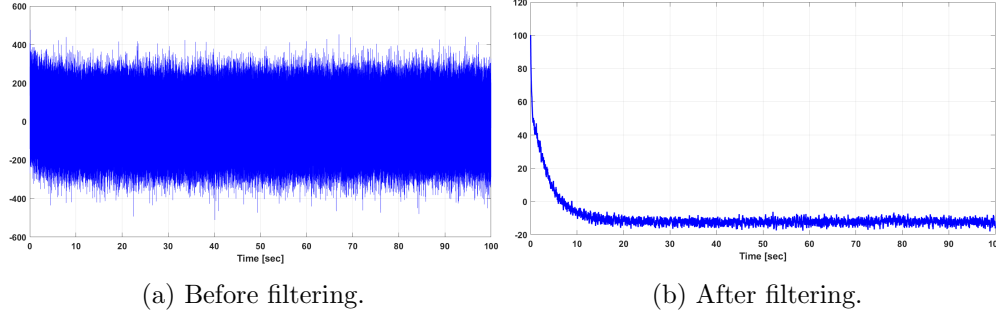
Figure 4.9: Output responses of the rotor current i_{qr} of the original and reduced-order system for voltage sag.

4.6 Conclusions

Optimal control techniques are applied to the DFIG wind turbine by decomposing the algebraic Riccati equation of the singularly perturbed wind turbine system into two reduced-order algebraic Riccati equations that correspond to the slow and fast time scales. The optimal regulator gains, with respect to the optimal pure-slow and pure-fast, reduced-order Kalman filters, and LQG controllers, are obtained. This decomposition allows the design of linear controllers for the slow and fast subsystems independently, thus, achieving the complete and exact separation of the linear-quadratic stochastic regulator problem. The Kalman filter was able to accurately track the state space states of the wind turbine system. The response of the reduced-order system was compared to that of the full-order system for the purpose of validating the performance of the proposed method. The effect of the applied white Gaussian noise is reduced successfully by the LQG regulator and its Kalman filter implementation. Moreover, the designed LQG controller showed good performance and robustness when wind turbulence and a large-signal disturbance are applied to the system. Additionally, we showed that the similarity transformation does not preserve the performance index value in the case of the Kalman filter and the corresponding LQG controller.

Chapter 5

Recursive Reduced-Order Algorithm for Singularly Perturbed Cross Gramian Algebraic Sylvester Equation

5.1   Introduction

Singularly perturbed systems span multiple time scales, corresponding to fast and slow state-space variables. For a system with two time scales, the slow time scale is related to the eigenvalues close to the imaginary axis and represent the slow state-space variables (slow modes) of the system, while the fast time scale is related to those eigenvalues far from the imaginary axis and represent the fast state-space variables (fast modes) of the system. Many algorithms exist in the literature for solving diverse problems related to the analysis and control of singularly perturbed linear systems. Fixed point recursive numerical methods were first proposed in [91] and used in [55, 92] to solve the closed and open loop optimal control problems. These methods led thereafter to the Hamiltonian approach, which solves the linear-quadratic optimal control and filtering problems by decomposing their algebraic Riccati equations into pure-slow and pure-fast reduced-order algebraic Riccati equations [89]. The exact decomposition into pure-slow and pure-fast subsystems led to the use of parallel algorithms [80, 93], which also provided the solutions to the algebraic Riccati equation of the linear-quadratic optimal control problem. Moreover, some iterative methods were used to solve this problem (see for example [94] and the references therein). Most of the previous studies considered solving the algebraic Reccati equation, as it represents the most important equation of the optimal control and filtering problems.

Sylvester equation has numerous applications in many areas including mathematics, control and system theory, model reduction, signal and image processing. The general

form of the continuous time algebraic Sylvester equation is given by

$$AX - XD = C \qquad (5.1)$$

where $A \in \Re^{n \times n}$, $D \in \Re^{m \times m}$, and $C \in \Re^{n \times m}$ are given matrices. A unique solution $X \in \Re^{n \times m}$ of (5.1) exists if and only if A and D matrices have disjoint eigenvalues. An important special case of the algebraic Sylvester equation is the algebraic Lyapunov equation, which plays an important role in control theory, and is given by

$$AX + XA^T = -BB^T \qquad (5.2)$$

where $A \in \Re^{n \times n}$, $B \in \Re^{n \times m}$, and $X \in \Re^{n \times n}$. A systematic approach for solving the Sylvester matrix equation is by using Bartels–Stewart [95] and the Hessenberg-Schur methods [96], which use the Hessenberg or Schur form to transform the matrices of the original system to the triangular form that can then be solved directly using backward substitution. These methods are efficient for small and medium-scale systems. To reduce the computational time and complexity when dealing with large-scale systems, several iterative algorithms have been proposed for solving the Sylvester equation; see for example [97–101].

In this chapter, we propose a new reduced-order recursive algorithm, which provides a solution for a class of Sylvester equation given by

$$AW_X + W_X A = BC \qquad (5.3)$$

where $B \in \Re^{n \times m}$, $C \in \Re^{m \times n}$, and the cross Gramian $W_X \in \Re^{m \times n}$ is the solution to the algebraic Sylvester equation (5.3), and is defined by

$$W_X = \int_0^\infty \mathrm{e}^{At} BC e^{At} \, \mathrm{d}t \qquad (5.4)$$

The system under investigation in this chapter must be asymptotically stable, controllable, observable, and square, i.e., the number of inputs equals the number of outputs

$m = p$. The test for controllability and observability of the system is usually performed separately using the controllability and observability Gramians. In many applications, lowering the computational complexity, as a result of the system order-reduction, is desirable. Model order-reduction retains only those state-space variables that are both strongly controllable and strongly observable. This requires investigating the behavior of the state-space variables, and balancing the controllability and observability Gramians, such that they are diagonal and identical. It has been shown in [46] that studying the system controllability and observability, separately, can be misleading; a method that directly assesses the combination of the two properties is preferred. Therefore, the cross Gramian matrix was defined in [71] as an alternative approach to the existing controllability and observability Gramian matrices. Unlike the controllability and observability Gramians, the cross Gramian contains information about both the controllability and observability of the system.

In this chapter, a new recursive algorithm is proposed to solve the algebraic Sylvester equation, of linear singularly perturbed systems, whose solution defines the cross Gramian matrix. The algorithm is obtained in terms of the reduced-order algebraic Sylvester equations corresponding to the slow and fast subsystems. The solutions of the full-order algebraic Sylvester equations, for finding the cross Gramian matrix, was considered in [102, 103].

The remainder of this chapter is organized as follows. The proposed recursive algorithm is described in Section 5.2. In Section 5.3, several case studies are considered to demonstrate the performance of the proposed algorithm. Then, the conclusions follow in Section 5.4.

5.2 A Recursive Algorithm for Finding Cross Gramians for Singularly Perturbed Linear Systems

The singularly perturbed structure can be obtained by partitioning the state space system

$$\dot{x}(t) = Ax(t) + Bu(t)$$
$$y(t) = Cx(t)$$

(5.5)

where $x(t) \in \Re^n$, are state variables, $u(t) \in \Re^m$ are control inputs, and $y(t) \in \Re^p$ are measured outputs, as follows [54, 80]

$$A = \begin{bmatrix} A_1 & A_2 \\ \frac{A_4}{\epsilon} & \frac{A_3}{\epsilon} \end{bmatrix}, \ B = \begin{bmatrix} B_1 \\ \frac{B_2}{\epsilon} \end{bmatrix}, \ C = \begin{bmatrix} C_1 & C_2 \end{bmatrix}$$

(5.6)

where ϵ is a small positive singular perturbation parameter. A, B, and C are constant matrices of appropriate dimensions. Based on the singular perturbation theory [54, 80], a singularly perturbed linear system in the explicit state variable standard form is given by

$$\frac{dx_1(t)}{dt} = A_1 x_1(t) + A_2 x_2(t) + B_1 u(t)$$
$$\epsilon \frac{dx_2(t)}{dt} = A_3 x_1(t) + A_4 x_2(t) + B_2 u(t)$$
$$y(t) = C_1 x_1(t) + C_2 x_2(t) + Du(t)$$

(5.7)

where $x_1(t) \in \Re^{n_1}$ are the slow state variables, and $x_2(t) \in \Re^{n_2}$ are the fast state variables, $n_1 + n_2 = n$. Assuming that A_4 is nonsingular, the eigenvalues of matrix A consists of two disjoint groups: one corresponds to the slow subsystem $\lambda_s(A)$ and the other corresponds to the fast subsystem $\lambda_f(A)$. If the two subsystems have a mixture of slow and fast eigenvalues, then a technique has to be applied to convert the system into its standard singularly perturbed form defined in (5.7). We will give examples on this case in Sections 5.3.2 and 5.3.3.

The nature of the cross Gramian matrix W_X defined in the algebraic Silvester's equation

$$AW_X + W_X A = BC$$

(5.8)

corresponding to the system singularly perturbed form defined in (5.7) is

$$W_X = \begin{bmatrix} W_1 & \epsilon W_2 \\ W_3 & W_4 \end{bmatrix} \tag{5.9}$$

Using (5.6) and (5.9) in (5.8), we get the partitioned form of the Sylvester equation as follows

$$
\begin{aligned}
A_1 W_1 + A_2 W_3 + W_1 A_1 + W_2 A_3 + B_1 C_1 &= 0 \\
\epsilon A_1 W_2 + A_2 W_4 + W_1 A_2 + W_2 A_4 + B_1 C_2 &= 0 \\
A_3 W_1 + A_4 W_3 + \epsilon W_3 A_1 + W_4 A_3 + B_2 C_1 &= 0 \\
\epsilon A_3 W_2 + A_4 W_4 + \epsilon W_3 A_2 + W_4 A_4 + B_2 C_2 &= 0
\end{aligned} \tag{5.10}
$$

Setting $\epsilon = 0$, we get the following approximate equations

$$
\begin{aligned}
A_1 W_1^{(0)} + A_2 W_3^{(0)} + W_1^{(0)} A_1 + W_2^{(0)} A_3 + B_1 C_1 &= 0 \\
A_2 W_4^{(0)} + W_1^{(0)} A_2 + W_2^{(0)} A_4 + B_1 C_2 &= 0 \\
A_3 W_1^{(0)} + A_4 W_3^{(0)} + W_4^{(0)} A_3 + B_2 C_1 &= 0 \\
A_4 W_4^{(0)} + W_4^{(0)} A_4 + B_2 C_2 &= 0
\end{aligned} \tag{5.11}
$$

The solution of equations (5.11) is given in terms of the following reduced-order algebraic Sylvester equations corresponding to the slow and fast subsystems

$$
\begin{aligned}
A_4 W_4^{(0)} + W_4^{(0)} A_4 + B_2 C_2 &= 0 \\
A_0 W_1^{(0)} + W_1^{(0)} A_0 + G_0 &= 0
\end{aligned} \tag{5.12}
$$

In addition we have from (5.11)

$$
\begin{aligned}
W_2^{(0)} &= -(B_1 C_2 + A_2 W_4^{(0)} + W_1^{(0)} A_2) A_4^{-1} \\
W_3^{(0)} &= -A_4^{-1}(B_2 C_1 + A_3 W_1^{(0)} + W_4^{(0)} A_3)
\end{aligned} \tag{5.13}
$$

where

$$A_0 = A_1 - A_2 A_4^{-1} A_3 \tag{5.14}$$

$$G_0 = -A_2 A_4^{-1}(B_2 C_1 + W_4^{(0)} A_3) - (A_2 W_4^{(0)} + B_1 C_2)A_4^{-1}A_3 + B_1 C_1 \qquad (5.15)$$

To find a unique solution of (5.12), we impose the following assumption.

Assumption 5.1 *Matrices A_0 and A_4 are asymptotically stable.*

In consequence, unique solutions of (5.12)–(5.13) exist. Defining the approximation error as

$$
\begin{aligned}
W_1 &= W_1^{(0)} + \epsilon E_1, \\
W_2 &= W_2^{(0)} + \epsilon E_2, \\
W_3 &= W_3^{(0)} + \epsilon E_3, \\
W_4 &= W_4^{(0)} + \epsilon E_4,
\end{aligned}
\qquad (5.16)
$$

subtracting (5.11) from (5.10), we get the following error equations, after some algebra,

$$
\begin{aligned}
A_4 E_4 + E_4 A_4 &= -A_3(W_2^{(0)} + \epsilon E_2) - (W_3^{(0)} + \epsilon E_3)A_2 \\
A_3 E_1 + A_4 E_3 + E_4 A_3 &= -(W_3^{(0)} + \epsilon E_3)A_1, \\
A_2 E_4 + E_1 A_2 + E_2 A_4 &= -A_1(W_2^{(0)} + \epsilon E_2), \\
A_1 E_1 + A_2 E_3 + E_1 A_1 + E_2 A_3 &= 0.
\end{aligned}
\qquad (5.17)
$$

From the first equation in (5.17), we can observe that the unknown errors E_2 and E_3 are multiplied by a small parameter ϵ. Similar situation is in the second and the third equations of (5.17). Therefore, we propose the following algorithm for solving the error equations (5.17).

Start with $E_2^{(0)} = 0$ and $E_3^{(0)} = 0$ and recursively evaluate

$$A_4 E_4^{(i+1)} + E_4^{(i+1)} A_4 = -A_3(W_2^{(0)} + \epsilon E_2^{(i)}) - (W_3^{(0)} + \epsilon E_3^{(i)}) A_2,$$

$$A_0 E_1^{(i+1)} + E_1^{(i+1)} A_0 = A_2 A_4^{-1}(W_3^{(0)} + \epsilon E_3^{(i)}) A_1 + A_1(W_2^{(0)} + \epsilon E_2^{(i)}) A_4^{-1} A_3$$

$$+ A_2 A_4^{-1} E_4^{(i+1)} A_3 + A_2 E_4^{(i+1)} A_4^{-1} A_3,$$

$$E_2^{(i+1)} = -(A_1(W_2^{(0)} + \epsilon E_2^{(i)}) + A_2 E_4^{(i+1)} + E_1^{(i+1)} A_2) A_4^{-1},$$

$$E_3^{(i+1)} = -A_4^{-1}((W_3^{(0)} + \epsilon E_3^{(i)}) A_1 + A_3 E_1^{(i+1)} + E_4^{(i+1)} A_3).$$

$$(5.18)$$

for $i = 0, 1, 2, \ldots$

The steps of the proposed algorithm are summarized in Algorithm 1

Algorithm 1: The proposed recursive algorithm

Input: A, B, C

Output: E_1, E_2, E_3, E_4

1: Find the cross-Gramian matrix W_X using (5.8)
2: Define the matrix partitions (5.6) and (5.9)
3: Initialize $W_1^{(0)}$, $W_2^{(0)}$, $W_3^{(0)}$, and $W_4^{(0)}$ using (5.12)–(5.15)
4: Initialize $E_2^{(0)} = 0$ and $E_3^{(0)} = 0$
5: Initialize $E_1^{(0)}$ and $E_4^{(0)}$ using (5.17)
6: Set $i = 0$
7: **while** $|W_X - W_X^{(i)}| > O(\epsilon)$ **do**
8:　Update $E_1^{(i+1)}$, $E_2^{(i+1)}$, $E_3^{(i+1)}$, and $E_4^{(i+1)}$ using (5.18)
9:　Update $W_1^{(i+1)}$, $W_2^{(i+1)}$, $W_3^{(i+1)}$, and $W_4^{(i+1)}$ using (5.16)
10:　Update $W_X^{(i+1)} = \begin{bmatrix} W_1^{(i+1)} & \epsilon W_2^{(i+1)} \\ W_3^{(i+1)} & W_4^{(i+1)} \end{bmatrix}$
11:　$i = i + 1$
12: **end while**

Theorem 5.1 Assuming that matrices A_0 and A_4 are asymptotically stable, algorithm (5.18) converges to the exact solution of (5.17) with a rate of convergence $O(\epsilon)$, that is

$$\|E_j^{(i+1)} - E_j^{(i)}\| = O(\epsilon)$$

$$(5.19)$$

$$\|E_j^{(i)} - E_j\| = O(\epsilon^i)$$

for $j = 1, 2, 3, 4$; and $i = 0, 1, 2, \ldots$

Therefore, the exact solution W_X can be obtained with an accuracy of $O(\epsilon^i)$ after performing i iterations on the proposed algorithm (5.18) as

$$W_j^{(i)} = W_j + \epsilon E_j^{(i)}, \tag{5.20}$$

for $j = 1, 2, 3, 4$; and $i = 0, 1, 2, \ldots$.

Proof 5.1 For $i = 0$, we have from (5.18)

$$A_4 E_4^{(1)} + E_4^{(1)} A_4 = -A_3 W_2^{(0)} - W_3^{(0)} A_2,$$

$$A_0 E_1^{(1)} + E_1^{(1)} A_0 = A_2 A_4^{-1} W_3^{(0)} A_1 + A_1 W_2^{(0)} A_4^{-1} A_3$$

$$+ A_2 A_4^{-1} E_4^{(1)} A_3 + A_2 E_4^{(1)} A_4^{-1} A_3 \tag{5.21}$$

$$E_2^{(1)} = -(A_1 W_2^{(0)} + A_2 E_4^{(1)} + E_1^{(1)} A_2) A_4^{-1},$$

$$E_3^{(1)} = -A_4^{-1} (W_3^{(0)} A_1 + A_3 E_1^{(1)} + E_4^{(1)} A_3).$$

Equations (5.21) are $O(\epsilon)$ approximates of (5.17). Subtracting these equations from the corresponding equations in (5.17), we have

$$A_4(E_4 - E_4^{(1)}) + (E_4 - E_4^{(1)})A_4 = O(\epsilon),$$

$$A_0(E_1 - E_1^{(1)}) + (E_1 - E_1^{(1)})A_0 = O(\epsilon),$$

$$A_2(E_4 - E_4^{(1)}) + (E_1 - E_1^{(1)})A_2 + (E_2 - E_2^{(1)})A_4 = O(\epsilon), \tag{5.22}$$

$$A_3(E_1 - E_1^{(1)}) + A_4(E_3 - E_3^{(1)})A_2 + (E_4 - E_4^{(1)})A_3 = O(\epsilon),$$

which implies

$$\|E_4 - E_4^{(1)}\| = O(\epsilon),$$

$$\|E_1 - E_1^{(1)}\| = O(\epsilon),$$

$$\|E_2 - E_2^{(1)}\| = O(\epsilon), \tag{5.23}$$

$$\|E_3 - E_3^{(1)}\| = O(\epsilon),$$

For $i = 1$, we have

$$A_4 E_4^{(2)} + E_4^{(2)} A_4 = -A_3(W_2^{(0)} + \epsilon E_2^{(1)}) - (W_3^{(0)} + \epsilon E_3^{(1)})A_2,$$

$$A_0 E_1^{(2)} + E_1^{(2)} A_0 = A_2 A_4^{-1}(W_3^{(0)} + \epsilon E_3^{(1)})A_1 + A_1(W_2^{(0)} + \epsilon E_2^{(1)})A_4^{-1} A_3$$

$$+ A_2 A_4^{-1} E_4^{(2)} A_3 + A_2 E_4^{(2)} A_4^{-1} A_3 \tag{5.24}$$

$$E_2^{(2)} = -(A_1(W_2^{(0)} + \epsilon E_2^{(1)}) + A_2 E_4^{(2)} + E_1^{(2)} A_2)A_4^{-1},$$

$$E_3^{(2)} = -A_4^{-1}((W_3^{(0)} + \epsilon E_3^{(1)})A_1 + A_3 E_1^{(2)} + E_4^{(2)} A_3),$$

subtracting (5.24) from (5.17) and using (5.19), we get

$$A_4(E_4 - E_4^{(2)}) + (E_4 - E_4^{(2)})A_4 = O(\epsilon^2),$$

$$A_0(E_1 - E_1^{(2)}) + (E_1 - E_1^{(2)})A_0 = O(\epsilon^2),$$

$$A_2(E_4 - E_4^{(2)}) + (E_1 - E_1^{(2)})A_2 + (E_2 - E_2^{(2)})A_4 = O(\epsilon^2), \tag{5.25}$$

$$A_3(E_1 - E_1^{(2)}) + A_4(E_3 - E_3^{(2)})A_2 + (E_4 - E_4^{(2)})A_3 = O(\epsilon^2),$$

which by Assumption 5.1 implies

$$\|E_4 - E_4^{(2)}\| = O(\epsilon^2),$$

$$\|E_1 - E_1^{(2)}\| = O(\epsilon^2),$$

$$\|E_2 - E_2^{(2)}\| = O(\epsilon^2), \tag{5.26}$$

$$\|E_3 - E_3^{(2)}\| = O(\epsilon^2),$$

continuing the same procedure, we come to

$$A_4(E_4 - E_4^{(i+1)}) + (E_4 - E_4^{(i+1)})A_4 = O(\epsilon^{i+1}),$$

$$A_0(E_1 - E_1^{(i+1)}) + (E_1 - E_1^{(i+1)})A_0 = O(\epsilon^{i+1}),$$

$$A_2(E_4 - E_4^{(i+1)}) + (E_1 - E_1^{(i+1)})A_2 + (E_2 - E_2^{(i+1)})A_4 = O(\epsilon^{i+1}), \tag{5.27}$$

$$A_3(E_1 - E_1^{(i+1)}) + A_4(E_3 - E_3^{(i+1)})A_2 + (E_4 - E_4^{(i+1)})A_3 = O(\epsilon^{i+1}),$$

which implies the results stated in Theorem 5.1, that is

$$\|E_j - E_j^{(i+1)}\| = O(\epsilon^{(i+1)})$$
$$\|E_j^{(i+1)} - E_j^{(i)}\| = O(\epsilon^i)$$

(5.28)

The proof is complete. $\square$

5.3   Case Studies

Three case studies are considered to demonstrate the proposed algorithm; **(a)** a fourth-order aircraft example whose mathematical model is in the explicit singularly perturbed form defined in (5.7), in which with accuracy of $O(\epsilon)$ the slow eigenvalues are all contained in the approximate slow subsystem represented by A_0 and all fast eigenvalues are contained in the approximate fast subsystem represented by A_4; **(b)** a fifth-order chemical plant model given in implicit singularly perturbed form (it has two slow and three fast eigenvalues, but the state variables have to be reordered to achieve explicit singularly perturbed form defined in (5.7); **(c)** a tenth-order hydrogen gas reformer used to provide hydrogen to a fuel cell from hydrogen rich fuels (natural gas, methanol).

5.3.1   L-1011 Aircraft

Here, we consider the lateral axis equations of the rigid body model of L-1011 aircraft at cruise condition [104]. The state variables are the bank angle, roll rate, yaw rate, and sideslip angle, which are respectively represented in the state vector $x(t) = [x_1 \quad x_2 \quad x_3 \quad x_4]^T$. The input vector consists of two variables: the rudder deflection δ_r and the aileron deflection δ_a, and is given as $u(t) = [\delta_r \quad \delta_a]^T$. The system matrices are given as

$$
A = \begin{bmatrix} 0 & 1 & 0 & 0 \\ 0 & -1.89 & 0.39 & -5.55 \\ 0 & -0.034 & -2.98 & 2.43 \\ 0.034 & -0.0011 & -0.99 & -0.21 \end{bmatrix}
$$

$$
B = \begin{bmatrix} 0 & 0 \\ 0.36 & -1.6 \\ -0.95 & -0.032 \\ 0.03 & 0 \end{bmatrix} , \quad C = \begin{bmatrix} 1 & 0 & 0 & 0 \\ 0 & 1 & 0 & 0 \end{bmatrix}
\tag{5.29}
$$

The eigenvalues of the matrix A are: $-0.1016, -1.4811 \pm 0.6292i$, and -2.0162. The system is asymptotically stable (all eigenvalues are in the left half plane), controllable, and observable. Moreover, there is only one slow mode with eigenvalue -0.0899, and three fast modes with eigenvalues: $-1.4891 \pm 0.7686i$ and -2.1017. The perturbation parameter is $\epsilon = 0.07$, which is the ratio between the fastest slow eigenvalue and the slowest fast eigenvalue. Solving the algebraic Sylvester equation (5.8), the cross Gramian matrix can be obtained as follows

$$
W_X = \begin{bmatrix} -3.77168467243 & -0.43134179103 & -0.14313989569 & 0.20967036557 \\ -2.25320146563 & -0.62940797540 & 0.00048741612 & 0.06408641105 \\ -4.60285451131 & -0.27809983914 & -0.01060057667 & -0.03861451004 \\ 12.68652326564 & 1.332572206696 & -0.02122054103 & 0.00250243909 \end{bmatrix}
$$

Using the proposed algorithm, the initial cross Gramian matrix $W^{(0)}$ is obtained as

$$
W^{(0)} = \begin{bmatrix} -3.98315817315 & -0.41906814039 & -0.14908955443 & 0.202330975578 \\ -2.25882783809 & -0.42418654922 & -0.00284907928 & 0.001553980682 \\ -4.46229986109 & -0.21443252362 & 0.00235249833 & 0.000836843461 \\ 12.32553354098 & 0.883962065453 & -0.00586646018 & -0.00419856136 \end{bmatrix}
$$

Comparing the exact solution W_X to the first-order approximate solution of the

Number of Iteration i	$\|W_X - W_X^{(i)}\|_2$
2	$7.50332862598 \times 10^{-4}$
3	$2.61112541747 \times 10^{-5}$
4	$9.08506250553 \times 10^{-7}$
5	$3.16109799914 \times 10^{-8}$
6	$1.09991811058 \times 10^{-9}$
7	$3.83066885862 \times 10^{-11}$
8	$1.36887465822 \times 10^{-12}$
9	$9.59811872673 \times 10^{-14}$
10	$6.47440768237 \times 10^{-14}$

Table 5.1: Error norm values for each iteration for L-1011 aircraft system

cross Gramian matrix by calculating the error norm, we get

$$\|W_X - W^{(0)}\|_2 = 0.624920763816596$$

Then, the cross Gramian matrix is calculated using the proposed recursive algorithm. The error norm at each iteration is shown in Table 5.1. By taking the error norm, it can be seen that the algorithm converges rapidly to the exact solution.

5.3.2 Chemical Plant

In this section, the linearized chemical plant considered in [105] is chosen to demonstrate the behavior of the proposed algorithm when the linear singularly perturbed system is not in the explicit standard form (5.7). The system matrices are given as follows

$$A = \begin{bmatrix} -0.1094 & 0.0628 & 0 & 0 & 0 \\ 1.306 & -2.136 & 0.9807 & 0 & 0 \\ 0 & 1.595 & -3.149 & 1.547 & 0 \\ 0 & 0.0355 & 2.632 & -4.257 & 1.855 \\ 0 & 0.0027 & 0 & 0.1636 & -0.1625 \end{bmatrix}$$

(5.30)

$$B = \begin{bmatrix} 0 & 0 \\ 0.0638 & 0 \\ 0.0838 & -0.1396 \\ 0.1004 & -0.206 \\ 0.0063 & -0.0128 \end{bmatrix}, \quad C = \begin{bmatrix} 1 & 0 & 0 & 0 & 0 \\ 0 & 0 & 0 & 0 & 1 \end{bmatrix}$$

The eigenvalues of matrix A are $-5.9822, -2.8408, -0.8954, -0.0141$, and -0.0774, which indicates that this system has two slow modes (eigenvalues). The small singular perturbation parameter ϵ is chosen as the ratio of the fastest slow eigenvalue to the slowest fast eigenvalue, and equals to $\epsilon = 0.0141/0.8954 = 0.086$. Introducing the following permutation matrix that exchanges the second row of matrix A, with its fifth row, that is

$$P = \begin{bmatrix} 1 & 0 & 0 & 0 & 0 \\ 0 & 0 & 0 & 0 & 1 \\ 0 & 0 & 1 & 0 & 0 \\ 0 & 0 & 0 & 1 & 0 \\ 0 & 1 & 0 & 0 & 0 \end{bmatrix}$$

the explicit singularly perturbed form of the system matrices can be obtained as follows

$$A_{SP} = PAP,$$

$$B_{SP} = PB, \quad C_{SP} = CP$$

(5.31)

Note $P = P^{-1}$. Thereby, they are calculated as

$$A = \begin{bmatrix} -0.1094 & 0 & 0 & 0 & 0.0628 \\ 0 & -0.1625 & 0 & 0.1636 & 0.0027 \\ 0 & 0 & -3.149 & 1.547 & 1.5950 \\ 0 & 1.8550 & 2.632 & -4.257 & 0.0355 \\ 1.3060 & 0 & 0.9807 & 0 & -2.1320 \end{bmatrix}$$

$$B = \begin{bmatrix} 0 & 0 \\ 0.0638 & -0.0128 \\ 0.0838 & -0.1396 \\ 0.1004 & -0.206 \\ 0.0638 & 0 \end{bmatrix}, \ C = \begin{bmatrix} 1 & 0 & 0 & 0 & 0 \\ 0 & 1 & 0 & 0 & 0 \end{bmatrix}$$

$$(5.32)$$

Matrices A_{SP} and A have the same eigenvalues and the same number of slow and fast modes. However, the slow and fast eigenvalues are now correctly separated into two disjoint groups. The slow mode has the eigenvalues -0.0788 and -0.0160, and the fast mode has the fast eigenvalues $-5.9521, -0.7933$, and -2.7925. Solving the algebraic Sylvester equation (5.8), the cross Gramian matrix can be obtained as follows

$$W_X = \begin{bmatrix} -0.07530866 & -0.11561658 & -0.00985227 & -0.00806596 & -0.00985946 \\ -0.23194836 & -0.49463876 & -0.03897379 & -0.03313413 & -0.03676743 \\ -0.07341430 & -0.42776115 & -0.02785663 & -0.02552098 & -0.02384797 \\ -0.12954567 & -0.52436133 & -0.03510447 & -0.03163354 & -0.03102749 \\ -0.05734203 & -0.26232141 & -0.01916962 & -0.01692499 & -0.01682689 \end{bmatrix}$$

Calculating the initial cross Gramian matrix $W^{(0)}$ using the proposed algorithm, and comparing the result to the exact solution of the cross Gramian, using the error

Number of Iteration i	$\|W_X - W_X^{(i)}\|_2$
2	$6.549205248602 \times 10^{-3}$
4	$3.305462486403 \times 10^{-4}$
6	$1.644553914568 \times 10^{-5}$
8	$7.961048437784 \times 10^{-7}$
10	$3.79165870750 \times 10^{-8}$
12	$1.79073797457 \times 10^{-9}$
14	$8.42125015994 \times 10^{-11}$
16	$3.94485224503 \times 10^{-12}$
18	$1.78105453794 \times 10^{-13}$
20	$1.74637224575 \times 10^{-14}$

Table 5.2: Error norm values for each iteration for the chemical plant

norm, we get the following results

$$W^{(0)} = \begin{bmatrix} -0.07894318 & -0.13640657 & -0.01124158 & -0.00932742 & -0.0110635 \\ -0.25878609 & -0.56732132 & -0.04537161 & -0.03829073 & -0.04292241 \\ -0.05767992 & -0.50330195 & 0 & 0 & 0 \\ -0.12521917 & -0.60940965 & 0 & 0 & 0 \\ -0.04496552 & -0.31507279 & 0 & 0 & 0 \end{bmatrix}$$

$$\|W_X - W^{(0)}\|_2 = 0.160161520985517$$

The cross Gramian matrix is then calculated using the proposed recursive algorithm. The error norm for each iteration is shown in Table 5.2, from which it can be observed that, the proposed algorithm converges to the exact solution according to the convergence result stated in the presented theorem.

5.3.3 Natural Gas Hydrogen Reformer

In this section, we investigate the behavior of the proposed algorithm in case of higher order singularly perturbed systems. The linearized 10th-order mathematical model of the gas hydrogen reformer introduced and studied in [106, 107] is chosen.

The system matrices are given as follows [106]

$A =$

$$
\begin{bmatrix}
-0.074 & 0 & 0 & 0 & 0 & 0 & -3.53 & 1.075 & 0 & 0 \\
0 & -1.47 & -25.3 & 0 & 0 & 0 & 0 & 0 & 2.56 & 13.91 \\
0 & 0 & -156 & 0 & 0 & 0 & 0 & 0 & 0 & 33.59 \\
0 & 0 & 0 & -124.5 & 212.6 & 0 & 112.69 & 112.7 & 0 & 0 \\
0 & 0 & 0 & 0 & -3.33 & 0 & 0 & 0 & 0 & 0 \\
0 & 0 & 0 & 0 & 0 & -32.43 & 32.30 & 32.30 & 0 & 0 \\
0 & 0 & 0 & 0 & 0 & 331.8 & -344 & -341 & 0 & 9.90 \\
0 & 0 & 0 & 221.97 & 0 & 0 & -253.2 & -254.9 & 0 & 32.53 \\
0 & 0 & 2.035 & 0 & 0 & 0 & 1.830 & 1.214 & -0.36 & -3.30 \\
0.018 & 0 & 8.164 & 0 & 0 & 0 & 5.6 & 5.39 & 0 & -13.61
\end{bmatrix}
$$

$$
B = \begin{bmatrix}
0 & 0 & 0 & 0 & 0.12 & 0 & 0 & 0 & 0 & 0 \\
0 & 0 & 0 & 0 & 0 & 0 & 0.1834 & 0 & 0 & 0
\end{bmatrix}^T ,
$$

$$
C = \begin{bmatrix}
1 & 0 & 0 & 0 & 0 & 0 & 0 & 0 & 0 & 0 \\
0 & 0.994 & -0.088 & 0 & 0 & 0 & 0 & 0 & 0 & 0
\end{bmatrix}
$$

$$
\tag{5.33}
$$

The eigenvalues of the system matrix A are as follows: -660.68, -157.9, -89.137, -12.175, -3.33, $-2.77 \pm 0.547i$, -1.468, -0.358, -0.0861. All real parts of those eigenvalues lie in the left part of the complex plane; hence, the system is asymptotically stable. Moreover, the system has multiple time scales (slow and fast) since there are three eigenvalues located very close to the imaginary axis while the other seven eigenvalues are located far from that axis. The perturbation parameter ϵ is chosen as the ratio of the fastest slow eigenvalue to the slowest fast eigenvalue, and equals $\epsilon = 0.52 = 1.468/2.77$.

What are supposed to be slow mode eigenvalues, obtained via (5.14), -1.468,

-0.0838, -128.4495 and what are supposed to be the fast mode eigenvalues ((eigen-values of A_4) -0.358, -660.68, -89.144, -13.954, -2.829 ± 0.886, and -3.333) do not display the slow-fast time scale separation. Similarly to the chemical plant example in the previous section, we can notice that the slow and fast eigenvalues are not well separated into two disjoint groups. However, since the gas reformer system is of higher order, it will be a little cumbersome to come up with a permutation matrix that would convert the system into its explicit singularly perturbed form. Therefore, the algorithm presented in [108], [54], and used by [107] to study the slow and fast dynamics of the gas reformer system, is also considered here to convert the system from an implicit singularly perturbed form to the explicit singularly perturbed form. The algorithm in [108] and [54] is based on introducing a similarity transformation T that transform the general linear system in implicit singularly perturbed form into the explicit singularly perturbed form defined in (5.7). The similarity transformation T is given by [107]

$$T = \begin{bmatrix} 4.8557 & 2.1797 & -0.3535 & 1.7829 & 113.74 & -52.659 & -5.1468 & 1 & 0 & 0 \\ 0 & 0 & 0 & 0 & 0 & 0 & 0 & 0 & 1 & 0 \\ -0.3794 & 0.7980 & -0.0771 & 0 & 0 & 5.2667 & 0.5148 & 0 & 0 & 1 \\ 0 & 0 & 1 & 0 & 0 & 0 & 0 & 0 & 0 & 0 \\ 0 & 0 & 0 & 1 & 0 & 0 & 0 & 0 & 0 & 0 \\ 0 & 0 & 0 & 0 & 1 & 0 & 0 & 0 & 0 & 0 \\ 0 & 0 & 0 & 0 & 0 & 1 & 0 & 0 & 0 & 0 \\ 0 & 0 & 0 & 0 & 0 & 0 & 1 & 0 & 0 & 0 \\ 0 & 0 & 0 & 0 & 0 & 0 & 0 & 1 & 0 & 0 \\ 0 & 0 & 0 & 0 & 0 & 0 & 0 & 0 & 0 & 1 \end{bmatrix}$$

The new transformed system matrices are defined as

$$A_{SP} = TAT^{-1}$$

$$B_{SP} = TB \qquad (5.34)$$

$$C_{SP} = CT^{-1}$$

thereby, they are calculated as

$A_{SP} =$

$$\begin{bmatrix}
-0.319 & 5.576 & -3.138 & -0.353 & 0.568 & 36.31 & -0.26 & -0.05 & 5.516 & 3.138 \\
0 & -0.358 & 0 & 2.035 & 0 & 0 & 0 & 1.83 & 1.214 & -3.30 \\
-0.087 & 2.041 & -1.232 & -0.125 & 0.154 & 9.85 & 1.925 & 0.190 & -0.319 & 1.231 \\
0 & 0 & 0 & -124.5 & 0 & 0 & 0 & 0 & 0 & 33.59 \\
0 & 0 & 0 & 0 & -124.5 & 212.63 & 0 & 112.69 & 112.69 & 0 \\
0 & 0 & 0 & 0 & 0 & -3.33 & 0 & 0 & 0 & 0 \\
0 & 0 & 0 & 0 & 0 & 0 & -32.43 & 32.30 & 32.30 & 0 \\
0 & 0 & 0 & 221.97 & 0 & 0 & 331.8 & -344 & -341 & 9.904 \\
0 & 0 & 2.035 & 0 & 221.97 & 0 & 0 & -253.2 & -254.9 & 32.53 \\
0.019 & 0 & 8.164 & 0 & -0.006 & -0.363 & 0.213 & 5.625 & 5.396 & -13.61
\end{bmatrix}$$

$$B_{SP} = \begin{bmatrix}
13.6488 & 0 & 0 & 0 & 0 & 0.12 & 0 & 0 & 0 & 0 \\
-9.6577 & 0 & 0.9659 & 0 & 0 & 0 & 0.1834 & 0 & 0 & 0
\end{bmatrix}^T ,$$

$$C_{SP} = \begin{bmatrix}
0.169 & 0 & -0.464 & 0.024 & -0.302 & -19.30 & 11.38 & 1.11 & -0.169 & 0.463 \\
0.080 & 0 & 1.03 & 0.019 & -0.143 & -9.124 & -1.183 & -0.115 & -0.08 & -1.026
\end{bmatrix}$$

$$(5.35)$$

The matrices A_{SP} and A have the same eigenvalues, since they are preserved under the similarity transformation. The slow mode eigenvalues are: -1.468, -0.08552, and -0.358 obtained as $(\lambda(A_s) + O(\epsilon))$, while the fast mode eigenvalues are: -660.682, -157.89, 89.137, -12.174, -2.7697 ± 0.60087, and -3.333 obtained as $(\lambda(A_f) + O(\epsilon))$. They are

Number of Iteration i	$\|W_X - W_X^{(i)}\|_2$
2	56.67074786107
5	13.26046318575
10	0.38648979991
12	$50.9580379513 \times 10^{-2}$
15	$5.949048480951 \times 10^{-3}$
20	$6.505261253303 \times 10^{-4}$
23	$6.630466299301 \times 10^{-5}$
25	$7.912793405030 \times 10^{-6}$
30	$7.210694103862 \times 10^{-7}$
35	$3.050169378906 \times 10^{-8}$
40	$8.638446874677 \times 10^{-10}$

Table 5.3: Error norm values for each iteration for the gas reformer system

clearly separated now into two disjoint groups.

Using our proposed algorithm to calculate the initial cross Gramian matrix $W^{(0)}$ and compare the result to the exact solution of the algebraic Sylvester equation, we get the error norm as

$$\|W_X - W^{(0)}\|_2 = 53.489147248362102$$

The cross Gramian matrix is then calculated using the proposed recursive algorithm. The error norm for each iteration is shown in Table 5.3.

5.4 Conclusions

The algorithm was developed to solve the algebraic Sylvester equation whose solution defines the cross Gramian of singularly perturbed linear systems. The algorithm is very efficient, defined in terms of reduced-order sub-problems corresponding to slow and fast subsystems, and converges rapidly to the required solution. The efficacy of the algorithm is demonstrated on three real physical examples. The algorithm can be directly applied to singularly perturbed systems in the explicit standard forms. A similarity transformation needs to be applied to singularly perturbed systems in implicit forms to convert them into their explicit forms, before the proposed algorithm can be applied to this class of systems.

Chapter 6

Conclusions and Future Work

6.1   Conclusions

In this dissertation, a DFIG-wind energy conversion system connected to the utility grid, as well as wind farms of different sizes were investigated for model order reduction and optimal control.

In Chapter 2, the balanced truncation and residualization and the singular perturbation methods were utilized to reduce the order of an eighth-order DFIG-based wind energy conversion system connected to the utility grid. In general, these two model order reduction techniques produce consistent results. However, in the case of the considered DFIG system, the reduction in model order achieved via singular perturbations outperformed the reduction achieved via the balancing methods in terms of both the transient step response and the linear-quadratic near-optimal control performance. The singular perturbation method allows the reduction of the system model order even to an order of two while the balancing method only allows the system model order to be reduced to the sixth order. Further order reduction using the balancing method would result in a significant increase in the error bound.

In Chapter 3, model order reduction, based on the balancing and cross Gramian methods, was considered for the state-space model of wind farms of different sizes. The cross Gramian method reduces the computational complexity by calculating only one Gramian without the need for balancing and shows comparable results to the balanced truncation methods. The order of the reduced system depends, significantly, on the selected threshold value. Furthermore, comparing the degree of controllability and observability of the system, in both the vector and diagonal forms of the control input matrix, showed a considerable loss of controllability and observability in the case of the

latter form.

In Chapter 4, based on time scale analysis, LQR, Kalman filter, and LQG controllers were designed for a fifth-order, single-cage DFIG wind turbine. The algebraic Riccati equation of the singularly perturbed wind turbine system was decomposed into two reduced-order AREs that correspond to the slow and fast time scales. These AREs were successfully solved using the Newton recursive algorithm. The obtained solutions are used to design an optimal LQR controller for the slow and fast subsystems, independently. Using the duality between the optimal filters and regulators, the same technique was applied to the full order Kalman filter to obtain two independent, reduced order, slow and fast Kalman filters which were able to accurately track the state-space states of the wind turbine system. The reduced-order LQG controller was obtained by combining the corresponding regulator and Kalman filter. The effect of the applied white Gaussian noise is reduced successfully by the LQG regulator and its Kalman filter implementation. Furthermore, the designed LQG controller showed good performance and robustness when a wind turbulence and a large-signal disturbance affect the system.

In Chapter 5, a new reduced-order recursive algorithm was developed to solve a class of Sylvester equation given by $AW_X + W_X A = BC$, whose solution W_X defines the cross Gramian of singularly perturbed linear systems. The system under investigation must be asymptotically stable, controllable, observable, and square. The algorithm is defined in terms of the reduced-order sub-problems corresponding to the slow and fast subsystems. The rate of convergence of the proposed algorithm is $O(\epsilon)$, where ϵ is a small singular perturbation parameter that indicates the separation of the slow and fast state variables. The algorithm can be directly applied to singularly perturbed systems in the explicit standard form. A similarity transformation needs to be applied to the singularly perturbed systems in implicit forms to convert them into their explicit form before the proposed algorithm can be applied to this class of systems.

6.2 Future Work

A number of possible directions for further developing the work presented in this dissertation can be pursued. The following directions may be considered for future work:

- Due to complexity of wind power electric energy production, variability of operating conditions, intermittency of wind power, disturbances, and integration of wind turbines into the power grid, it is important that the research work presented in this dissertation that focused mostly on modeling and controls, be expanded to a system integration level and include other researchers and practitioners of the smart power grid community. The problems of wind turbines integration with transmissions lines, grouping within different areas of wind farms, coordination of the control with supervision systems, integration with other distributed energy resources, such as energy storage systems, and microgrids, would provide variety of topics for future multidisciplinary research.

- Verify the analytical results obtained in Chapter 2 using different wind turbine generator setups. For example, a two-mass model of WECS with different wind speeds, load levels, and power grid models can be investigated and compared using the the considered order reduction methods.

- In Chapter 3, a general setup of the following two linear systems, differing in the forms of their input matrices

$$
\dot{x}(t) = Ax(t) + \begin{bmatrix} B_1 \\ B_2 \end{bmatrix} u(t) \quad \text{and} \quad \dot{x}(t) = Ax(t) + \begin{bmatrix} B_1 & 0 \\ 0 & B_2 \end{bmatrix} \begin{bmatrix} u(t) \\ u(t) \end{bmatrix} \tag{6.1}
$$

  can be studied analytically in more detail. The controllability Gramians of these systems can be compared in terms of their input matrix representation; earlier, we concluded that representing the input matrix in the diagonal form causes a controllability loss of the system.

- For the optimal linear controllers designed in Chapter 4, evolutionary optimization algorithms may be used in constructing the optimal weighting matrices R and Q.

Nonlinear controllers can also be designed to eliminate the need for linearization and to improve the dynamic response of the considered wind turbine system during grid disturbances.

- A major hindrance associated with the cross Gramian-based solution is that this technique is applicable to square systems only. The proposed algorithm in Chapter 5 may be extended to include the non-square systems.

- The presented algorithms are suitable to be implemented as the modern reinforcement learning algorithms, since the reinforcement learning methods for dynamic systems are in fact approximate optimal control (approximate dynamic programming) methods.

Appendix A

A.1 Wind Turbine with DFIG Energy System Parameters

$C_1 = 0.5176, \quad C_2 = 116, \quad C_3 = 0.4, \quad C_4 = 5, \quad C_5 = 21, \quad C_6 = 0.0068,$

$v_p = 690V, \quad T_{sp} = 0.8064, \quad v = 9m/s, \quad C_p = 0.48, \quad P_{nom} = 2MVA,$

$H_t = 3.5, \quad k_{opt} = 0.56, \quad \omega_s = 1, \quad F_b = 50, \quad \omega_b = 2\pi F_b, \quad V_{SC} = 16MVA,$

$S_b = 2, \quad VA = 16, \quad Z_e = \frac{S_b}{VA} = 0.125,$

$X_{ls} = 0.09241, \quad X_{lr} = 0.09955, \quad X_m = 3.95279, \quad X_{tr} = 0.05, \quad X_R = 10,$

$R_r = 0.00549, \quad R_s = 0.00488,$

$X_{ss} = X_{ls} + X_m = 4.0452,$

$X_{rr} = X_{lr} + X_m = 4.0452,$

$X_T = X_e + X_{tr} = 0.1744,$

$R_e = \frac{Z_e}{\sqrt{1+X_R^2}} = 0.0124,$

$X_e = R_e X_R = 0.1244,,$

$R_T = R_s + R_e = 0.0173$

A.2 Wind Turbine with DFIG Energy System Operating Points

$i_{ds0} = -0.035, \quad i_{qs0} = 0.343, \quad i_{dr0} = 0.217, \quad i_{qr0} = 0.367$

$v_{ds0} = -0.06, \quad v_{qs0} = 0.998, \quad v_{dr0} = -0.025, \quad v_{qr0} = 0.206,$

$v_{s0} = 0.9998, \quad \omega_{r0} = 0.8, \quad s_0 = 0.2$

A.3 Wind Turbine with DFIG Energy System Matrices

$$a_{11} = \frac{W_b}{(X_{rr}X_{ss} - X_m^2)}\{(-R_T X_{rr} + \frac{K_{p2}}{V_{s0}W_s})(R_T V_{ds0} + X_T V_{qs0})\},$$

$$a_{12} = \frac{W_b}{(X_{rr}X_{ss} - X_m^2)}\{(X_{rr}X_{ss} - s_0 X_m^2)W_s + X_T X_{rr} +$$

$$(K_{p2}/V_{s0}W_s)(R_T V_{qs0} - X_T V_{ds0})\},$$

$$a_{13} = \frac{W_b}{(X_{rr}X_{ss} - X_m^2)}\{-X_m(R_r + K_{p2})\},$$

$$a_{14} = \frac{W_b}{(X_{rr}X_{ss} - X_m^2)}\{(-X_m X_{rr} + s_0 X_m X_{rr})W_s\},$$

$$a_{15} = \frac{W_b}{(X_{rr}X_{ss} - X_m^2)}\{(X_m i_{qs0} - X_{rr} i_{qr0})X_m\},$$

$$a_{16} = \frac{W_b X_m}{(X_{rr}X_{ss} - X_m^2)}, \quad a_{17} = 0, \quad a_{18} = \frac{W_b X_m K_{p2}}{(X_{rr}X_{ss} - X_m^2)},$$

$$a_{21} = \frac{W_b}{(X_{rr}X_{ss} - X_m^2)}\{(-X_{rr}X_{ss} + s_0 X_m^2)W_s - X_T X_{rr}$$

$$+ (K_{p1}K_{opt}X_{ss}W_s W_{r0}^2/V_{s0}^3)(R_T V_{ds0} + X_T V_{qs0})\},$$

$$a_{22} = \frac{W_b}{(X_{rr}X_{ss} - X_m^2)}\{(-R_T X_{rr} + (K_{p1}K_{opt}X_{ss}W_s W_{r0}^2/V_{s0}^3)(R_T V_{qs0} - X_T V_{ds0})\},$$

$$a_{23} = -a_{14}, \quad a_{24} = \frac{W_b}{(X_{rr}X_{ss} - X_m^2)}\{-X_m(R_r + K_{p1})\},$$

$$a_{25} = \frac{W_b}{(X_{rr}X_{ss} - X_m^2)}\{(-X_m i_{ds0} + X_{rr} i_{dr0})X_m\}, \quad a_{26} = 0, \quad a_{27} = a_{16}, \quad a_{28} = 0,$$

$$a_{31} = \frac{W_b}{(X_{rr}X_{ss} - X_m^2)}\{-R_T X_m + (K_{p1}X_{ss}/(X_m V_{s0}W_s))(R_T V_{ds0} + X_T V_{qs0})\}$$

$$a_{32} = \frac{W_b}{(X_{rr}X_{ss} - X_m^2)}\{(X_m X_{ss} - s_0 X_m X_{ss})W_s + X_T X_{rr}$$

$$+ (K_{p2}X_{ss}/(X_m V_{s0}W_s))(R_T V_{qs0} - X_T V_{ds0})\},$$

$$a_{33} = \frac{W_b}{(X_{rr}X_{ss} - X_m^2)}\{-X_{ss}(R_r + K_{p2}),$$

$$a_{34} = \frac{W_b}{(X_{rr}X_{ss} - X_m^2)}\{(-X_m^2 + s_0 X_{ss} X_{rr})W_s\},$$

$$a_{35} = \frac{W_b}{(X_{rr}X_{ss} - X_m^2)}\{(X_m i_{qs0} - X_{rr} i_{qr0})X_{ss}\},$$

$$a_{36} = \frac{W_b X_{ss}}{(X_{rr}X_{ss} - X_m^2)}, \quad a_{37} = 0,$$

$$a_{38} = \frac{W_b}{(X_{rr}X_{ss} - X_m^2)}\{X_{ss}K_{p2}\},$$

$$a_{41} = \frac{W_b}{(X_{rr}X_{ss} - X_m^2)}\{(-X_mX_{ss} + s_0X_mX_{ss})W_s - X_TX_{rr}$$

$$+ (K_{p1}K_{opt}X_{ss}^2W_sWr0^2/(V_{s0}^3X_m))(R_TV_{ds0} + X_TV_{qs0})\},$$

$$a_{42} = \frac{W_b}{(X_{rr}X_{ss} - X_m^2)}\{-R_TX_m + (K_{p1}K_{opt}X_{ss}^2W_sW_{r0}^2/(V_{s0}^3X_m))(R_TV_{qs0} - X_TV_{ds0})\},$$

$$a_{43} = \frac{W_b}{(X_{rr}X_{ss} - X_m^2)}\{(X_m^2 - s_0X_{ss}X_{rr})W_s\},$$

$$a_{44} = \frac{W_b}{(X_{rr}X_{ss} - X_m^2)}\{-X_{ss}(R_r + K_{p1})\},$$

$$a_{45} = \frac{W_b}{(X_{rr}X_{ss} - X_m^2)}\{(-X_mi_{ds0} + X_{rr}i_{dr0})X_{ss} + 2(K_{p1}X_{ss}/X_m)\},$$

$$a_{46} = 0 \quad a_{47} = a_{36}, \quad a_{48} = 0,$$

$$a_{51} = X_mi_{qr0}/(2H_{tot}), \quad a_{52} = -X_mi_{dr0}/(2H_{tot}), \quad a_{53} = -X_mi_{qs0}/(2H_{tot}),$$

$$a_{54} = X_mi_{ds0}/(2H_{tot}), \quad a_{55} = 0, \quad a_{56} = 0, \quad a_{57} = 0, \quad a_{58} = 0,$$

$$a_{61} = (K_{i2}/(V_{s0}W_sX_m))(R_TV_{ds0} + X_TV_{qs0}),$$

$$a_{62} = (K_{i2}/(V_{s0}W_sX_m)) * (R_TV_{ds0} - X_TV_{ds0}),$$

$$a_{63} = -K_{i2}, \quad a_{64} = 0 \quad a_{65} = 0, \quad a_{66} = 0, \quad a_{67} = 0, \quad a_{68} = K_{i2},$$

$$a_{71} = (K_{i1}K_{opt}X_{ss}W_sW_{r0}^2/(V_{s0}^3X_m))(R_TV_{ds0} + X_TV_{qs0}),$$

$$a_{72} = (K_{i1}K_{opt}X_{ss}W_sW_{r0}^2/(V_{s0}^3X_m))(R_TV_{qs0} - X_TV_{ds0}),$$

$$a_{73} = 0, \quad a_{74} = -K_{i1}, \quad a_{75} = 2K_{i1}K_{opt}X_{ss}W_sW_{r0}/(X_mV_{s0}),$$

$$a_{76} = 0, \quad a_{77} = 0, \quad a_{78} = 0,$$

$$a_{81} = (-K_{p3}/V_{s0})(R_TV_{ds0} + X_TV_{qs0}),$$

$$a_{82} = (K_{p3}/V_{s0})(R_TV_{qs0} - X_TV_{ds0}), \quad a_{83} = 0,$$

$$a_{84} = 0, \quad a_{85} = 0, \quad a_{86} = 0, \quad a_{87} = 0, \quad a_{88} = 0,$$

$$b_{61} = -Ki2, \quad b_{62} = 0, \quad b_{63} = -K_{i2}K_{p3} + \frac{K_{i2}}{W_s X_m}, \quad b_{64} = K_{i2}K_{p3}, \quad b_{65} = 0,$$

$$b_{71} = 0, \quad b_{72} = -K_{i1}, \quad b_{73} = -\frac{K_{i1}X_{ss}Tsp}{W_s X_m V_{s0}^2},$$

$$b_{74} = 0, \quad b_{75} = \frac{K_{i1}X_{ss}}{W_s X_m V_{s0}},$$

$$b_{81} = 0 \quad b_{82} = 0 \quad b_{83} = -K_{p3} \quad b_{84} = K_{p3} \quad b_{85} = 0,$$

$$E = \frac{1}{\omega_b} \begin{bmatrix} -X_{ss} & 0 & X_m & 0 & 0 \\ 0 & -X_{ss} & 0 & X_m & 0 \\ -X_m & 0 & X_{rr} & 0 & 0 \\ 0 & -X_m & 0 & X_{rr} & 0 \\ 0 & 0 & 0 & 0 & 2H_{tot}\omega_b \end{bmatrix},$$

$$B_{conv} = \begin{bmatrix} b_{61} & b_{62} & b_{63} & b_{64} & b_{65} \\ b_{71} & b_{72} & b_{73} & b_{74} & b_{75} \\ b_{81} & b_{82} & b_{83} & b_{84} & b_{85} \end{bmatrix}, \quad B = \begin{bmatrix} E^{-1} \\ B_{conv} \end{bmatrix}$$

Appendix B

B.1 Direct Quadrature Zero Transformation

In order to simplify the mathematical model analysis, and to eliminate the effect of time-varying inductances, the three-phase stator and rotor quantities (voltages, currents, and flux linkages) are transformed into a single rotating reference frame $dq0$ using the direct-quadrature-zero transformation (DQZ). The DQZ transformation is the product of the Clarke and Park transformation matrices. The Clarke transformation matrix is given by

$$T_{Clarke} = \sqrt{\frac{2}{3}} \cdot \begin{bmatrix} 1 & -\frac{1}{2} & -\frac{1}{2} \\ 0 & -\frac{\sqrt{3}}{2} & -\frac{\sqrt{3}}{2} \\ \frac{1}{\sqrt{2}} & \frac{1}{\sqrt{2}} & \frac{1}{\sqrt{2}} \end{bmatrix} \tag{B.1}$$

The Park transformation matrix is given by

$$T_{Park} = \begin{bmatrix} cos\theta & sin\theta & 0 \\ -sin\theta & cos\theta & 0 \\ 0 & 0 & 1 \end{bmatrix} \tag{B.2}$$

where θ is an arbitrary rotation angle. Together, the Clarke and Park transforms form the DQZ transform:

$$T_{PC} = T_{Park} \cdot T_{Clarke} \tag{B.3}$$

Let $x_{abc} = [x_a, x_b, x_c]^T$ and $x_{dq0} = [x_d, x_q, x_0]^T$, then, in matrix notation, we have

$$x_{dq0} = T_{PC}x_{abc} = \sqrt{\frac{2}{3}} \cdot \begin{bmatrix} cos\theta & cos(\theta - \frac{2\pi}{3}) & cos(\theta + \frac{2\pi}{3}) \\ -sin\theta & -sin(\theta - \frac{2\pi}{3}) & -sin(\theta + \frac{2\pi}{3}) \\ \frac{1}{\sqrt{2}} & \frac{1}{\sqrt{2}} & \frac{1}{\sqrt{2}} \end{bmatrix} \begin{bmatrix} x_a \\ x_b \\ x_c \end{bmatrix} \tag{B.4}$$

where the subscripts d, q, and 0 represent the direct, quadrature, and zero components. The angle θ, here, is the reference angle or reference phase and is typically chosen as $\omega_s t$ where ω_s is the frequency of the infinite bus or is fixed to the rotor angle of one of the synchronous machines [109]. T_{PC} is an orthogonal transformation matrix. Thus, the inverse transform is

$$
x_{abc} = T_{PC}^{-1} x_{dq0} = \sqrt{\frac{2}{3}} \begin{bmatrix} cos\theta & -sin\theta & \frac{1}{\sqrt{2}} \\ cos(\theta - \frac{2\pi}{3}) & -sin(\theta - \frac{2\pi}{3}) & \frac{1}{\sqrt{2}} \\ cos(\theta + \frac{2\pi}{3}) & -sin(\theta + \frac{2\pi}{3}) & \frac{1}{\sqrt{2}} \end{bmatrix} \begin{bmatrix} x_d \\ x_q \\ x_0 \end{bmatrix} \tag{B.5}
$$

The stator and rotor voltages of the DFIG, respectively, in the three phase frame are given by

$$
\begin{bmatrix} v_{as}(t) \\ v_{bs}(t) \\ v_{cs}(t) \end{bmatrix} = R_s \begin{bmatrix} i_{as}(t) \\ i_{bs}(t) \\ i_{cs}(t) \end{bmatrix} + \frac{d}{dt} \begin{bmatrix} \psi_{as}(t) \\ \psi_{bs}(t) \\ \psi_{cs}(t) \end{bmatrix}
$$

$$
\begin{bmatrix} v_{ar}(t) \\ v_{br}(t) \\ v_{cr}(t) \end{bmatrix} = R_r \begin{bmatrix} i_{ar}(t) \\ i_{br}(t) \\ i_{cr}(t) \end{bmatrix} + \frac{d}{dt} \begin{bmatrix} \psi_{ar}(t) \\ \psi_{br}(t) \\ \psi_{cr}(t) \end{bmatrix}
$$

(B.6)

where subscripts a, b, and c stand for the three phase quantities in the abc-frame, while subscripts s and r stand for the stator and rotor, respectively. v, i, ψ, R_s, and R_r are the voltages, currents, flux linkages, and stator and rotor winding resistances, respectively.

The flux linkages are related to the currents as follows

$$
\begin{bmatrix} \psi_{as}(t) \\ \psi_{bs}(t) \\ \psi_{cs}(t) \end{bmatrix} = L_s \begin{bmatrix} i_{as}(t) \\ i_{bs}(t) \\ i_{cs}(t) \end{bmatrix} + L_m \begin{bmatrix} i_{ar}(t) \\ i_{br}(t) \\ i_{cr}(t) \end{bmatrix}
$$

$$
\begin{bmatrix} \psi_{ar}(t) \\ \psi_{br}(t) \\ \psi_{cr}(t) \end{bmatrix} = L_r \begin{bmatrix} i_{ar}(t) \\ i_{br}(t) \\ i_{cr}(t) \end{bmatrix} + L_m^T \begin{bmatrix} i_{as}(t) \\ i_{bs}(t) \\ i_{cs}(t) \end{bmatrix}
$$

(B.7)

The inductance matrices are defined by

$$
L_s = \begin{bmatrix} L_{ls} + L_m & -\frac{1}{2} L_m & -\frac{1}{2} L_m \\ -\frac{1}{2} L_m & L_{ls} + L_m & -\frac{1}{2} L_m \\ -\frac{1}{2} L_m & -\frac{1}{2} L_m & L_{ls} + L_m \end{bmatrix}
$$

(B.8)

$$
L_r = \begin{bmatrix} L_{lr} + L_m & -\frac{1}{2} L_m & -\frac{1}{2} L_m \\ -\frac{1}{2} L_m & L_{lr} + L_m & -\frac{1}{2} L_m \\ -\frac{1}{2} L_m & -\frac{1}{2} L_m & L_{lr} + L_m \end{bmatrix}
$$

(B.9)

$$
L_m = \hat{L}_m \begin{bmatrix} \cos(\theta_r) & \cos(\theta_r + \frac{2\pi}{3}) & \cos(\theta_r - \frac{2\pi}{3}) \\ \cos(\theta_r - \frac{2\pi}{3}) & \cos(\theta_r) & \cos(\theta_r + \frac{2\pi}{3}) \\ \cos(\theta_r + \frac{2\pi}{3}) & \cos(\theta_r - \frac{2\pi}{3}) & \cos(\theta_r) \end{bmatrix}
$$

(B.10)

where subscripts l and m stand for the leakage and magnetizing inductances, respectively. $\hat{L}_m$ is the maximum mutual inductance between the stator and the rotor. $\theta_r(t)$ is the electrical rotor speed.

Applying (B.4) to the DFIG equations (B.6) and (B.7) in the abc-frame gives the DFIG model in the dq-frame. The stator and rotor voltage and flux dynamic equations

in the dq synchronous reference frame are given, respectively, by [5, 15, 40].

$$
\begin{bmatrix} v_{ds} \\ v_{qs} \end{bmatrix} = R_s \begin{bmatrix} i_{ds} \\ i_{qs} \end{bmatrix} + \omega_s \begin{bmatrix} -\psi_{qs} \\ \psi_{ds} \end{bmatrix} + \frac{d}{dt} \begin{bmatrix} \psi_{ds} \\ \psi_{qs} \end{bmatrix}
$$

$$
\begin{bmatrix} v_{dr} \\ v_{qr} \end{bmatrix} = R_r \begin{bmatrix} i_{dr} \\ i_{qr} \end{bmatrix} + s\omega_s \begin{bmatrix} -\psi_{qr} \\ \psi_{dr} \end{bmatrix} + \frac{d}{dt} \begin{bmatrix} \psi_{dr} \\ \psi_{qr} \end{bmatrix}
$$

$$(B.11)$$

$$
\begin{bmatrix} \psi_{ds} \\ \psi_{qs} \end{bmatrix} = \begin{bmatrix} L_{ls} + \frac{3}{2}L_m & 0 \\ 0 & L_{ls} + \frac{3}{2}L_m \end{bmatrix} \begin{bmatrix} i_{ds} \\ i_{qs} \end{bmatrix} + \begin{bmatrix} \frac{3}{2}L_m & 0 \\ 0 & \frac{3}{2}L_m \end{bmatrix} \begin{bmatrix} i_{dr} \\ i_{qr} \end{bmatrix}
$$

$$(B.12)$$

$$
\begin{bmatrix} \psi_{dr} \\ \psi_{qr} \end{bmatrix} = \begin{bmatrix} L_{lr} + \frac{3}{2}L_m & 0 \\ 0 & L_{lr} + \frac{3}{2}L_m \end{bmatrix} \begin{bmatrix} i_{dr} \\ i_{qr} \end{bmatrix} + \begin{bmatrix} \frac{3}{2}L_m & 0 \\ 0 & \frac{3}{2}L_m \end{bmatrix} \begin{bmatrix} i_{ds} \\ i_{qs} \end{bmatrix}
$$

where the subscripts s and r denote the stator and rotor quantities, whereas subscripts q and d denote the components aligned with the q-axis and d-axis reference frames, respectively. In (B.11), ω_s and ω_r are the synchronous stator and rotor angular frequencies, respectively. s is defined as the slip of the generator, and is given by $s = (\omega_s - \omega_r)/\omega_s$.

B.2   Per Unit System

In order to simplify the calculations when dealing with different quantities in the power systems, such as the different voltage levels separated by multiple transformers, the per unit system can be used to obtain the normalized values of all quantities. The per unit quantity is defined by the ratio between the original value and the base value

$$
\text{per unit value} = \frac{\text{original value}}{\text{base value}}
$$

$$(B.13)$$

The power and the voltage are usually chosen as the base quantities, and all other base quantities are derived after that by the laws of electrical circuits. The base power S_{base}

is chosen considering the rated power of the generator. For the base voltage V_{base}, the nominal voltage is considered, with the low and high voltage sides of the transformers being related to each other through the appropriate turn ratio [110]. Similarly, the synchronous speed is chosen as the base values, with the different base speeds on the low and high speed sides of the gearboxes being related to each other through the gearbox ratio. More details on the chosen and deduced base quantities for the DFIG generator can be found in [110].

References

[1] R. H. Wiser and M. Bolinger, "2018 Wind Technologies Market Report," 2019.

[2] M. Ram, M. Child, A. Aghahosseini, D. Bogdanov, A. Lohrmann, and C. Breyer, "A comparative analysis of electricity generation costs from renewable, fossil fuel and nuclear sources in g20 countries for the period 2015-2030," *Journal of Cleaner Production*, vol. 199, pp. 687–704, 2018.

[3] E. Hau, *Wind Turbines: Fundamentals, Technologies, Application, Economics*. Springer Science & Business Media, 2013.

[4] C. Dao, B. Kazemtabrizi, and C. Crabtree, "Wind turbine reliability data review and impacts on levelised cost of energy," *Wind Energy*, vol. 22, no. 12, pp. 1848–1871, 2019.

[5] O. Anaya-Lara, N. Jenkins, J. Ekanayake, P. Cartwright, and M. Hughes, *Wind Energy Generation: Modelling and Control*. John Wiley & Sons, 2011.

[6] F. D. Bianchi, H. De Battista, and R. J. Mantz, *Wind Turbine Control Systems: Principles, Modelling and Gain Scheduling Design*. Springer Science & Business Media, 2006.

[7] K. E. Johnson, L. Y. Pao, M. J. Balas, and L. J. Fingersh, "Control of variable-speed wind turbines: standard and adaptive techniques for maximizing energy capture," *IEEE Control Systems Magazine*, vol. 26, no. 3, pp. 70–81, 2006.

[8] B. Boukhezzar and H. Siguerdidjane, "Comparison between linear and nonlinear control strategies for variable speed wind turbines," *Control Engineering Practice*, vol. 18, no. 12, pp. 1357–1368, 2010.

[9] C. E. Ugalde-Loo and J. B. Ekanayake, "State-space modelling of variable-speed wind turbines: A systematic approach," in *2010 IEEE International Conference on Sustainable Energy Technologies (ICSET)*. IEEE, 2010, pp. 1–6.

[10] C. E. Ugalde-Loo, J. B. Ekanayake, and N. Jenkins, "State-space modeling of wind turbine generators for power system studies," *IEEE Transactions on Industry Applications*, vol. 49, no. 1, pp. 223–232, 2013.

[11] B. Mehta, P. Bhatt, and V. Pandya, "Small signal stability enhancement of dfig based wind power system using optimized controllers parameters," *International Journal of Electrical Power & Energy Systems*, vol. 70, pp. 70–82, 2015.

[12] I. Al-Iedani and Z. Gajic, "Order reduction of a wind turbine energy system via the methods of system balancing and singular perturbations," *International Journal of Electrical Power & Energy Systems*, vol. 117, p. 105642, 2020.

[13] I. Al-Iedani and Z. Gajic, "Optimal control of wind turbine systems via time-scale decomposition," *Energies*, vol. 13, no. 2, p. 287, 2020.

[14] I. Al-Iedani and Z. Gajic, "Recursive reduced-order algorithm for singularly perturbed cross grammian algebraic sylvester equation," *Mathematical Problems in Engineering*, vol. 2016, 2016.

[15] P. Kundur, N. J. Balu, and M. G. Lauby, *Power System Stability and Control*. McGraw-hill New York, 1994, vol. 7.

[16] A. Feijóo, J. Cidrás, and C. Carrillo, "A third order model for the doubly-fed induction machine," *Electric Power Systems Research*, vol. 56, no. 2, p. 121, 2000.

[17] J. B. Ekanayake, L. Holdsworth, and N. Jenkins, "Comparison of 5th order and 3rd order machine models for doubly fed induction generator (dfig) wind turbines," *Electric Power Systems Research*, vol. 67, no. 3, pp. 207–215, 2003.

[18] P. Ledesma and J. Usaola, "Effect of neglecting stator transients in doubly fed induction generators models," *IEEE Transactions on Energy Conversion*, vol. 19, no. 2, pp. 459–461, 2004.

[19] A. Rolán and J. Pedra, "Doubly fed induction generator-based variable-speed wind turbine: Proposal of a simplified model under a faulty grid with short-duration faults," *Wind Energy*, vol. 22, no. 8, pp. 1121–1133, 2019.

[20] J. Slootweg and W. Kling, "Aggregated modelling of wind parks in power system dynamics simulations," in *2003 IEEE Bologna Power Tech Conference Proceedings,*, vol. 3. IEEE, 2003, pp. 6–pp.

[21] L. Fernandez, C. Garcia, J. Saenz, and F. Jurado, "Equivalent models of wind farms by using aggregated wind turbines and equivalent winds," *Energy conversion and management*, vol. 50, no. 3, pp. 691–704, 2009.

[22] H. Liu and Z. Chen, "Aggregated modelling for wind farms for power system transient stability studies," in *2012 Asia-Pacific Power and Energy Engineering Conference*. IEEE, 2012, pp. 1–6.

[23] H. A. Pulgar-Painemal and P. W. Sauer, "Reduced-order model of type-c wind turbine generators," *Electric Power Systems Research*, vol. 81, no. 4, pp. 840–845, 2011.

[24] S. Ghosh and N. Senroy, "Balanced truncation based reduced order modeling of wind farm," *International Journal of Electrical Power & Energy Systems*, vol. 53, pp. 649–655, 2013.

[25] H. A. Mohammadpour, A. Ghaderi, H. Mohammadpour, and E. Santi, "Ssr damping in wind farms using observed-state feedback control of dfig converters," *Electric Power Systems Research*, vol. 123, pp. 57–66, 2015.

[26] B. G. Rawn, P. W. Lehn, and M. Maggiore, "Control methodology to mitigate the grid impact of wind turbines," *IEEE Transactions on Energy Conversion*, vol. 22, no. 2, pp. 431–438, 2007.

[27] D. Fu and Y. Xing, "Study on linear dynamic model and analysis of operating characteristics of high-power vscf wind energy conversion system," in *2009 World Non-Grid-Connected Wind Power and Energy Conference*. IEEE, 2009, pp. 1–6.

[28] R. Zarouala, C. Vivas, J. Á. Acosta, and L. El Bakkali, "On singular perturbations of flexible and variable-speed wind turbines." *International Journal of Aerospace Engineering*, 2012.

[29] X. Li, X. Chen, and G. Tang, "Output feedback control of doubly-fed induction generator based on multi-time scale model," in *2008 Third International Conference on Electric Utility Deregulation and Restructuring and Power Technologies*. IEEE, 2008, pp. 2798–2802.

[30] P. Han, Y. Zhang, L. Wang, Y. Zhang, and Z. Lin, "Model reduction of dfig wind turbine system based on inner coupling analysis," *Energies*, vol. 11, no. 11, p. 3234, 2018.

[31] S. Ganjefar and A. Mohammadi, "Variable speed wind turbines with maximum power extraction using singular perturbation theory," *Energy*, vol. 106, pp. 510–519, 2016.

[32] S. Xia, S. Bu, X. Zhang, Y. Xu, B. Zhou, and J. Zhu, "Model reduction strategy of doubly-fed induction generator-based wind farms for power system small-signal rotor angle stability analysis," *Applied energy*, vol. 222, pp. 608–620, 2018.

[33] Y. Ni, C. Li, Z. Du, and G. Zhang, "Model order reduction based dynamic equivalence of a wind farm," *International Journal of Electrical Power & Energy Systems*, vol. 83, pp. 96–103, 2016.

[34] G. Abad, J. Lopez, M. Rodriguez, L. Marroyo, and G. Iwanski, *Doubly Fed Induction Machine: Modeling and Control for Wind Energy Generation*. John Wiley & Sons, 2011, vol. 85.

[35] H. Jadhav and R. Roy, "A comprehensive review on the grid integration of doubly fed induction generator," *International Journal of Electrical Power & Energy Systems*, vol. 49, pp. 8–18, 2013.

[36] I. Ngamroo, "Review of dfig wind turbine impact on power system dynamic performances," *IEEJ Transactions on electrical and electronic engineering*, vol. 12, no. 3, pp. 301–311, 2017.

[37] M. Rahimi, "Dynamic performance assessment of dfig-based wind turbines: A review," *Renewable and Sustainable Energy Reviews*, vol. 37, pp. 852–866, 2014.

[38] F. Wu, X.-P. Zhang, K. Godfrey, and P. Ju, "Small signal stability analysis and optimal control of a wind turbine with doubly fed induction generator," *IET Generation, Transmission & Distribution*, vol. 1, no. 5, pp. 751–760, 2007.

[39] S. Chatterjee, A. Naithani, and V. Mukherjee, "Small-signal stability analysis of dfig based wind power system using teaching learning based optimization," *International Journal of Electrical Power & Energy Systems*, vol. 78, pp. 672–689, 2016.

[40] C. Hamon, K. Elkington, and M. Ghandhari, "Doubly-fed induction generator modeling and control in digsilent powerfactory," in *2010 International Conference on Power System Technology*. IEEE, 2010, pp. 1–7.

[41] A. Wu, B. Zhao, J. Mao, B. Wu, and F. Yu, "Adaptive active fault-tolerant mppt control for wind power generation system under partial loss of actuator effectiveness," *International Journal of Electrical Power & Energy Systems*, vol. 105, pp. 660–670, 2019.

[42] R. Pena, J. Clare, and G. Asher, "Doubly fed induction generator using back-to-back pwm converters and its application to variable-speed wind-energy generation," *IEE Proceedings-Electric power applications*, vol. 143, no. 3, pp. 231–241, 1996.

[43] S. Muller, M. Deicke, and R. W. De Doncker, "Doubly fed induction generator systems for wind turbines," *IEEE Industry applications magazine*, vol. 8, no. 3, pp. 26–33, 2002.

[44] A. D. Hansen, P. Soerensen, F. Iov, and F. Blaabjerg, "Control of variable speed wind turbines with doubly-fed induction generators," *Wind Engineering*, vol. 28, no. 4, pp. 411–432, 2004.

[45] J. Mohammadi, S. Vaez-Zadeh, S. Afsharnia, and E. Daryabeigi, "A combined vector and direct power control for dfig-based wind turbines," *IEEE Transactions on Sustainable Energy*, vol. 5, no. 3, pp. 767–775, 2014.

[46] B. Moore, "Principal component analysis in linear systems: Controllability, observability, and model reduction," *IEEE transactions on automatic control*, vol. 26, no. 1, pp. 17–32, 1981.

[47] C.-T. Chen, *Linear System Theory and Design*. Oxford University Press, Inc., 1995.

[48] Z. Gajic and M. Lelic, "Improvement of system order reduction via balancing using the method of singular perturbations," *Automatica*, vol. 37, no. 11, pp. 1859–1865, 2001.

[49] K. Glover, "All optimal hankel-norm approximations of linear multivariable systems and their l,infinity error bounds," *International journal of control*, vol. 39, no. 6, pp. 1115–1193, 1984.

[50] R. Samar, I. Postlethwaite, and D.-W. Gu, "Model reduction with balanced realizations," *International Journal of Control*, vol. 62, no. 1, pp. 33–64, 1995.

[51] Y. Liu and B. D. Anderson, "Singular perturbation approximation of balanced systems," *International Journal of Control*, vol. 50, no. 4, pp. 1379–1405, 1989.

[52] K. Kodra and Z. Gajic, "Order reduction via balancing and suboptimal control of a fuel cell–reformer system," *International journal of hydrogen energy*, vol. 39, no. 5, pp. 2215–2223, 2014.

[53] A. Sinha, *Linear Systems: Optimal and Robust Control*. CRC Press, 2007.

[54] P. Kokotovic, H. K. Khalil, and J. O'Reilly, *Singular Perturbation Methods in Control: Analysis and Design*. SIAM, 1999, vol. 25.

[55] Z. Gajic and M.-T. Lim, *Optimal Control of Singularly Perturbed Linear Systems and Applications*. Marcel Dekker, 2001.

[56] K. Kodra, N. Zhong, and Z. Gajić, "Multi-time-scale systems control via use of combined controllers," in *2016 European Control Conference (ECC)*. IEEE, 2016, pp. 2638–2643.

[57] G. H. Golub and C. F. Van Loan, *Matrix Computations*. JHU press, 2012, vol. 3.

[58] I. IEC, "61400e1: Wind turbines part 1: design requirements," *International Electrotechnical Commission*, 2005.

[59] J. L. Rodriguez-Amenedo, S. Arnalte, and J. C. Burgos, "Automatic generation control of a wind farm with variable speed wind turbines," *IEEE Transactions on energy conversion*, vol. 17, no. 2, pp. 279–284, 2002.

[60] A. Tapia, G. Tapia, J. Ostolaza, J. Saenz, R. Criado, and J. Berasategui, "Reactive power control of a wind farm made up with doubly fed induction generators. I." in *Power Tech Proceedings, 2001 IEEE Porto*, vol. 4. IEEE, 2001, pp. 6–pp.

[61] V. Akhmatov and H. Knudsen, "An aggregate model of a grid-connected, large-scale, offshore wind farm for power stability investigations—importance of windmill mechanical system," *International Journal of Electrical Power & Energy Systems*, vol. 24, no. 9, pp. 709–717, 2002.

[62] J. B. Ekanayake, L. Holdsworth, X. Wu, and N. Jenkins, "Dynamic modeling of doubly fed induction generator wind turbines," *IEEE Transactions on Power systems*, vol. 18, no. 2, pp. 803–809, 2003.

[63] L. M. Fernández, F. Jurado, and J. R. Saenz, "Aggregated dynamic model for wind farms with doubly fed induction generator wind turbines," *Renewable energy*, vol. 33, no. 1, pp. 129–140, 2008.

[64] Y. Ni, Z. Du, C. Li, and G. Zhang, "Cross-gramian-based dynamic equivalence of wind farms," *IET Generation, Transmission & Distribution*, vol. 10, no. 6, pp. 1422–1430, 2016.

[65] S. Ghosh, Y. J. Isbeih, M. S. El Moursi, and E. F. El-Saadany, "Cross-gramian model reduction approach for tuning power system stabilizers in large power networks," *IEEE Transactions on Power Systems*, vol. 35, no. 3, pp. 1911–1922, 2019.

[66] Z. Gajic and M. Lelic, *Modern Control Systems Engineering*. Prentice-Hall, Inc., 1996.

[67] H. Lee and Y. Park, "Degree of controllability for linear unstable systems," *Journal of Vibration and Control*, vol. 22, no. 7, pp. 1928–1934, 2016.

[68] Y. Xia, M. Yin, C. Cai, B. Zhang, and Y. Zou, "A new measure of the degree of controllability for linear system with external disturbance and its application to wind turbines," *Journal of Vibration and Control*, vol. 24, no. 4, pp. 739–759, 2018.

[69] Y. Xia, M. Yin, R. Li, D. Liu, and Y. Zou, "Integrated structure and maximum power point tracking control design for wind turbines based on degree of controllability," *Journal of Vibration and Control*, vol. 25, no. 2, pp. 397–407, 2019.

[70] T. Sadamoto and A. Chakrabortty, "Improving controllability and plug-and-play operation of wind farms using b2b converters," *IEEE Control Systems Letters*, vol. 4, no. 2, pp. 379–384, 2019.

[71] K. Fernando and H. Nicholson, "On the structure of balanced and other principal representations of siso systems," *IEEE Transactions on Automatic Control*, vol. 28, no. 2, pp. 228–231, 1983.

[72] P. Lancaster and M. Tismenetsky, *The Theory of Matrices: with Applications*. Elsevier, 1985.

[73] A. Laub, L. Silverman, and M. Verma, "A note on cross-grammians for symmetric realizations," *Proceedings of the IEEE*, vol. 71, no. 7, pp. 904–905, 1983.

[74] K. Fernando and H. Nicholson, "On a fundamental property of the cross-gramian matrix," *IEEE transactions on circuits and systems*, vol. 31, no. 5, pp. 504–505, 1984.

[75] K. Fernando and H. Nicholson, "Reachability, observability, and minimality of mimo systems," *Proceedings of the IEEE*, vol. 72, no. 12, pp. 1820–1821, 1984.

[76] K. Fernando and H. Nicholson, "On the cross-gramian for symmetric mimo systems," *IEEE Transactions on Circuits and Systems*, vol. 32, no. 5, pp. 487–489, 1985.

[77] C. Himpe and M. Ohlberger, "Cross-gramian-based combined state and parameter reduction for large-scale control systems," *Mathematical Problems in Engineering*, vol. 2014, 2014.

[78] P. V. Kokotovic, J. J. Allemong, J. R. Winkelman, and J. H. Chow, "Singular perturbation and iterative separation of time scales," *Automatica*, vol. 16, no. 1, pp. 23–33, 1980.

[79] K. W. Chang, "Singular perturbations of a general boundary value problem," *SIAM Journal on Mathematical Analysis*, vol. 3, no. 3, pp. 520–526, 1972.

[80] Z. Gajic and X. S. Shen, *Parallel Algorithms for Optimal Control of Large Scale Linear Systems*. Springer Science & Business Media, 2012.

[81] K. Kodra and Z. Gajic, "Optimal control for a new class of singularly perturbed linear systems," *Automatica*, vol. 81, pp. 203–208, 2017.

[82] J. G. Njiri and D. Söffker, "State-of-the-art in wind turbine control: Trends and challenges," *Renewable and Sustainable Energy Reviews*, vol. 60, pp. 377–393, 2016.

[83] Y. Yuan and J. Tang, "On advanced control methods toward power capture and load mitigation in wind turbines," *Engineering*, vol. 3, no. 4, pp. 494–503, 2017.

[84] E. J. N. Menezes, A. M. Araújo, and N. S. B. da Silva, "A review on wind turbine control and its associated methods," *Journal of cleaner production*, vol. 174, pp. 945–953, 2018.

[85] H. M. Nguyen and D. S. Naidu, "Time scale analysis and control of wind energy conversion systems," in *2012 5th International Symposium on Resilient Control Systems*. IEEE, 2012, pp. 149–154.

[86] Y. Zhang, H. Nguyen, D. S. Naidu, Y. Zou, and C. Cai, "Time scale analysis and synthesis for model predictive control," in *Proceedings of the WSEAS-NAUN 4th International Conference on Circuits, Systems, Control, Signals (CSCS'13)*, 2013, pp. 27–32.

[87] S. Jaison, D. S. Naidu, and D. Zydek, "Time scale analysis and synthesis of deterministic and stochastic wind energy conversion systems," *WSEAS Transactions on Systems and Control*, vol. 9, no. 1, pp. 189–198, 2014.

[88] Z. Gajic and M. T. Lim, "A new filtering method for linear singularly perturbed systems," *IEEE Transactions on Automatic Control*, vol. 39, no. 9, pp. 1952–1955, 1994.

[89] W. C. Su, Z. Gajic, and X. M. Shen, "The exact slow-fast decomposition of the algebraic ricatti equation of singularly perturbed systems," *IEEE Transactions on Automatic Control*, vol. 37, no. 9, pp. 1456–1459, 1992.

[90] M. L. Shanoob, K. Iqbal, and A. Al-Maliki, "Wind turbine transient response and fault ride-through improvements with optimal control," *International Transactions on Electrical Energy Systems*, vol. 27, no. 11, p. e2412, 2017.

[91] Z. Gajic, *Multimodel Control and Estimation of Linear Stochastic Systems*, 1984.

[92] T. Grodt and Z. Gajic, "The recursive reduced-order numerical solution of the singularly perturbed matrix differential riccati equation," *IEEE transactions on automatic control*, vol. 33, no. 8, pp. 751–754, 1988.

[93] I. Borno and Z. Gajic, "Parallel algorithms for optimal control of weakly coupled and singularly perturbed jump linear systems," *Automatica*, vol. 31, no. 7, pp. 985–988, 1995.

[94] H. Mukaidani, H. Xu, and K. Mizukami, "New iterative algorithm for algebraic riccati equation related to h-infinity control problem of singularly perturbed systems," *IEEE transactions on automatic control*, vol. 46, no. 10, pp. 1659–1666, 2001.

[95] R. H. Bartels and G. W. Stewart, "Solution of the matrix equation ax+ xb= c [f4]," *Communications of the ACM*, vol. 15, no. 9, pp. 820–826, 1972.

[96] G. Golub, S. Nash, and C. Van Loan, "A hessenberg-schur method for the problem ax+ xb= c," *IEEE Transactions on Automatic Control*, vol. 24, no. 6, pp. 909–913, 1979.

[97] D. Y. Hu and L. Reichel, "Krylov-subspace methods for the sylvester equation," *Linear Algebra and its Applications*, vol. 172, pp. 283–313, 1992.

[98] F. Ding and T. Chen, "Iterative least-squares solutions of coupled sylvester matrix equations," *Systems & Control Letters*, vol. 54, no. 2, pp. 95–107, 2005.

[99] X. Wang, L. Dai, and D. Liao, "A modified gradient based algorithm for solving sylvester equations," *Applied Mathematics and Computation*, vol. 218, no. 9, pp. 5620–5628, 2012.

[100] Z.-Z. Bai, "On hermitian and skew-hermitian splitting iteration methods for continuous sylvester equations," *Journal of Computational Mathematics*, pp. 185–198, 2011.

[101] Y.-F. Ke and C.-F. Ma, "A preconditioned nested splitting conjugate gradient iterative method for the large sparse generalized sylvester equation," *Computers & Mathematics with Applications*, vol. 68, no. 10, pp. 1409–1420, 2014.

[102] V. Sreeram, "Recursive technique for computation of grammians," in *IEE Proceedings-D*, vol. 140, no. 3, 1993, pp. 160–166.

[103] K. Wan and V. Sreeram, "Solution of the bilinear matrix equation using åström-jury-agniel algorithm," *IEE proceedings. Control theory and applications*, vol. 142, no. 6, pp. 603–610, 1995.

[104] A. Andry, J. Chung, and E. Shapiro, "Modalized observers," *IEEE transactions on automatic control*, vol. 29, no. 7, pp. 669–672, 1984.

[105] V. Gourishankar and K. Ramar, "Pole assignment with minimum eigenvalue sensitivity to plant parameter variations," *International Journal of Control*, vol. 23, no. 4, pp. 493–504, 1976.

[106] J. T. Pukrushpan, A. G. Stefanopoulou, and H. Peng, *Control of Fuel cell Power Systems: Principles, Modeling, Analysis and Feedback Design*. Springer Science & Business Media, 2004.

[107] M. Skataric and Z. Gajic, "Slow and fast dynamics of a natural gas hydrogen reformer," *International Journal of Hydrogen Energy*, vol. 38, no. 35, pp. 15 173–15 179, 2013.

[108] H. K. Khalil, "Time scale decomposition of linear implicit singularly perturbed systems," *IEEE transactions on automatic control*, vol. 29, no. 11, pp. 1054–1056, 1984.

[109] Y. Levron, J. Belikov, and D. Baimel, "A tutorial on dynamics and control of power systems with distributed and renewable energy sources based on the dq0 transformation," *Applied Sciences*, vol. 8, no. 9, p. 1661, 2018.

[110] F. Mei, *Small-Signal Modelling and Analysis of Doubly-Fed Induction Generators in Wind Power Applications*. Ph.D. dissertation, Imperial College London, Univ. London, London, 2008.